

---

---

# Phenomenology of bulk scalar production at the LHC

---

---

Pierre-Hugues Beauchemin  
Center for High Energy Physics  
Department of Physics  
McGill University  
Montréal, Québec  
Canada  
August 2004

A Thesis submitted to McGill University  
in partial fulfillment of the requirements for the degree of  
Doctor of Philosophy

© Pierre-Hugues Beauchemin, 2004



Library and  
Archives Canada

Bibliothèque et  
Archives Canada

Published Heritage  
Branch

Direction du  
Patrimoine de l'édition

395 Wellington Street  
Ottawa ON K1A 0N4  
Canada

395, rue Wellington  
Ottawa ON K1A 0N4  
Canada

*Your file* *Votre référence*  
*ISBN: 978-0-494-21621-7*  
*Our file* *Notre référence*  
*ISBN: 978-0-494-21621-7*

#### NOTICE:

The author has granted a non-exclusive license allowing Library and Archives Canada to reproduce, publish, archive, preserve, conserve, communicate to the public by telecommunication or on the Internet, loan, distribute and sell theses worldwide, for commercial or non-commercial purposes, in microform, paper, electronic and/or any other formats.

The author retains copyright ownership and moral rights in this thesis. Neither the thesis nor substantial extracts from it may be printed or otherwise reproduced without the author's permission.

#### AVIS:

L'auteur a accordé une licence non exclusive permettant à la Bibliothèque et Archives Canada de reproduire, publier, archiver, sauvegarder, conserver, transmettre au public par télécommunication ou par l'Internet, prêter, distribuer et vendre des thèses partout dans le monde, à des fins commerciales ou autres, sur support microforme, papier, électronique et/ou autres formats.

L'auteur conserve la propriété du droit d'auteur et des droits moraux qui protègent cette thèse. Ni la thèse ni des extraits substantiels de celle-ci ne doivent être imprimés ou autrement reproduits sans son autorisation.

---

In compliance with the Canadian Privacy Act some supporting forms may have been removed from this thesis.

Conformément à la loi canadienne sur la protection de la vie privée, quelques formulaires secondaires ont été enlevés de cette thèse.

While these forms may be included in the document page count, their removal does not represent any loss of content from the thesis.

Bien que ces formulaires aient inclus dans la pagination, il n'y aura aucun contenu manquant.

  
**Canada**

*“Et moi je participais maintenant de cette expérience suprême, moi qui pourtant me mouvais avec tout et avec le tout, mais pouvais voir Cela, le Non-mouvant, la Forteresse, la Garantie, le brouillard très lumineux qui n’est corps, n’a figure forme poids quantité ou qualité, et ne voit, n’entend, ni ne tombe sous la sensibilité, n’est pas en un lieu, en un temps ou en un espace, n’est âme, intelligence, imagination, opinion, nombre, ordre, mesure, substance, éternité, n’est ni ténèbre ni lumière, n’est pas erreur et n’est pas vérité.”*

Unberto Eco,  
Le Pendule de Foucault

---



---

# CONTENTS

---



---

Abstract	x
Résumé	xi
Acknowledgments	xii
<b>1 INTRODUCTION</b>	<b>1</b>
1.1 Framework . . . . .	1
1.2 Research project . . . . .	4
<b>2 MOTIVATION: SUPERSYMMETRIC LARGE EXTRA-DIMENSION (SLED)</b>	<b>6</b>
2.1 Motivation for the SLED scenario . . . . .	7
2.1.1 What is a cosmological constant? . . . . .	7
2.1.2 What is the problem? . . . . .	11
2.1.3 How can we solve it? . . . . .	12
2.2 Ingredients needed for a solution . . . . .	13
2.2.1 Large Extra Dimension (LED) . . . . .	13
2.2.2 6D Supergravity (SLED) . . . . .	18
2.3 Consequences of SLED . . . . .	24
2.3.1 String inspired . . . . .	24
2.3.2 Phenomenology . . . . .	25
2.3.3 New SUSY realization . . . . .	29
2.4 Present state research on an explicit SLED model . . . . .	31
2.4.1 Salam-Sezgin model . . . . .	31
2.4.2 Other possible quantum effects . . . . .	33
2.4.3 Hidden fine tuning . . . . .	34
2.4.4 Astrophysical bounds . . . . .	35
2.5 Conclusion on this chapter . . . . .	37
<b>3 PHYSICAL PREDICTIONS ON SEARCH FOR BULK SCALAR AT LHC</b>	<b>39</b>
3.1 Low-Energy bulk scalar coupling . . . . .	39
3.1.1 Four-dimensional extended SUSY . . . . .	39
3.1.2 Coupling of bulk scalar with SM fields . . . . .	50
3.2 Bulk scalar production at LHC . . . . .	59
3.2.1 Parton-level cross section of the hadronic processes . . . . .	60
3.2.2 Proton-Proton Cross Sections of the hadronic processes . . . . .	66
3.2.3 Validity of the Low-Energy Approximation . . . . .	67
3.2.4 $h - \phi$ production at colliders . . . . .	71

<b>4</b>	<b>LHC AND ATLAS DETECTOR</b>	<b>81</b>
4.1	LHC . . . . .	82
4.2	ATLAS . . . . .	86
4.2.1	Transverse momentum observables . . . . .	87
4.2.2	The ATLAS Inner Detector . . . . .	90
4.2.3	ATLAS calorimetry . . . . .	92
4.2.4	ATLAS Muon system . . . . .	94
4.2.5	Trigger . . . . .	95
<b>5</b>	<b>PHENOMENOLOGICAL ANALYSIS</b>	<b>97</b>
5.1	Simulations . . . . .	98
5.2	jet+bulk scalar signal . . . . .	100
5.2.1	Standard Model Backgrounds . . . . .	101
5.2.2	Analysis . . . . .	101
5.2.3	Results . . . . .	106
5.2.4	Graviton-Bulk Scalar Confusion . . . . .	110
5.2.5	Summary and Conclusions on the jet+ $\cancel{E}_T$ signal . . . . .	112
5.3	Higgs+bulk scalar signal . . . . .	112
5.3.1	Standard Model Backgrounds . . . . .	113
5.3.2	Analysis . . . . .	115
5.3.3	Summary and Conclusions on scalar-Higgs coupling . . . . .	118
<b>6</b>	<b>UNIVERSAL EXTRA DIMENSION</b>	<b>125</b>
6.1	Why Universal Extra Dimensions? . . . . .	125
6.2	Extra dimension and gauge coupling unification . . . . .	130
6.3	The Universal Extra Dimension model . . . . .	136
6.4	Decay mechanism of the lowest-lying KK mode . . . . .	143
<b>7</b>	<b>PHENOMENOLOGICAL ANALYSIS OF THE UED SCENARIO</b>	<b>147</b>
7.1	Physical predictions . . . . .	147
7.2	Detailed Simulations . . . . .	151
7.2.1	Standard Model Backgrounds . . . . .	152
7.2.2	Analysis . . . . .	153
7.2.3	Results . . . . .	155
<b>8</b>	<b>SUMMARY AND CONCLUSION</b>	<b>159</b>
	<b>BIBLIOGRAPHY</b>	<b>162</b>

---



---

## LIST OF FIGURES

---



---

3.1	The parton-level Feynman graphs which contribute to bulk scalar production with an associated jet in proton-proton scattering. . . . .	64
3.2	Comparison of the graviton cross section computed by Giudice <i>et al.</i> (left) and the one obtained by our numerical integration (right). We see that these results are consistent . . . . .	67
3.3	Total jet + nothing cross section for bulk scalar production at LHC to evaluate the validity limit of the phase space volume when: top) only the bulk scalar-gluons coupling is present; bottom) only the bulk scalar-fermions coupling is present. The curves are normalized to the cross section for graviton production at a value of $E_{T,jet}^{min}$ of 500 GeV. . . . .	69
3.4	Evaluation of the minimum (4+n)-dimensional Planck scale for which the effective model is valid, at the 90% level, given a cut $E_{T,jet}^{min}$ , as explained in the text . . . . .	70
3.5	Branching ratio for the various decay channels of the Higgs boson in function of the mass of this particle. . . . .	72
3.6	ATLAS sensitivity for the discovery of a Standard Model Higgs boson for each individual decay channels in function of the mass of this particle. This assume an integrated luminosity of $100 \text{ fb}^{-1}$ and a statistical significance computed as $\frac{\text{signal}}{\sqrt{\text{bkg}}}$ . This figure is taken from [52] . . . . .	73
3.7	Parton-level Feynman graphs which dominate the Higgs/bulk-scalar production at the LHC. . . . .	74
3.8	Parton-level Feynman graphs which could contribute to the Higgs/bulk scalar production at the LHC. We argued in the text that this contribution is too weak to be considered in this first analysis. . . . .	75
3.9	Effective parton-level Feynman graph for the direct production of Higgs/bulk-scalar production at the LHC. . . . .	76
4.1	Picture of the LHC location in the Geneva area. . . . .	82
4.2	Picture of the four experiments on the underground LHC ring. . . . .	83
4.3	Picture of the LHC injector complex and of the main LHC ring. . . . .	83
4.4	The cross section of an LHC standard two-in-one dipole in its cryostat. . . . .	84
4.5	A cut-away view of the ATLAS detector. . . . .	87
4.6	Cut-away view of the ATLAS inner detector. . . . .	91
4.7	Cut-away view of the ATLAS calorimetry. . . . .	93
4.8	Architecture of the three level trigger system of ATLAS. . . . .	96
5.1	Distribution of the difference in the azimuthal angle between the two most energetic jets of an event for: (top) each of the backgrounds; (bottom) the signal and the total background on top of it. . . . .	102
5.2	Significance of the signal for different values of cut 2 . . . . .	103

5.3	Contributions of different processes to the total background after application of the cuts, for an integrated luminosity of $100 \text{ fb}^{-1}$ . . . . .	104
5.4	Distributions of missing $E_T$ for background and signal when: (top) the cross section for bulk scalar production is the same as the graviton one; (bottom) this cross section is at its discovery limit. . . . .	120
5.5	Parameters region for bulk scalar theory at second order in $E/M_D$ that allows testable and valid physical predictions at ATLAS, for different number of extra dimensions. The bulk scalar-fermions and bulk scalar-gluons dimensionless couplings are effectively combinations $(g^2 + g_5^2)^{1/2}$ and $(c^2 + c_5^2)^{1/2}$ . . . . .	121
5.6	Feynman graphes of the irreducible backgrounds. In a) we have the Born process, in b) the box diagram process and in c) the quark bremsstrahlung process. . . . .	121
5.7	Expected $h + \phi$ signal for $M_H = 120$ . GeV, for an integrated luminosity of $100 \text{ fb}^{-1}$ and with $hh\phi$ coupling value chosen as $a = 0.5$ . The left panel shows the signal on top of the irreducible background, while the right one shows the reconstruction of the mass pic. . . . .	122
5.8	Distribution of $\cancel{E}_T$ for the Higgs + bulk scalar signal, assuming $a = 0.5$ (top), the total background (bottom-left) including the $Zh \rightarrow \gamma\gamma \nu\nu$ production (dashed blue) and the $pp \rightarrow h$ process, with $m_H = 120$ GeV (bottom-right). The plots are normalized for an integrated luminosity of $100 \text{ fb}^{-1}$ . . . . .	122
5.9	Value of the $hh\phi$ coupling needed for different significances of the signal, as function of a cut on $\cancel{E}_T$ . . . . .	123
5.10	Number of events (including backgrounds) for $h\phi$ and standard $h$ production, as a function of the two-photon invariant mass. This plot assumes the smallest-detectable coupling $a = 0.09$ . and uses the optimal missing-energy cut, $\cancel{E}_T > 78$ GeV. . . . .	123
5.11	The significance of the $\gamma\gamma$ signal alone as function of the Higgs mass for different values of the cut on $\cancel{E}_T$ . The figure assumes the choices $a = 0.5$ and an integrated luminosity of $100 \text{ fb}^{-1}$ . The dotted line corresponds to what can be obtained from the standard $h \rightarrow \gamma\gamma$ process making no cut on $\cancel{E}_T$ . This shows that a considerable gain in Higgs reach is possible should Higgs production be possible in association with missing energy. . . . .	124
6.1	Unification of the electromagnetic, weak and strong coupling constants for the Standard Model (left) and the MSSM (right) . . . . .	126
6.2	(top) Scales involved in the UED scenario, with $R$ being the size of the small extra dimensions; (bottom) scales involved in the SLED scenario, with $r$ being the size of the large extra dimensions. . . . .	133
6.3	Unification of gauge couplings in the presence of extra space-time dimensions in the case where only gauge bosons and Higgs field propagate in the extra dimensions as computed by ref. [61]. Four cases have been considered: $\mu_0 = 10^5$ GeV (top left), $\mu_0 = 10^8$ GeV (top right), $\mu_0 = 10^{11}$ GeV (bottom left) and $\mu_0 = 10^{15}$ GeV (bottom right). In each case they considered only one small extra dimension ( $\delta = 1$ ). . . . .	135

6.4	Relative coupling strengths of vertices involving $q_n^\bullet$ and $q_n^\circ$ [63]. Only the overall factors are shown: these vertices also involve the usual $SU(3)$ matrix element and the Dirac $\gamma^\mu$ matrix. Here, $n$ and $m$ are distinct positive integers ( $n \neq m$ ) and the projection operators are defined in the text. . . . .	141
6.5	Width for the decay of the first excited KK state (even-top left panel, odd-top right panel) into the corresponding zero mode and a graviton tower as a function of the mass of the KK state. The solid (dashed) lines are for $M_D = 5(10)$ TeV and from top to bottom in each case the curves correspond to $\delta = 2, 4, 6$ largeextra dimensions respectively. The lower panel shows the missing energy distribution for these decays for the same cases assuming a KK mass of 1 TeV. These graphs have been taken from [66] . . . . .	145
7.1	The total cross section for the production of two KK final states at the LHC is shown in function of the KK mass of these states. A annual luminosity of $100 \text{ fb}^{-1}$ has been considered here. The dashed line mark 100 events at this luminosity. . . . .	152
7.2	Comparison of the $p_T$ distributions of the two most energetic jets for the signal and the background. . . . .	154
7.3	top: Distribution of the difference in the azimuthal angle between the two most energetic jets of an event for the signal and the each background on top of it. A KK mass of 1.3 TeV is used as reference. Cuts 1-3 have been applied. bottom: Significance of the signal for different values of a cut on the difference in the azimuthal angle between the most energetic jets of an event. . . . .	156
7.4	Left: Comparison of $\cancel{E}_T$ distribution for signal and background events. Right: Variation of the significance of the signal as a function of the cut on $\cancel{E}_T$ . . . . .	157
7.5	Variation of the significance of the signal in function of the mass of the first KK excitation state. . . . .	157

---



---

## LIST OF TABLES

---



---

3.1	Number of states for each helicity value $\lambda$ associated to a spin-2 graviton by a N-extended supersymmetry . . . . .	48
3.2	Cross-sections for the signal process $pp \rightarrow h\phi$ using the coupling value $a = 0.5$ , and for $pp \rightarrow hX$ as a function of the Higgs mass. Also shown are the branching ratio for Higgs decay into two photons and the mass resolutions ( $\sigma_H$ ) at high luminosity in ATLAS. . . . .	79
4.1	Some parameters of the LHC . . . . .	85
4.2	Performance objectives for the ATLAS calorimetry. Here, the granularity is defined in terms of the pseudorapidity $\eta$ and the azimuthal angle $\phi$ . Note that the numbers that are quote here are indicative. For example, the granularity change in the EM end-cap detector with decreasing $\eta$ because of the geometry of that sub-detector. . . . .	88
4.3	Performance objectives for the ATLAS inner detector. Here, the granularity is defined in terms of the transverse distance $R$ to the beam-pipe in the pseudorapidity-azimuthal angle space (for any $\phi$ ). . . . .	89
5.1	S.M. backgrounds to the bulk scalar production at ATLAS and their cross section for different phase space volume. . . . .	101
5.2	Number of signal ( $M_D = 5$ TeV, $n = 2$ , $g = 0.70$ and $c = 0.41$ ) and background events that survive each cut for an integrated luminosity of $100 \text{ fb}^{-1}$ . The cuts are defined in the text. Remember finally that the value of the coupling constants has each been chosen for rough comparison with the graviton production and are independent of the $5\sigma$ reach of the bulk scalar production. . . . .	104
5.3	Sensitivity of the ATLAS detector to the fundamental Planck scale $M_D$ through the discovery of a bulk scalar signal, for $c = 0$ and for an integrated luminosity of $100 \text{ fb}^{-1}$ . For $n \geq 4$ , observation of a signal is not possible. . . . .	108
5.4	Sensitivity of the ATLAS detector to the fundamental Planck scale $M_D$ through the discovery of a bulk scalar signal, for $g = 0$ and for an integrated luminosity of $100 \text{ fb}^{-1}$ . For $n \leq 6$ , observation of a signal is possible. . . . .	109

5.5	With $c=0$ : comparison of the sensitivity of ATLAS to $M_D$ for bulk scalar and graviton signals under the conditions $E_T^{min} > 1\text{TeV}$ , $\frac{S}{\sqrt{7B}}$ and with indirect constraints from cosmology. The integrated luminosity is $100\text{ fb}^{-1}$ . For $n \geq 3$ , observation of a bulk scalar signal is not possible since $M_D^{min} > M_D^{max}$ . For the cosmology bounds, Scenario A means limits to neutron star heating by KK-decays, while scenario B corresponds to bounds from the cooling of SN1987A by KK-modes emission. . . . .	109
5.6	With $g=0$ : comparison of the sensitivity of ATLAS to $M_D$ for bulk scalar and graviton signals under the conditions $E_T^{min} > 1\text{TeV}$ , $\frac{S}{\sqrt{7B}}$ and with indirect constraints from cosmology. The integrated luminosity is $100\text{ fb}^{-1}$ . For $n \leq 4$ , observation of a bulk scalar signal is possible. . .	110
5.7	SM backgrounds to the production of bulk scalars in association with the Higgs at ATLAS, their cross section (for an $E_T^{cut}$ of 23 GeV) and the total number of events expected at ATLAS for an integrated luminosity of $100\text{ fb}^{-1}$ (after application of rejection factors). . . . .	114
7.1	Cross sections for the different processes that yield a KK pair production at LHC assuming $M_{KK} = 1.3\text{ TeV}$ and an integrated luminosity of $100\text{ fb}^{-1}$ . . . . .	151
7.2	S.M. backgrounds to the production at ATLAS of a pair of KK partons which each decay in a jet plus an undetectable graviton and their cross sections for 2 different phase space regions. . . . .	153

---

---

## Abstract

---

---

We examine the sensitivity of the ATLAS detector to extra-dimensional scalars in scenarios having the extra-dimensional Planck scale in the TeV range and  $n = 2$  large extra dimensions. Such scalars appear as partners of the graviton in higher-dimensional supersymmetric theories. Using first the scalar's lowest-dimensional effective couplings to quarks and gluons, we compute the rate of production of a hard jet together with missing energy. We find a nontrivial range of bulk scalar couplings for which ATLAS could observe a signal, and in particular, higher sensitivity to couplings to gluons than to quarks.

Bulk scalar emission increases the missing-energy signal by adding to graviton production, and so complicates the inference of the extra-dimensional Planck scale from the observed rate of jet +  $E_T^{\text{miss}}$ . Because bulk scalar differential cross sections resemble those for gravitons, it is unlikely that these can be experimentally distinguished should a missing energy signal be observed. However, given, for example, the Supersymmetric Large Extra Dimension (SLED) scenario, which can provide a framework for a solution to the cosmological constant problem, the D-dimensional Planck scale is approximately fixed and so is the graviton production rate. An excess of events would then be due to graviton superpartners like bulk scalars.

Next, we identify the lowest-dimension interaction which is possible between Standard Model brane fields and bulk scalars. The lowest-dimension interaction is unique and involves a trilinear coupling between the Standard Model Higgs and a bulk scalar. We compute its influence on Higgs physics at ATLAS and identify how large a coupling can be detected at the LHC. Besides providing a potentially interesting signal in Higgs searches, such couplings provide a major observational constraint on 6D large-extra-dimensional models with scalars in the bulk.

Finally we consider the Universal Extra Dimensions scenario in which all the SM fields propagate. Tree-level KK number conservation dictates that the associated KK excitations cannot be singly produced. We recalculate the cross sections obtained by Macesanu *et al.* for the direct production of KK excitations of the gluon,  $g^*$ , and two distinct towers of quarks,  $q^\bullet$  and  $q^\circ$ , in proton-proton collisions at the LHC. According to the SLED scenario, these KK states will quickly decay in a parton plus a graviton. We find that the LHC mass bound for KK quark and gluon final states is 2675 GeV at its nominal luminosity of  $100 \text{ fb}^{-1}$ .

---

---

## Résumé

---

---

Nous étudions la sensibilité du détecteur ATLAS à la production de particules scalaires pouvant se propager dans des dimensions supplémentaires, tel que prédit par les théories supersymétriques de grandes dimensions supplémentaires (SLED). Dans de tels scénarios, ces particules scalaires sont des superpartenaires du graviton. Dans un premier temps, nous étudions les couplages dominants de ces particules aux quarks et aux gluons. Après avoir calculé le taux de production de jets durs accompagnés d'énergie manquante dans le détecteur, nous démontrons que le détecteur ATLAS sera sensible à un important intervalle de valeurs des couplages de ce scalaire, particulièrement pour le couplage aux gluons. Un tel signal s'ajoutera à celui de la production directe de gravitons. Comme la section efficace de ce dernier processus est du même ordre de grandeur que celle de la production de scalaire et comme leurs distributions sont équivalentes, il sera a priori impossible de les distinguer. Cependant, dans le scénario SLED pour lequel le problème de la constante cosmologique reçoit une solution satisfaisante, l'échelle de Planck en  $D = 4 + 2$  dimensions est approximativement déterminée. Le taux de production de gravitons le sera donc également. La mesure d'un excès dans des événements de ce type ne pourra alors être attribuée qu'à des superpartenaires du graviton comme le scalaire étudié ici.

Ensuite nous identifions l'interaction dominante entre un scalaire extra-dimensionnel et une particule du Modèle Standard. Il s'agit du couplage trilineaire, de dimension nulle, d'un tel scalaire avec deux bosons de Higgs. Ce processus est exclusif au scénario SLED. Après avoir calculé son influence sur la physique du Higgs au LHC, nous évaluons la grandeur que ce couplage doit avoir pour pouvoir être clairement détecté avec ATLAS. Cette étude fournira les contraintes majeures à l'observabilité des signaux de modèles supersymétriques avec dimensions supplémentaires. Elle offrira également de nouvelles possibilités pour la recherche du Higgs.

Finalement, on considèrera le scénario de dimensions supplémentaires universelles dans lequel toutes les particules du Modèle Standard ont accès à une cinquième dimension. Nous avons recalculé les sections efficaces, évaluées par Maccesanu *et al.*, pour les divers processus de production d'états KK du gluon,  $g^*$ , ainsi que pour deux types de quarks distincts,  $q^\bullet$  and  $q^\circ$ . Nous avons corrigé certaines erreurs de leur calcul. Nous avons montré que la limite de masse à laquelle sera sensible le LHC est de 2675 GeV, à une luminosité de  $100 \text{ fb}^{-1}$ .

---

---

## Acknowledgments

---

---

Firstly, I want to thank my supervisors, Cliff Burgess and Georges Azuelos, because this work results from the good influence they had on me. More precisely:

Cliff is the great architect behind all this work. He develop the brilliant and exciting idea of the SLED framework which provides the complete motivation of my research. Having the opportunity to work on such physics is a privilege and an honor, and I owe this to Cliff. The clearness and the keenness of its understanding of high energy and cosmology theories struck me and incite me to learn from him. I'm particularly compelled to Cliff for the effective field theory approach and for helping me to understand the structure of theories in terms of symmetries. This was really helpful for understanding models behind my work, but, on a more philosophical point of view, it also provided me with an epistemological insight of how scientific discourses are structured. Cliff helped me in that by orienting my study and my work, by the course that he gave me and by the discussion we had. Finally I'm thankful to him because he always encouraged me to go back on the working bench when problems or errors arose and because he taught me methods to overcome these difficulties. I would say that Cliff has been the lighthouse of my mind during my PHD.

Si la partie théorique de mon travail est tributaire à Cliff, mon travail phénoménologique, qui constitut l'essentiel de mon apport à la physique des particules, est complètement redevable à Georges. C'est lui, en effet, qui a amené le contexte expérimental dans lequel j'ai établi la pertinence empirique des modèles SLED. Avec Georges, c'est une toute autre facette de la physique que j'ai appris à sonder: celle d'établir un contact entre les idées et la réalité. Cela aussi est fondamental à une compréhension épistémologique de ce qu'est une science et constitue donc un élément essentiel à la formation d'un scientifique. Ainsi, Georges m'a appris à analyser des résultats empiriques et à en soutirer de l'information physique. Bien sûr, pour accomplir des analyses de ce genre, un tas d'outils techniques sont nécessaires à utiliser, mais aussi à comprendre et là encore Georges fut d'une aide exemplaire. Mais au-delà de tous ces enseignements, il y a deux choses que je retiens particulièrement de Georges: son pertinent sens critique et sa patience extrême. Georges ne prend rien pour acquis et ses remarques nous ont permis d'éviter bon nombre de catastrophes. De plus, les innombrables heures que nous avons passées assis à son ordinateur

à coder, “debugger” ou comprendre des résultats d’analyse font de ma collaboration avec Georges un exemple que je souhaiterais renouvelable éternellement. Georges est donc en quelque sorte le forgeron de mon esprit scientifique.

Finally, I want to thank both Cliff and Georges because they provided me the funding without which I would not have been able to continue my studies. They also made me travel around the world to meet people and give talks about my research. This introduced me to the scientific community. Finally the contacts that they provided gave me the opportunity to continue a career in physics. Unfortunately I made another choice, but I’m really thankful to them because by offering me the possibility to continue, they offered me the possibility to choose.

Je voudrais également remercier les gens de mon entourage, à McGill, comme au Laboratoire René J.A. Lévesque, qui m’ont aidé, ci et là, en répondant à mes questions ou en m’aidant en informatique. C’est gens sont nombreux, mais je tiens particulièrement à remercier Simon Turbide, Jean-Sébastien Gagnon, Yashar Aghababaie, John Idárraga et Jonathan Ferland.

Bien sûr, je ne passerai pas sous silence ma famille et mes amis qui par leur support moral et affectif m’ont offert les conditions nécessaires pour que je puisse me consacrer, l’esprit libre, à mon travail. Voici donc les noms (sans ordre de préférence) de ces personnes que ma mémoire n’oubliera jamais: mon père et ma mère, Geneviève et Marie-Élyse, Philippe et Pascal, Ervig, Thomas, Jean-François, Philippe, Phanie, Patrick, les François (Lemieux et Fillion), les Oliviers (“l’ancien” et le “jeune”), Pierre-Antoine, Marie-Hélène, Marie et Maxime.

J’offrirai en terminant quelques mots à ma charmante épouse qui a partagé avec moi mes bons moments, mais surtout qui a toujours cherché à m’épauler lors des moments difficiles. Elle a même déjà essayé de trouver où était passé mon facteur  $2\pi$ ! Geneviève, tu rends chaque jour meilleur que le précédent et c’est là le plus beau cadeau qu’on peut faire à quelqu’un. Merci, merci à tous!!!

## INTRODUCTION

---

---

### *1.1 Framework*

The paradigm of particle physics is so far provided by the Standard Model, a theory that properly describes the electro-weak interactions at experimental energies, ie below the TeV scale. It also includes a consistent and calculable description of the strong interaction at the partonic level. However, it fails in providing a good theory of the gravitational interaction which is manifest in our everyday life. In order to complete our knowledge of particle physics, we therefore need to incorporate the Standard Model in a more general and complete theory that will include gravity but will also provide a solution to at least some of the most fundamental problems of particle physics such as the question of the origin of mass, the problem of the huge hierarchy between the fundamental scales of nature, the explanation of why there are only three families of quarks and leptons, and the problem of the smallness of the cosmological constant compared to the Standard Model predictions. All these problems demonstrate our fundamental misunderstanding of the true structure of Nature. Much effort have been devoted to find a solution to some of these problems and from these efforts, many theories beyond the Standard Model have emerged. Up to now, the most promising and popular such theory is certainly the supersymmetric extension of the Standard Model which is called, in its minimal version, the Minimal Supersymmetric Standard Model (MSSM).

The study of the MSSM and of its phenomenological properties is one of the greatest challenges of the next few years in high-energy physics, both at the theoretical

and at the experimental levels. To detect the superparticles predicted by this theory is one of the big challenges of the Large Hadron Collider (LHC). The LHC will become in 2008 the most powerful particle collider ever built, and provide an incomparable empirical framework for the discovery of what is called “new physics”. The three fundamental reasons why serious research efforts have been devoted so far to supersymmetry by the high-energy physicists are that:

1. it has a large and concrete predictive power that allows for direct tests at the LHC;
2. it is motivated by a more fundamental theory: string theory (that incorporates gravity);
3. it provides a natural solution to some of the most challenging problems of microphysics (namely the hierarchy problem, the question of gauge unification and the problem of finding dark matter candidates)

These fundamental features of a good theoretical high-energy physics framework are not exclusive to the MSSM. In fact, every experimentally testable theory that describes at low energy some of the fundamental features of string theory and which uses them to solve some of the most important problems of particle physics will be justified to get as much attention as the MSSM has had so far. This, I believe, will be the case for the theoretical framework considered in this thesis.

String theory hitherto offers the most powerful theoretical motivation that an effective low-energy theory can provide because it is the most promising framework in which we can hope to consistently describe quantum gravity and predict the unification of all the fundamental forces of Nature [1]. Among other things, string theory predicts a small value for the cosmological constant at high energies [1], which is a good thing since our observations already reveal a small value for this quantity at low energies [3, 4]. However, our low energy theories today predict a large value for this cosmological constant, indicating that there is still a profound lack in our understanding of particle physics and of the vacuum in our Universe. Even if string theory

seems to provide good hints for solving this refractory problem, it will not be able to explain why the cosmological constant stays small at low energies. In fact, the difficulty with this theory is that, in the orthodoxy in high-energy physics, it can only affect the physics at the Planck scale which is of  $10^{19}$  GeV, 16 orders of magnitude higher than the energy that will be achieved at the LHC. Except for supersymmetry itself, none of the string predictions seems testable in a near future. String theory is therefore a good theoretical motivation for low-energy theories but does not, for the moment, provide a solution testable at low energy experiments.

However, recent developments in string theory [5] have sparked renewed interest in its phenomenology at low energies. In fact, it has been shown that the extra dimensions predicted by the theory could be much larger than what was considered before ( $\lesssim 0.1$  mm rather than  $\lesssim 10^{-31}$  mm). This would allow the  $(4 + n)$ -dimensional Planck scale to be of the order of the weak scale (TeV scale). If this turns out to be true, important gravitational effects would then be observable at the LHC and this could have important consequences on the quest for a solution to the cosmological constant problem at available energies. In the last few years, major research effort has thus been put on the phenomenology of string inspired effective field theory with coupling to a gravitational interaction that can propagate in large extra dimensions. However, the effort has been mostly concentrated so far on non-supersymmetric versions of such a theory [6, 7, 8, 9, 10]. Since supersymmetry is also a prediction from string theory, there is no a priori reason for neglecting this feature. More than that, adding supersymmetry will turn out to be a fundamental step toward a better understanding of our world.

It has recently been suggested [11, 12, 13] that supersymmetric theories with large extra dimensions (SLED) can provide the suitable framework for solving the cosmological constant problem. Moreover, such a scenario requires that supersymmetry be strongly broken on the brane where the Standard Model lives, but only weakly broken in the bulk space where gravity propagates. The SLED scenario will therefore provide a completely new way (different from MSSM) in which supersymmetry

can be realized at low energy. Finally, since the SLED proposal predicts coupling between Standard Model particles and bulk graviton superpartners at relatively low energies (below the weak scale), the LHC will therefore have the possibility to test the theory in a near future. Because Supersymmetric Large Extra Dimensional theories are well motivated by string theory, because they can solve some of the most fundamental problems of high-energy physics and cosmology (the cosmological constant problem and the hierarchy problem) and because they predict testable phenomenologies for collider experiments, they constitute a rich, inescapable and exciting research framework for theorists, cosmologists, phenomenologists and experimentalists as well. Moreover, the novelty of this subject ensures that almost nothing has been done so far from the phenomenological point of view. The object of this thesis will be to examine phenomenological aspects of SLED and predict the extent to which the LHC can test the theory.

## 1.2 *Research project*

In the SLED scenario, our empirical world is confined to a 4-dimensional hyperplane called *3-brane*, but gravitons and their superpartners will also propagate in two transverse extra dimensions. Because these dimensions are compactified, the bulk particles will appear to a brane observer as a complete tower of Kaluza-Klein states of different masses (see section 3.1.1). It is the experimental analysis of the direct production of such KK-states that constitutes the subject of this thesis. Since SLED theoretical modelling is not yet completed, our work will consist in establishing the experimental limit of detectability for such bulk particles at the LHC. We will therefore be interested in evaluating the minimal values of couplings of bulk scalars to Standard Model particles that can yield a signature in the ATLAS detector a real discovery potential. We will also try to find out up to which energy scale we can expect such signals. This work will thus provide the information that will allow experimentalists to conclude on the validity of this SLED scenario, when data will become available.

Our work will be organized as follow. In the next chapter we will describe the

SLED scenario. There, we will discuss the cosmological constant problem, how it can be solved and how the SLED scenario may provide a solution. In the third chapter we will concentrate on physical predictions that can be made from generic SLED models. We will show how bulk scalars can emerge, how they can couple to Standard Model particles and what effective low-energy four-dimensional Lagrangian describes these interactions. We will then use this Lagrangian to compute the cross sections for direct production of bulk scalar particles in association with final state partons or Higgs particles. This last case will be particularly important for testing our proposal since this process has no equivalent in any other new theory involving gravity, this interaction being dimensionless. In the fourth chapter we will briefly describe the LHC and the ATLAS detector, which provide the experimental set up in which our physical predictions will be tested. The chapter 5 will present the complete phenomenological analysis. The most important results of our work will be given in this chapter.

The last two chapters constitute a complementary analysis on an extension of the SLED scenario that will be presented in chapter 2. In fact, in order to allow for a unification of the Standard Model gauge couplings within the SLED proposal, we will add a small thickness to our brane. The Standard Model fields will therefore be described by a 5D Lagrangian. This is what we call the Universal Extra Dimension scenario (UED). In chapter 6 we will explain the theoretical motivation for such a SLED extension and sketch an explanation of how it can lead to coupling unification. In chapter 7 we will show our physical predictions on the direct production of a pair of UED KK states. We will finally perform a brief phenomenological analysis on the experimental discovery potential of this physics at the LHC.

This thesis constitutes a synthesis of the work that I have done in the last four years.

---

---

## MOTIVATION: SUPERSYMMETRIC LARGE EXTRA-DIMENSION (SLED)

---

---

The goal of this chapter is to introduce the SLED scenario, developed by C.P. Burgess *et al.* [11, 12, 13], from which the physical predictions constituting the subject of this thesis will be made. This will provide the fundamental motivations and the theoretical background for our work. Since our phenomenological analysis will concentrate on collider signals at a relatively low energy scale ( $\lesssim \mathcal{O}(\text{TeV})$ ), our physical predictions will be made from an effective theory which displays the general features of the SLED scenario, but which will not correspond to an explicit and complete model of this proposal. For that reason, this chapter will only focus qualitatively on the big picture of SLED, trying to justify in simple terms its general features (2 large extra dimensions, 6D SUGRA with a small supersymmetry breaking scale in the bulk, etc). All these properties will then, in the next chapters, be explicitly used for our physical predictions for colliders. What we want to point out in the next few pages, therefore, is that the SLED scenario offers serious possibilities to greatly improve our understanding of particle physics at our scale and beyond, thus justifying the work performed for this thesis.

We will first give the fundamental motivations for this proposal. Then we will show how the fundamental properties of SLED answer these motivations. Afterwards, we will briefly dwell on the physical implications and point out the strong scientific value of the SLED scenario. Finally, since research on the elaboration of this proposal is still underway, we will present a quick overview of what has not been done yet. This will emphasize the fact that this proposal is involved in actual scientific research.

## 2.1 Motivation for the SLED scenario

As mentioned already, the recent realization [5, 14, 15] that some fundamental features of string theory (extra dimensions, gravity and supersymmetry as examples) can possibly affect the physics at the TeV scale and even below has sparked considerable effort in analyzing the theoretical and experimental [16, 17, 18, 6] consequences on particle physics. They can, in fact, provide particle physics with new testable solutions to fundamental problems that have escaped the reach of an explanation within the Standard Model (SM). The fundamental purpose of the SLED proposal (and its primary interest) is then to take advantage of these features to provide a complete framework in which to build models that solve in a testable way one of the most refractory problems of modern physics: the cosmological constant problem. Before seeing what features such a framework must exhibit in order to achieve this goal, let us first explain the problem.

### 2.1.1 What is a cosmological constant?

Einstein's theory of general relativity tells us that the evolution of the Universe is determined by the form of the energy that it contains and by the curvature of space. This is expressed by what is known as the Einstein equation [19]:

$$R_{\mu\nu} - \frac{1}{2}g_{\mu\nu}R = -8\pi GT_{\mu\nu} \quad (2.1)$$

where  $R_{\mu\nu}$  is called the Ricci tensor,  $R$  is the curvature,  $g_{\mu\nu}$  the metric tensor,  $G$  Newton's constant of gravity and finally  $T_{\mu\nu}$  is the stress-energy tensor of the system under study. Einstein later added a cosmological constant term  $-\Lambda g_{\mu\nu}$  to the left-handed part of his equation in order to obtain solutions for which the Universe would be static. However when in the 1920s Hubble's observations showed that the Universe was not static but in expansion, Einstein recognized his error and dropped this term from his equation. The Hubble discovery then brought the picture of an isotropic, homogeneous and expanding Universe which can properly be described by the Robertson-Walker solution to the Einstein equation [19]:

$$ds^2 = dt^2 - R^2(t) \left[ \frac{d\bar{r}^2}{1 - k\bar{r}^2} + \bar{r}^2(d\theta^2 + \sin^2\theta d\phi^2) \right] \quad (2.2)$$

where  $k = +1$  for a closed Universe,  $0$  for a flat Universe and  $-1$  for an open one,  $R(t) = R_0 a(t)$ ,  $\bar{r} = r/R_0$ , and  $a(t)$  is a dimensionless factor giving the expansion scaling of the Universe.

Following this equation, we can imagine the Universe as a cake that is expanding in an oven, increasing the distance between the raisins that it contains. The values of the expansion rate  $a(t)$  can be obtained by putting back equation 2.2 in the Einstein's equation and then solving for a given energy distribution  $T_{\mu\nu}$  of the Universe. This has been done under the hypothesis that the Universe is a galactic fluid of average energy density  $T_0^0 = \rho$  and of average internal pressure  $T_i^i = -P$  (all the other components of  $T_{\mu\nu}$  being null) yielding two Friedman equations. These equations are of particular interest since they provide an interpretation of the cosmological constant that, because of the recent observations, reintroduce the question of its non-zero value. Einstein's first guess was thus right, but for a different reason. To see this, let us first adopt co-moving coordinates, ie coordinates for which the Universe expands (or contracts) as  $a(t)$ , but for which galaxies conserve fixed  $r, \theta, \phi$  positions, and let us make the following change of variables:  $\bar{r} = a \sin \chi$  and  $t = a\eta$ . Using these new coordinates, we can express the Robertson-Walker metric in a simpler form [19]:

$$g_{\mu\nu} = a^2 \begin{pmatrix} 1 & 0 & 0 & 0 \\ 0 & -1 & 0 & 0 \\ 0 & 0 & -\sin^2 \chi & 0 \\ 0 & 0 & 0 & -\sin^2 \chi \sin^2 \theta \end{pmatrix} \quad (2.3)$$

We can now use this to compute the Christoffel symbols  $\Gamma_{00}^0$ ,  $\Gamma_{kn}^0$ ,  $\Gamma_{0n}^k$ ,  $\Gamma_{k0}^0$  and  $\Gamma_{00}^k$  which are totally determined by the metric tensor as:

$$\Gamma_{\mu\nu}^\alpha = \frac{1}{2} g^{\alpha\beta} \left( \frac{\partial g_{\beta\mu}}{\partial x^\nu} + \frac{\partial g_{\nu\beta}}{\partial x^\mu} - \frac{\partial g_{\mu\nu}}{\partial x^\beta} \right) \quad (2.4)$$

From the definition of the Riemann tensor ( $R_{\beta\mu\nu}^{\alpha} = -\Gamma_{\beta\mu,\nu}^{\alpha} + \Gamma_{\beta\nu,\mu}^{\alpha} + \Gamma_{\beta\nu}^{\sigma}\Gamma_{\sigma\mu}^{\alpha} - \Gamma_{\beta\mu}^{\sigma}\Gamma_{\sigma\nu}^{\alpha}$  where  $\Gamma_{\beta\mu,\nu}^{\alpha} = \partial_{\nu}\Gamma_{\beta\mu}^{\alpha}$ ) and of the Ricci tensor ( $R_{\mu\nu} = R_{\mu\nu\alpha}^{\alpha}$ ) we can now compute the the curvature ( $R = R_{\mu}^{\mu}$ ) and the 00-component of the Ricci tensor and express them in term of the expansion scale of the Universe as:

$$R_{00} = \frac{3}{a^2}(a\ddot{a} - \dot{a}^2) \quad \text{and} \quad R = \frac{6}{a^3}(ka + \ddot{a}) \quad (2.5)$$

where  $\dot{a} = \frac{da}{dt}$ . Substituting equations 2.5 in Einstein's equation multiplied by  $g^{00}$  and adding a non-zero cosmological constant term  $\Lambda$  will finally yield the first Friedman equation:

$$-\frac{3}{a^4}(ka^2 - \dot{a}^2) = 8\pi G\rho + \Lambda \quad (2.6)$$

which allows us to solve for  $a(t)$ .

Now we want to relate this equation to measurable quantities in order to obtain an experimental evaluation of  $\Lambda$ . To achieve this, the first thing to do is to relate the expansion rate factor  $a$  to the Hubble constant  $H = \frac{1}{a} \frac{da}{dt} = \frac{\dot{a}}{a}$  and rewrite the Friedman equation as:

$$H^2 = \frac{8\pi G}{3}\rho - \frac{k}{a^2} + \frac{\Lambda}{3} \quad (2.7)$$

Given the actual observed value  $H_0$  of the Hubble constant ( $H_0 = \frac{100\text{km}}{\text{s.Mpc}} \cdot h$  with  $h = 0.71_{-3}^{+4}$  [20]) and defining the measurable critical density of the Universe  $\rho_c = \frac{3H_0^2}{8\pi G} = 1.05369(16) \times 10^{-5} h^2 \text{ GeV cm}^{-3}$ , we can express equation 2.7 in terms of the total cosmological density  $\Omega = \frac{\rho}{\rho_c}$  of the Universe, each term of the equation hence corresponding to a different contribution to  $\Omega$  as:

$$\Omega \equiv \Omega_{\text{matter}} + \Omega_{\Lambda} = 1 + \frac{k}{H_0^2 a^2} \quad (2.8)$$

where  $\Omega_{\Lambda}$  is the cosmological constant contribution defined as  $\Omega_{\Lambda} = \frac{1}{\rho_c} \frac{\Lambda}{8\pi G}$ . By measuring this cosmological density of the Universe we can now confront the cosmological constant with experiment.

The recent measurements of anisotropy of the cosmic microwave background radiation by the WMAP experiment [2] have shown that the value of  $\Omega$  is centered on 1 ( $\Omega = 1.02 \pm 0.02$  at a 95% of confidence level [2]) such that the Universe is flat and  $k = 0$  to a very good approximation. Any contribution to the total energy density of the Universe must then come from matter and from the cosmological constant. The question is then whether experiments can tell us the relative size of each contribution.

To this end, observations of distant supernova provide us with a surprising outcome: the expansion of the Universe is accelerating (inflation). To see how this could be possible, we have to solve Einstein's equation with the Robertson-Walker metric for the diagonal components. Given that the Ricci tensor takes the form:

$$R_i^i = \frac{1}{a^4}(2a^2 + \dot{a}^2 + a\ddot{a})g_i^i \quad (2.9)$$

and that the stress-energy tensor is  $T_i^i = -P$ , we have, using equations 2.1 and 2.5, the acceleration in the expansion of the Universe given by the second Friedman equation:

$$\frac{d^2 a}{dt^2} = -\frac{4\pi G}{3}(\rho + 3P)a + \frac{\Lambda a}{3} \quad (2.10)$$

From this equation we clearly see that if the pressure is negative ( $\rho + 3P < 0$ ), then  $\frac{d^2 a}{dt^2} > 0$  and the Universe will be in inflation, as could be measured with telescopes. An energy density that has such a negative pressure is called Dark Energy. We can see in equation 2.10 that the cosmological constant term corresponds to such a Dark Energy. Because an acceleration has been experimentally observed [4], we expect a non-zero contribution of Dark Energy sources such as the cosmological constant to the total energy density of the Universe. Moreover, if we consider the most precise measurements that could be made on the mass (via the observations of the "clustering of matter"), the acceleration (using supernova) and curvature (from the analysis of the cosmic microwave background) of the Universe, we will be able to determine which cosmological model concerning the composition of the energy density of the Universe is the most viable, according to these observations. Recent data [2, 4] confirm the

model for which the contribution of Dark Energy is:

$$\Omega_\Lambda \simeq \frac{2}{3} \quad (2.11)$$

This means that the energy density of the cosmological constant must be about  $\rho_\Lambda = \rho_c \Omega_\Lambda \simeq 1 \times 10^{-47} \text{ GeV}^4$ .

How can we interpret this small but non-zero cosmological constant? Lorentz invariance tells us that in the vacuum, the energy-momentum tensor must be of the form [21]:

$$\langle T_{\mu\nu} \rangle = \langle \rho \rangle g_{\mu\nu} \quad (2.12)$$

If we put this in the equation 2.1, we find that this vacuum energy density  $\langle \rho \rangle$  has exactly the same behavior as a cosmological constant term. We can then define an effective cosmological constant  $\Lambda_{eff} = \Lambda + 4\pi G \langle \rho \rangle$  which will correspond to the measured Dark Energy.

What is important to retain from this section is that the cosmological constant is a form of Dark Energy which defines the energy density of the vacuum and which contributes to 2/3 of the total energy density of the Universe:  $\rho_\Lambda = v^4$  where  $v \sim 1 \text{ meV}$ .

Let us now state the problem of the cosmological constant.

### 2.1.2 *What is the problem?*

The problem shows up when we compute the contributions of the quantum degrees of freedom of our world to this vacuum energy density. We know that the vacuum is not empty because the Heisenberg principle tells us that a permanent fundamental state of zero energy is forbidden: quantum fluctuations of each quantum field will contribute to the vacuum energy density by an amount that can be computed from  $\rho = \langle 0|H|0 \rangle$  [22]. But the Feynman diagrams that allow us to compute this correlation function correspond to loop diagrams with a superficial divergence of degree 4, which means that the corresponding amplitude is proportional to the fourth power of the cutoff scale  $M$  of the theory describing the known physics, ie  $\rho \sim M^4$ . We see then that the physics manifest at the Weak scale ( $\mathcal{O}(10^3) \text{ GeV}$ ) contributes

an amount  $\rho \sim M_W^4 \sim 10^{12} \text{ GeV}^4$  to the cosmological constant. This estimate is 60 orders of magnitude in error compared to what is actually measured for Dark Energy. To cope with this, we are obliged to consider that the vacuum energy density evaluated from quantum field theory is canceled by a cosmological constant such that the effective cosmological constant  $\Lambda_{eff} = \Lambda + 8\pi G \langle \rho \rangle$  obtains its measured value of  $\sim 10^{-47} \text{ GeV}^4$ . This means a fine tuning of 60 decimal places on the values of  $\langle \rho \rangle$  and  $\Lambda$ . Clearly, there must be a fundamental misunderstanding of the microphysics, ie of the physics that stand at scales higher than what is actually probed in our experiments.

Of course, the fact that we don't understand what we cannot experiment is not surprising. The worse aspect of this problem is that it shows that we have a fundamental misunderstanding of the physics at low energy as well, ie at scales for which we thought that our theories properly describe nature with good precision. In fact, if we integrate out all the degrees of freedom down to the electron mass, we will still have a contribution to the vacuum energy density that is 36 orders of magnitude bigger than what is actually measured. The fact that the most precise and successful theory that we have in physics (the description of the quantum behavior of the electron) yields such a large discrepancy is really worrying. Understanding the value of the cosmological constant is therefore one of the most urging and difficult problems of physics.

### 2.1.3 *How can we solve it?*

What we ought to do is to find a way to cut down the contributions of each quantum oscillator to the effective cosmological constant by using a symmetry or a space property which has slipped one's mind so far. For example, since loop diagrams contribute to vacuum energy density and, because fermion and boson loops have a relative sign difference, if we have a symmetry like supersymmetry which relates each fermionic degree of freedom to a bosonic one (and vice versa), the contributions of these fermions to the vacuum energy density will be canceled by the contribution of their associated boson and the net vacuum energy will be null. However, all such symmetries that can

preserve the cosmological constant from being huge have not been proven so far by experiment and are therefore expected to be broken at scale at least  $M_W \sim \text{TeV}$ , if valid. This means that every degree of freedom lighter than the symmetry breaking scale  $M_W$  will contribute to  $\rho$  by an amount of  $M^4 \gg v^4$ , which is catastrophic (we recall that  $v \sim \text{meV}$ ).

We must then find other ingredients that prevent the various quantum oscillators from contributing to too big a cosmological constant. We can conclude from the last section that a solution to this problem must indeed answer two questions [11]:

1. Why is the vacuum energy small at the microscopic scales  $M \gtrsim 10^3 \text{ GeV}$  where the fundamental theory is couched?
2. Why does it remain small when all scales between  $M$  and  $v \simeq 10^{-12} \text{ GeV}$  are integrated out?

The second problem is the most troubling one because it proves our misunderstanding of low energy physics such as that of the electron. It is also this problem that makes the MSSM (minimal supersymmetric model) not an appropriate solution to the cosmological constant problem (the degrees of freedom integrated out below the SUSY breaking scale, above which stands the fundamental theory, will not be protected from contributing to a huge cosmological constant by this symmetry). Therefore, our strategy will be to first find a way to address the second problem and then to use this solution framework for solving the first one.

## 2.2 *Ingredients needed for a solution*

### 2.2.1 *Large Extra Dimension (LED)*

A hypothesis is usually made in every attempt to find a solution to this second problem but which, as string theory teaches us, we are not obliged to make: the world is 4-dimensional. Changing this hypothesis will turn out to be the key to a solution to the cosmological constant problem. If our description of the Universe involves

compactified (ie closed) extra dimensions that are unreachable to known particles which are thus confined on a (3+1)-dimensional surface called 3-brane (topological object predicted by string theory), then the vacuum energy generated by the quantum fluctuations of the different degrees of freedom trapped on that brane will not be a cosmological constant but will rather be considered as a brane tension [11]. Indeed, this brane tension is an energy density, located at the position of the brane in the extra dimensions, that will satisfy the equation of state of the Dark Energy  $\rho \leq -3P$  as we saw in equation 2.10. It will however be a source of a gravitational field propagating in these extra dimensions, rather than a uniform vacuum energy density spread everywhere in the Universe. Thus instead of contributing to a cosmological constant, all the degrees of freedom integrated out from the scale  $M_C$  where the theory must become 4-dimensional, to infinity, will contribute to a gravitational field in the bulk space [11], as general relativity teaches us (see beginning of section 2.1.1).

In this picture [11, 12, 13], only the degrees of freedom that are lighter than  $M_C$  will be allowed to run in the loops quantum corrections that yield a non-zero vacuum energy density to the Universe. The contribution of brane fields to the cosmological constant can therefore be at most  $\rho \sim M_C^4$ . If the size  $r$  of the extra dimensions is given by  $M_C \sim \frac{1}{r} \sim v$ , the theory will thus predict a value for the cosmological constant which will be consistent with the observed Dark Energy. We will thus have a solution to problem 2 stated earlier, ie we will protect the cosmological constant from becoming big when integrating out energy scales down to  $M_C$ , provided that it is already small at scales  $\gtrsim M_W$ , ie provided that we find an extra dimensional solution with gravity to problem one. Before addressing this problem, let us see how viable our assumptions are.

The first question one has to ask is whether it is possible to have extra dimensions of radius  $r \sim \frac{1}{v} \sim 10 \mu\text{m}$  without running into immediate conflict with experiment. Recent developments in string theory from which the idea of extra dimensions originate indicate that such an issue is possible [5, 14, 26, 27]. In fact, in the braneworld scenario just presented, it is possible to infer the size of a string from the effective

strength of gravitational and electromagnetic interactions in 4D. Since Coulomb's and Newton's laws reflect the spread of flux lines into space, the connection between these effective couplings and the size of a string will depend on the size of the extra dimensions because the force laws fall faster in higher dimensions, having more space to dilute in.

We would like to know if there is a relationship between the size of a string, the size of extra dimensions and the value of the electromagnetism and gravitational effective couplings that is consistent with our requirement for  $r$ . Having such a relation would guarantee the viability of our assumptions. Now, our scenario assumes that the known interactions of particle physics (electromagnetism, weak and strong forces) are confined to a 3-brane such that the usual scalar potential of electromagnetism (that will later be related to the gravitational potential via string coupling in order to reduce the number of non-measured parameters in our evaluation of the effective Newton's constant) applied in 4D and is given by:

$$A_0 \propto \frac{\alpha_{eff} Q}{r} \quad (2.13)$$

where the dependence of  $\alpha_{eff}$  on the coupling  $\lambda$  and the length  $\ell_s$  of a string is for this specific case [26]:

$$\alpha_{eff} = \frac{\lambda \ell_s^{p-3}}{a^{p-3}} \quad (2.14)$$

with  $p$  the dimension of the brane on which the electromagnetic interaction is confined and  $a$  is the size of the extra dimensions. On the other hand, since gravity is free to propagate in the extra dimensions, the gravitational potential will correspond to Newton's potential only when the probed distance is much larger than the size of the extra dimensions. We can therefore possibly have from the  $4 + n$ -dimensional gravitational potential a deviation from Newton's law at scales smaller than about 0.13 mm because it is the smallest distance at which the  $\frac{1}{r^2}$  power law has been tested so far [23]. Applying Gauss' law to a 3-brane embedded in  $n$  extra dimensions hence

allows us to find the gravitational force law for different distance scales:

$$F = \frac{GM_1M_2}{r^{2+n}} \quad \text{for } r < a \quad (2.15)$$

$$F = \frac{G_{eff}M_1M_2}{r^2} \quad \text{for } r > a \quad (2.16)$$

where  $G$  is the fundamental Newton constant related to the fundamental Planck mass  $M_D$  in  $D = 4 + n$  dimensions. If we compare both expressions for  $r \sim a$  we will have a relationship between the two different Newton constants:  $G_{eff} = \frac{G}{a^n}$ . By not being trapped on a  $p$ -dimensional brane, the gravitational interaction will have a coupling constant which will depend on  $\lambda$  and  $\ell_s$  according to the following equation [26]:

$$G = \lambda^2 \ell_s^{n+2} \quad (2.17)$$

Substituting the equation 2.14 with  $p = 3$  in the equation 2.17 will yield the following equation:

$$G_{eff} = \alpha_{eff}^2 \left(\frac{\ell_s}{a}\right)^n \ell_s^2 \quad (2.18)$$

which relates, as we wanted, the length of a string to the number and size of the extra dimensions such that the effective 4D electromagnetic interaction satisfies Coulomb's law and that the effective  $(4+n)$ -dimensional gravitational interaction at large distance scale satisfies Newton's law.

The relation (2.18) does not require  $\ell_s$  to be extremely small, contrary to the case where standard particles are not confined to a brane. So, according to this picture, if the length of a string is of the order of the electroweak distance scale  $\ell_W \sim 10^{-3}$  fm (in the unwarped case [26]), equation 2.18 will predict extra dimensions of radius  $a = 10 \mu\text{m}$  in the case where  $n = 2$ . This means that string theory and the experimental measurements of the effective electromagnetic and gravitational strengths predict that the extra dimensions would be of the size needed to achieve a small cosmological constant, provided that there are two large extra dimensions accessible only to gravity and that the string scale is close to the weak scale, which is absolutely consistent with this picture.

Moreover, this choice of string scale is not arbitrary. In fact, this scale is of the same order of magnitude as the fundamental  $(4 + n)$ -dimensional Planck scale  $M_D$ ,

ie the one at which a consistent and complete theory of quantum gravity is needed (this is not surprising since string theory is the only theory that makes sense of gravity at the quantum level). We know from dimensional analysis that the effective Newton constant at large distance is related to the traditional 4D Planck mass  $M_{Pl}$  according to:  $M_{Pl}^2 \sim G_{eff}^{-1}$ . Anticipating the corresponding relationship (also based on dimensional analysis) between  $M_D$  and  $G$  to be  $M_D^{n+2} \sim G^{-1}$  and using  $G_{eff} = \frac{G}{a^n}$  the following result is obtained:

$$M_{Pl}^2 \sim M_D^{n+2} a^n \quad (2.19)$$

According to this equation, if the number of extra dimensions is 2 and their size is  $r \sim 10 \mu\text{m}$ , we will have a fundamental Planck scale (and so the string scale) of the order of the weak scale, because  $M_{Pl} \sim 10^{19}$  GeV. This means that there is one and only one fundamental scale in nature, the weak scale  $M_W$ , and therefore one of the most critical problems of particle physics (besides the cosmological constant problem), the hierarchy problem [14, 11], is absent<sup>1</sup>. Equation 2.19 thus tells us that the reason why gravity seems incredibly weak from our 4D point of view is that it is radiated in large extra dimensions where it “spends most of its time”. Resolving the hierarchy between  $M_{Pl}$  and  $M_W$  requires that quantum gravity should be manifest immediately above the weak scale and provides the justification for having  $\ell_s \sim \ell_W$  and thus the possibility to solve the cosmological problem, at least the second version of the problem.

In summary, from our knowledge of physics at low energy (4D electromagnetism and Newtonian gravity) and borrowing a few concepts of string theory applied at low energy (3-brane, compactified large extra dimensions), we can explain the weakness of

---

<sup>1</sup>To completely eliminate hierarchy between energy scales, we have to explain why  $r$ , the radius of the extra dimensions, is so big, otherwise we will have a hierarchy in the low energy regime between  $1/r \sim 1$  meV and  $M_W \sim 1$  TeV. In SLED cosmology, this radius  $r$  is a scalar field, which potential and mass values allow a time-dependent dark energy during the present epoch. Understanding what happens shortly after the big bang (ie at high energy) and how the scalar  $r$  field evolves up to the present time could solve completely the hierarchy problem. We can therefore expect such a solution from SLED cosmology. [28]

the gravitational interaction at the particle level by considering only one fundamental energy scale: the weak scale  $M_W$ . More than that, this conceptual framework tells us that, provided there are two and only two extra dimensions (of size  $\mathcal{O}(10 \mu\text{m})$  according to equation 2.19), every degree of freedom tied to our world (3-brane) will contribute to a cosmological constant only below the scale  $M_C \sim \frac{1}{a} \sim \text{meV}$  for which the theory cannot be considered as  $(4+2)$ -dimensional (ie for which the 0-point correlation function will stop to contribute to the brane tension). This provides all the fundamental ingredients for a justified and empirically viable solution to the second version of the cosmological constant problem. Other scenarios of extra dimensions cannot achieve this because they predict a radius  $r$  too small to solve this problem in this way, even if they consider only one fundamental scale: for example, in the 5D Randall-Sundrum scenario [15], the fundamental Planck scale is related to the observed one by the relationship  $M_{Pl} = M_D e^{kr\pi}$  where  $k$  is constrained by  $0.01 < \frac{k}{M_{Pl}} < 0.1$  and  $M_D$  is of the order of 1 TeV, yielding an extremely small  $r$ ! Finally, this solution is valid at the classical level as well as at the quantum level because quantum fluctuation of brane fields will also indistinctly contribute to the brane tension for scales higher than  $M_C$ . However, as we have said, this solution is conditional on the fact that we have solved also problem one using these ingredients, ie that we provide a framework in which the cosmological constant will be small at a scale  $M \gtrsim M_W$ . To find this solution, we will have to add more structure than what has been considered so far in our scenario: we will need supersymmetry.

### 2.2.2 6D Supergravity (SLED)

The large extra dimension scenario proposed above, in which the large vacuum energy of quantum oscillators for scales between  $M$  and  $v$  is a brane tension rather than a cosmological constant, just shifts the problem elsewhere since it leaves two unsolved problems related to problem 1 [11]:

1A: Why is the cosmological constant not big in the two extra dimensions?

1B: Why doesn't this large brane tension unacceptably curve the space from the

point of view of a brane observer<sup>1</sup>?

Let us dwell first on the problem 1A which constitutes a residue of problem 2 and on the solution that it receives. We saw that, in order for such a solution to be valid, we considered that the bulk also has degrees of freedom (gravity), generated by the brane energy. These fields should not contribute to a too large cosmological constant. Moreover, when integrating out the quantum fluctuations of all these modes down to the scale  $v$ , the cosmological constant must remain small. These degrees of freedom are then extremely dangerous because they are not tied to a brane and so their 0-point function will not represent a brane tension [11].

To remove these difficulties we will again use one of the fundamental properties of string theory and apply it to our field-theory-approximate scenario: supersymmetry. At the scale  $M \gtrsim M_W$  where the full theory is exactly 6-dimensional, supersymmetry is not broken by the presence of the brane [11, 12]. As we explained in section 2.1.3, if every bulk gravitational field is part of a superfield, then every bosonic field of this gravitational supermultiplet will have its contribution to the vacuum energy density  $\rho$  canceled by the superpartner fermionic contribution, and the cosmological constant will be small in the bulk. This will also be true of any other multiplets that lives above the scale  $M_W$  such that the cosmological constant will be small for any supersymmetric exact theory that properly describes the physics for  $M \gtrsim M_W$ . The question is then whether supersymmetry, which now ensures a small cosmological constant at scale  $M \gtrsim M_W$ , will help protect this cosmological constant from becoming big when we integrate out bulk quantum degrees of freedom at scale  $M_C$ , corresponding to the measured Dark Energy in our 4D point of view (this is the residue of problem 2). The answer will be yes!

The crucial point of the large extra dimension scenario with supersymmetry in the bulk (SLED) is that the contribution of every bulk quantum degree of freedom to the

---

<sup>1</sup>Recall that in our solution of problem 2, every dimension must appear to be flat at relatively large distance scale compared to  $\frac{1}{M_W}$ , and that measurements of the anisotropy of the cosmic microwave background radiation give evidence of the flatness of our brane

vacuum energy density from the 4D point of view is proportional to the fourth power of the supersymmetry breaking scale in the bulk  $m_{sb}$ , ie  $\rho_{eff} \sim m_{sb}^4$ . The proof of this is beyond the scope of the present work (for more detail see [11, 29]). We can however understand this intuitively: supersymmetry is spontaneously broken if the vacuum is not invariant under a SUSY transformation, ie  $Q|0\rangle \neq 0$  where  $Q$  is the SUSY generator. This implies that  $\langle 0|Q^*Q|0\rangle \neq 0$ . Now, since  $Q^*Q$  is the Hamiltonian,  $\langle 0|Q^*Q|0\rangle$  will correspond to a vacuum energy density which is proportional, when we evaluate the relevant Feynman graphs [39, 30, 47], to the fourth power of the cutoff mass scale  $M$  as explained in 2.1.2, ie  $\langle 0|Q^*Q|0\rangle = \langle 0|H|0\rangle = \rho \sim M^4$ . The vacuum energy density is then precisely the quantity which tells if SUSY is broken or not and at which scale this is achieved. We then have  $\rho \sim m_{sb}^4$ . This sets the scale up to which we can integrate out bulk degrees of freedom that do not contribute to the vacuum energy density because bosonic and fermionic contributions cancel each other. Note that this is fundamental to the SLED scenario because it is the interaction terms that involve fields from Supergravity that naturally give non-zero vacuum energy [1, 30].

Now that we know that supersymmetry can control the contribution of bulk modes to a 4D effective cosmological constant through its symmetry breaking scale, let us find out the order of magnitude of  $m_{sb}$ . Here again supergravity (SUGRA) has a critical role to play because it ensures that  $m_{sb} \sim v \sim \frac{1}{a}$  [11]. In fact, it is the coupling of SUGRA bulk particles to particles on the brane that generates this supersymmetry breaking in the bulk. We thus expect  $m_{sb} \sim GM^2$ , where  $M$  is the energy scale of gravity and  $G$  is the value of the coupling of these bulk modes to the brane particles. Since this coupling is of gravitational strength from the 4D point of view, ie  $G = \frac{1}{M_{Pl}}$ , and since  $M$  is close to the weak scale for two extra dimensions of about 10 microns, we then have that SLED implies  $m_{sb} \sim \frac{M_W^2}{M_{Pl}} \sim \frac{1}{r} \sim v$ . This corresponds to the SUSY breaking mass splitting between graviton and gravitino [11]. This supersymmetry in the bulk gravity sector provides precisely the correct order of magnitude to account for the Dark Energy density as it appears in our recent observations. Our scenario

seems thus to be a suitable framework for a solution to the cosmological constant problem. However, before concluding that it is indeed the case, we still have to solve with this framework, problem 1B. This will allow us to add a last ingredient in our scenario: the minimal bulk spectrum.

Problem 1B will be solved, ie the brane tension will not curve in the extra dimensions at large distance scale  $r > \frac{1}{M_W}$ , if a cancellation occurs between the brane tension and the contribution of this tension to the curvature of the space in the bulk. This is what we call a self-tuning solution to the cosmological constant problem [11]. Let us see how such a cancellation is possible.

We recall that the classical and quantum brane modes contribute to the brane tension at all scales down to  $M_C$ , at which the degrees of freedom that will not be integrated out will contribute to the cosmological constant. This brane tension is then, from the 4D point of view, an effect of large distances (at small distances we see explicitly each mode in a 6D action and not a tension  $T$ ). Therefore, we must compute the contribution of bulk modes (generated by the energy of the brane) to the effective bulk curvature, as seen by a 4D observer at large distances, and hope that these two quantities will cancel. For this, we must first integrate out every bulk degree of freedom at small distance scales. We already did that for the quantum fluctuations of bulk fields and found that they were contributing to the cosmological constant for energy scales smaller than  $m_{sb}$  and not for higher energy scales (bosonic contributions to  $\rho$  cancel the fermionic ones). Thus, in order to compute the curvature in the bulk we must work only with bulk classical degrees of freedom. From the 4D point of view at large distance, the small distance degrees of freedom are eliminated by substituting their equation of motion in the action and by integrating on the two extra dimensions.

In reference [11], it is argued that the knowledge of the exact form of the action is not required for this self-tuned solution. This is because Lorentz invariance ensures that the solution to the 4D equation of motion of the Kaluza-Klein (KK) modes<sup>1</sup> of

---

<sup>1</sup>KK modes are 4D states corresponding to the bulk degrees of freedom as seen by a 4D observer, ie to the eigen-modes of the bulk momentum components  $P_y$ , quantized because the extra dimensions

every bulk field, except the effective 4D flat metric and 4D scalar, is the zero solution. Substituting 0 in the action is equivalent to not including these terms. Adopting the large distance 4D point of view, we don't need to know explicitly the action, but only to include the 4D metric (term describing gravitons) and scalars. Where these scalars come from in the 6D SUGRA is model-dependent. What is important is that such scalars come from the bosonic sector of the bulk supermultiplet and that bulk bosonic fields are sufficient for constructing a self-tuned framework like SLED.

Now, if we consider the most general minimal 6D SUGRA (ie with N=2 Supersymmetry which includes both a metric and a scalar), it can be shown that the two-dimensional Ricci scalar  $R_2$  that describes the curvature of the two extra dimensions due to localized energy sources (brane tension) is [11]:

$$R_2 = \frac{-2}{\sqrt{\det g_{mn}}} \sum_i T_i \delta^2(y - y_i) + \dots \quad (2.20)$$

where  $y_i$  is the position of the brane  $i$  in the extra dimensions (depending on the model, our brane could be one specific brane among many others) and where the ellipse (...) denotes any smooth contribution to  $R_2$  at the position of our brane. in contrast with the main term of equation eq. 2.20 which describe a conical singularity in the curvature at the position of that brane.

Now if we compute the contribution of the tension of our brane to the vacuum energy density at large distance from the 4D point of view (first term of eq 2.21) and add to this the contribution of the curvature in the bulk space (second term of eq 2.21) we will have [11]:

$$\rho_{class.} = \sum_i T_i + \int_M d^2y \sqrt{\det g_{mn}} \left[ \frac{1}{2} R_2 + \dots \right] \quad (2.21)$$

where  $M$  denotes here the internal two-dimensional bulk manifold on which we integrate the extra dimensions and where the ellipse represents all other terms beside the Einstein-Hilbert term in the supersymmetric bulk action. We clearly see in this expression that if we substitute equation 2.20 into equation 2.21, then the first term are compactified. We will show this formally in chapter 3.

describing the brane tension contribution will be canceled by the singular part of the curvature  $R_2$  in the extra dimensions. More than that, references [11, 31] argue that all the other terms will exactly cancel if there are bulk scalars that are smooth at the position of the 3-brane. Finally, this cancellation will not depend upon the particular value of the brane tension, and this self-tuned solution will still be correct if we consider brane quantum degrees of freedom, as expected. We then see that our SLED scenario for which the bulk space is populated by the fields of an extended  $N=2$  supergravity theory (remember that bulk scalars have a role to play in the self-tuning of the solution) will provide the needed cancellation between brane tension and the curvature it generates in the bulk in order to achieve a small cosmological constant without conflict with our low energy experiments. The mechanism of such a cancellation is fairly general and does not need equations of 6D SUGRA to be solved explicitly.

To summarize this section, we have seen that the SLED scenario offers all the necessary and sufficient conditions required for a theoretically and experimentally viable solution to the cosmological constant. These conditions are: exactly two large extra dimensions of about 10 microns in which gravitons and their “extended” superpartners (which will be properly described at the scale  $M \gtrsim M_W$  where they live) propagate. The Standard Model particles are confined to a 3-brane. Consequently:

1. brane degrees of freedom will not contribute to the cosmological constant at energy scales higher than  $v \sim 10^{-12}$  GeV;
2. the brane tension at which these modes contribute will be exactly canceled by the extra dimensional curvature that this tension creates;
3. the bulk degrees of freedom will not contribute to a cosmological constant at the scales  $M \gtrsim M_W$  (because of SUSY);
4. quantum fluctuation of every possible field will at most contribute to the cosmological constant by a factor  $\rho \sim m_{sb}^4$  where  $m_{sb}$  is the supersymmetry breaking scale of size  $m_{sb} \sim \frac{1}{r}$ .

It is thus possible to build from this scenario theoretical models beyond the Standard Model of particle physics that possess the virtue of this SM theory but which eliminate the worrying problem of an excessive contribution of Standard Model particles, even as light as the electrons, to the vacuum energy density, and which predict a value for the cosmological constant that is in agreement with recent Dark Energy evaluations. Furthermore, this is of real scientific value since it will be possible to test the SLED scenario in a near future at the LHC. Models built from this scenario will also have a rich phenomenology, while solving the hierarchy problem and proposing a completely new way in which supersymmetry could be realized. This, together with the solution proposed to the cosmological constant, will provide a fundamental and strong motivation for any research carried in this context.

Let us now summarize the fundamental predictions of the SLED scenario, which will justify spending a serious research effort on this subject.

## 2.3 *Consequences of SLED*

The fact that SLED offers the possibility to solve the cosmological constant problem, is, in itself, enough to justify to devote a large amount of work to SLED studies. However, we want to stress in this section that the SLED scenario is also strongly motivated by the fact that it is predicted by a more fundamental theory, that it provides testable phenomenological predictions, and that it provides a new way in which supersymmetry is realized.

### 2.3.1 *String inspired*

As was stated in the introduction, one of the principal motivations for the supersymmetric Standard Model comes from the plausibility that it arises as the low-energy limit of a well-motivated, more fundamental theory at higher energies. What is probably our best-motivated fundamental supersymmetric theory is the string theory. In fact, this theory, the only one that we have which succeeds in making sense of quantum gravity, needs supersymmetry in its fundamental structure. The question is then

if the SLED scenario can consistently be considered as a low-energy approximation of this well-motivated fundamental string theory. At first sight, it seems indeed plausible that the answer to this question is yes, since all along in our construction of this scenario we drew concepts from string theory that we applied consistently at low energy. However, to achieve a successful embedding of SLED into string theory, we have to identify the string vacuum for which low-energy excitations describe both 6D supergravity of the bulk and the degrees of freedom trapped on the branes [12]. There are two fundamental difficulties with this. First, there are too many vacua consistent with the requirements of string theory and they predict typically too many degrees of freedom in the low-energy approximation of the theory. The question will be whether it's possible to find such a vacuum or not. However, these problems affect also the supersymmetric Standard Model (MSSM). The challenge is then similar for SLED and for MSSM. A solution will have to specify how the other 4 small extra dimensions (remember that strings are 10-dimensional objects) will be compactified and how the branes will arise within string theory. Although a complete construction has not yet been accomplished and is certainly far beyond the scope of the present work, it is worth mentioning that there are good prospects coming from Type IIA and Type IIB string theory [12, 13]. This puts SLED and MSSM on an equal footing for the question of their fundamental origin. To the same extent that MSSM is recognized as being theoretically motivated by string theory, so it must also be the case for the SLED scenario.

### 2.3.2 *Phenomenology*

We have seen that the inspiration for the SLED solution to the cosmological constant problem comes from the superstring theory: brane, extra dimensions, supersymmetry and quantum gravity. However, little interest has been given, so far, on string theory by experimental particle physicists because of the lack of testable predictions that could be made from this theory. SLED does not suffer from these empirical difficulties. It applies at a low energy scale and provides a rich set of phenomenological possibilities. Moreover, the gravity scale has been fixed at  $O(10 \text{ TeV})$ , close to

the expected range of the LHC. Thus, the SLED scenario clearly provides exciting possibilities for experimental testing.

It is important to study these phenomenological consequences of SLED, not only to decide if this proposal has some truth in it, but also, if we adopt the point of view of experimentalists, to offer different elements of understanding for certain generic signals observed in future experiments (for example, the origin of missing  $\cancel{E}_T$ ). This is important, even if SLED should be experimentally non-viable, because some of its general features can still be true. Therefore, besides the fact that this scenario is well motivated and apparently robust, its phenomenological implications are interesting in themselves. Let us summarize now the rich phenomenological implications provided by this proposal.

### Signature at colliders:

The most direct evidence for such new physics will come from high energy colliders. The main signature of SLED will be an excess of events with large missing transverse energy. This signature is a consequence of any LED scenario, as has been shown in previous work [6, 7, 8, 9, 10, 33]. From a 4D point of view, bulk particles will appear as towers of Kaluza-Klein modes<sup>1</sup> whose coupling to ordinary particles is very small (gravitational strength), but with such a huge phase space factor at TeV energies that the cross section becomes large enough to provide an observable signal [6]. The signal of bulk particles escaping into the extra dimensions will thus be a large amount of missing transverse energy in the detector. (The conservation of momentum in the extra dimensions is ensured by the brane recoil). This will constitute the principal signal for LED scenarios, but SLED has additional degrees of freedom since it postulates the existence of superpartners of the graviton and of the other bulk fields. The signal will then be stronger than for LED, and will allow a non-ambiguous test of the models at colliders.

Moreover, if collider energies come close to the 6D gravitational scale, it will be

---

<sup>1</sup>see chap. 3

possible to produce and detect reactions resembling strings collisions near the Planck energies (in the case of unwarped extra dimensions) [34], as well as mini black holes with horizon radius  $r_H < r$ . These will decay mainly by Hawking radiation, providing striking signatures in the detector [9, 35]. These two types of phenomena would be abundant and spectacular at the LHC.

The study of the production of one type of SLED KK states will be the subject of this thesis. We will come to this in the next chapter. For now, let us give a quick overview of other possible phenomenological implications of SLED, not directly by colliders.

### Cosmology:

Because it provides an explanation for the observed Dark Energy density  $\rho$ , SLED, like the MSSM, is intrinsically related to cosmology. But it makes many other predictions for Dark Energy. Perhaps the most important one (after  $\rho$ ) is that it predicts a dynamically evolving Dark Energy that must not be seen as a cosmological constant in time but rather as quintessence, due to a cosmologically evolving 4D scalar field [12, 28]. SLED in fact predicts a very specific form for the quintessence field scalar potential, and therefore specific predictions on Dark Energy evolution. This has an influence on our understanding of inflation but the topic is beyond the scope of this work. Ref. [12, 28] argues that a viable cosmology can be built using extremely light scalars that happen to be naturally stable against quantum effects in the SLED (radion of  $m \sim 10^{-33}$  eV) and for which the couplings evolve over cosmological time scale, satisfying all current bounds on long range scalar-mediated force.

### Dark Matter:

The fact that SLED differs completely from MSSM in the way in which supersymmetry is realized (more on this later), obliges us to rethink the Dark Matter paradigm. However, the standard particle physics picture of Dark Matter will not be invalidated by SLED since it has been argued ([12]) that the usual WIMP (Weakly Interacting

Massive Particles) proposal (a stable particle with weak scale mass and weak strength coupling) can naturally have the correct present-day abundance in SLED. A specific model for a promising WIMP candidate from SLED is not yet available although it is a generic prediction. We can reasonably think that more research in SLED will provide a definite model for the WIMP, adding a testable prediction to the already exciting set of SLED phenomena.

### Tests of Gravity:

There are two types of changes to gravitational physics which must follow any variant of the SLED proposal [12]. These involve tests of Newton's inverse-square law at small distance as well as very-long distance modifications to gravity over scales up to the present-day Hubble length  $H_0^{-1}$ . Concerning the short distance scales, we saw in equation 2.15 that for distances smaller than the radius of the extra dimensions, we must expect deviations from Newton's inverse-square law. In the case of the SLED scenario, where there are two extra dimensions, we therefore expect a gravitational force acting as  $\frac{1}{r^4}$ . For small  $r$  of  $\mathcal{O}(10\mu\text{m})$  as is the case in SLED, this force will be stronger than what is expected from the  $\frac{1}{r^2}$  Newton's law. The range at which present searches for this effect is sensitive is unfortunately just at the upper limit of the distance scale at which we expect an effect [23]. However there are hopes for future tests based on precision measurements of the Casimir effect [12]. Moreover, SLED cannot evade the micron scale at which we necessarily expect an effect. So, we will soon be able to conclude definitively if SLED is empirically viable or not.

Concerning the very-long distance modifications to gravity, the extremely light scalars predicted by SLED leading to Dark Energy evolution can have small enough couplings at the present cosmological time to be compatible with known cosmology. They can, however, be probed by solar-system tests as well as in more exotic settings like the recently-discovered system consisting of two pulsars which orbit one another [12].

### 2.3.3 *New SUSY realization*

As was already explained in the introduction and in the subsection 2.3.1 the combination of good theoretical motivations and of distinctive experimental signatures has brought theorists, phenomenologists, experimentalists and even cosmologists to devote a great deal of effort on exploring the implications of supersymmetry over the last few years. What has been argued so far is that theoretical motivations and phenomenological implications of the SLED scenario are potentially as important as those of the Supersymmetric Standard Model. There is however another reason why it is fundamental to compare both theoretical frameworks: the SLED proposal offers a radically different way in which supersymmetry could be realized at low energies.

In the MSSM, supersymmetry is broken at the weak scale ( $\mathcal{O}(\text{TeV})$ ) by the inclusion of soft symmetry breaking terms in the 4D action. These are terms with coefficient having a positive dimension (of mass) which don't change anything substantial about the ultraviolet behavior of the amplitudes (super-renormalizable terms). For instance, the cancellation of the quadratic divergences to the Higgs mass is still guaranteed to hold, even after having added the soft SUSY terms. This kind of supersymmetry breaking should be thought of as a complete analogue to the Higgs breaking of the electroweak symmetry. Therefore, as is the case in SM electroweak theory, we expect that the resulting superpartners will have mass splitting much smaller than the SUSY breaking scale. The superpartners of our Standard Model fields should then be observable at upcoming experiments (LHC).

On the other hand, in the SLED scenario, supersymmetry, which is a 6D symmetry, is broken at the TeV scale because it must explicitly include the brane (which does not have supersymmetric counterpart) in the action. The mass splitting between ordinary particles and their superpartners must therefore be of the order of a few TeV, and there are no deviations from the Standard Model spectrum at low-energy, in contrast with the MSSM. However, as we have seen in section 2.2.2, the supersymmetry breaking scale in the bulk is extremely small, such that bulk particles forming a 6D supermultiplet are expected to interact with brane modes at scales

lower than  $\sim \text{TeV}$ . As such, SLED provides a counterexample to the statement that supersymmetric Standard Model is the sole low-energy manifestation of TeV-scale supersymmetry breaking [12].

Besides the fact that both scenarios are very well-motivated by string theory and that they predict testable phenomenologies, they also both address the hierarchy problem, although in a different way. As we saw in section 2.2.1, the SLED scenario solves this problem by considering that the natural scale for Dark Energy is the only fundamental scale of Nature, the difference between the weak scale and the 4D Planck scale being due to an effect of the large extra dimensions. The key claim of SLED is then that this remains true even when we consider loop corrections [11]. The MSSM cannot explain why the force of gravity should be weak compared with the electroweak force at low-energy scale, but it nevertheless provides a way to understand the natural stability of the weak scale against loop corrections, as is the case in SLED.

Many theoreticians object that Large Extra Dimensions scenarios are not a true solution to this hierarchy problem because they substitute the hierarchy of mass scale by a fine tuning of distance scale. This criticism is less pertinent to SLED because the theory constrains the compactification radii and number of extra dimensions not only to solve the hierarchy problem, but also to be consistent with observation of Dark Energy. The smallness of the cosmological constant would therefore be considered as an indication for the similarity between the gravity and the weak scales.

Finally that the SLED scenario does not offer a natural explanation for the apparent coupling unification at the GUT scale, which is considered as the triumph of the MSSM. However, SLED can allow for a small thickness ( $\text{TeV}^{-1}$ ) of the brane, which would then predict unification of the running gauge couplings at a scale much lower than the SM GUT scale, in a way which can have testable effects in colliders. This will be the subject of chapters 6 and 7. We will come back later on these issues. For now, let us see briefly what is at stake in building of explicit model within this scenario.

## 2.4 Present state research on an explicit SLED model

Using a top-down approach, having found one way to solve the cosmological constant problem, it is now important to construct concrete models in the SLED framework from which precise physical predictions can be made. Our ignorance of the physics beyond  $\sim 200$  GeV means that details of the theory (compactification form of the extra dimensions, exact mechanism of how SUSY is broken, complete spectrum in the bulk and on other branes, etc) must be described by a model rather than by an exact and complete theory. We will, in this section, discuss a model example and present difficulties not yet solved. This will give a general overview of the present state of research on this subject and about what has still to be done.

### 2.4.1 Salam-Sezgin model

The first thing an explicit model of SLED will have to achieve is to generate the classical cancellation between the huge brane tension and the curvature in the extra dimensions as explained on a general basis in subsection 2.2.2. Of course, such a model will have to specify the brane, bulk and brane-bulk interaction actions. It will also have to consider a specific way by which the extra dimensions will be compactified. Ref [13] argues that such a self-tuning solution to the cosmological constant problem is possible within a specific version of Salam-Sezgin model. This is a complete model of  $N=2$ , 6D supergravity compactified on a sphere with a brane localized at each pole of the sphere, with magnetic monopole background and with Yang-Mills and matter couplings. Without going in details (which is beyond the scope of the present thesis, see however [13, 36]), it must be said that the field content of the theory consists of a supergravity-tensor multiplet<sup>1</sup> coupled to a  $U(1)$  gauge multiplet (containing gauge potentials  $A_M$  and gauginos  $\lambda^i$ ) and  $n_H$  hypermultiplets (with scalars  $\Phi^a$  and fermions  $\Psi^{\hat{a}}$ ). From this spectrum, the bosonic part of the classical 6D supergravity Lagrangian, that will provide the needed self-tuned solution of the

<sup>1</sup>which contains a metric  $g_{MN}$ , an antisymmetric Kalb-Ramond field  $B_{MN}$ , a dilaton  $\varphi$  (scalar field which appears in Kaluza-Klein theory as the component  $g_{55}$  of the metric tensor), a gravitino  $\psi_M^i$  and a dilatino  $\chi^i$  (fermions)

cosmological constant problem, is:

$$e_g^{-1} \mathcal{L}_B = -\frac{1}{2}R - \frac{1}{2}\partial_M \varphi \partial^M \varphi - \frac{1}{2}G_{ab}(\Phi) D_M \Phi^a D^M \Phi^b - \frac{1}{12}e^{-2\varphi} G_{MNP} G^{MNP} - \frac{1}{4}e^{-\varphi} F_{MN}^\alpha F_\alpha^{MN} - e^{-\varphi} \nu(\Phi) \quad (2.22)$$

and the brane action giving the coupling of a 3-brane to the bulk fields is:

$$S_b = -T \int d^4x e^{\lambda\varphi} (-\det g_{MN} \partial_\mu x^M \partial_\nu x^N)^{1/2} \quad (2.23)$$

where the index  $\alpha = 1, \dots, \dim(\mathbf{G})$  runs over the gauge-group generators,  $e_g = |\det e_M^A| = \sqrt{-\det g_{MN}}$ ,  $T$  is the brane tension,  $G_{MNP} = \partial_M B_{NP} + F_{MN} A_P + (\text{cyclic permutations})$ ,  $F_{MN}$  is the usual Abelian gauge field strength,  $G_{ab}(\Phi)$  is the metric on the Kähler manifold,  $D_M$  are gauge and Kähler covariant derivatives and units has been chosen such that 6D Planck mass is unity ( $\kappa_6^2 = 8\pi G_6 = 1$ ). The details about Kähler covariant derivatives and manifold are not important for our purpose. In fact, we just need the spectrum in order to justify, in chapter 2, the couplings that we will consider in our low-energy 4D SLED theory. A complete description of this model, including discussions on the transformation of each field under supersymmetry, the fermionic part of the action, the anomaly cancellation, the compactification on a sphere and the 4D formulation of the theory is provided in ref [11, 13]. What is important here is that contributions of the bosonic bulk and brane actions to the vacuum energy with few conditions (flat metric, constant scalar fields, equal tension on each brane and no brane-dilaton coupling ( $\lambda = 0$ ) [11, 13]) will explicitly provide the cancellation between brane tension and bulk space curvature explained in 2.2.2, therefore demonstrating that there are indeed models that can achieve this particular feature of SLED scenario.

However, although the Salam-Sezgin model is a good and simple (for theoreticians!) model predicting a self-tuned solution to the cosmological constant problem (thus escaping from the Weinberg's No Go Theorem [21, 11, 13]), it cannot be retained as a good candidate for an explicit SLED model. This is because this model has

anomalies that must be canceled by introducing chiral supermultiplets in the bulk spectrum, increasing significantly the bulk gravity-mediated degrees of freedom, to an extent that is in conflict with astronomical bounds (we will come to these bounds later in this section). A good specific SLED model will then have to have a bosonic behavior similar to the Salam-Sezgin model one, but which leads towards a non-chiral, ungauged version of 6D supergravity. Such a model still has to be constructed. There are also few more difficulties that an explicit SLED model will have to face. Let us stop briefly on the most important ones (as stated in [11]).

### 2.4.2 Other possible quantum effects

We argued earlier, in section 2.2.2, that one of the central issues of the SLED scenario is that its estimate of the contribution of the bulk quantum degrees of freedom to the vacuum energy density is  $\rho \sim m_{sb}^4$ . Is this all the story? Power-counting arguments will tell us no!

In fact, the key feature of SLED is that interactions must be considered local in 6 dimensions at all scales down to the observed cosmological constant  $v = 10^{-12}$  GeV. Above this scale, the *effective action*<sup>1</sup> of the theory will thus take the schematic form of typical six-dimensional interactions:

$$S_{eff} = \int d^6x \sqrt{-g_6} [c_0 M^6 + c_1 M^4 R + c_2 M^2 R^2 + c_3 \log(M/\mu) R^3 + \dots] \quad (2.24)$$

where  $R$  is the 6D curvature scalar,  $c_i$  are dimensionless and arbitrary coupling constants,  $M$  is the scale where the theory lives,  $\mu$  is the scale at which the effective approximation is produced and the ellipse (...) stands for other terms suppressed in  $M$ . Now, if we evaluate the integral over the extra dimensions, we obtain a factor proportional to the volume  $r^2$  of these extra dimensions, and if we evaluate this action for the SLED vacuum configuration, we will have to make the substitution  $R \sim 1/r^2$ . The ultraviolet-sensitive terms in the effective 4D scalar potential for  $r$  will therefore be given by:

<sup>1</sup>an explicit example of an effective interaction is given in section 3.1.2

$$\delta V_{eff} = c_0 M^6 r^2 + c_1 M^4 + c_2 M^2 / r^2 + c_3 \log(M/\mu) / r^4 + \dots \quad (2.25)$$

Since  $m_{sb} \sim 1/r^4$ , we clearly see in the potential 2.25 that the first three terms are not of the form  $m_{sb}^4$  and could thus potentially yield too big contributions of bulk quantum degrees of freedom to the vacuum energy density. Note however that the terms of order  $M^6$  are excluded because supersymmetry forbids a bare cosmological constant in 6 dimensions (therefore enforcing  $c_0 = 0$ ) [11] and that the terms of order  $M^4$  correspond to the classical supergravity action which has been shown to be canceled by the brane tension. The only worrying terms are therefore those of the order  $M^2 m_{sb}^2$ .

It can however be argued ([11, 12, 13]) that within the SLED proposal the only dangerous bulk-loop contributions to the cosmological constant arise at one loop, making their vanishing easier to arrange than the complete N-loops contributions. This result is related to the small size predicted for the dilaton field, showing that the explicit model used as a self-tuning solution to the cosmological constant has also a role to play on the contribution to the vacuum energy at the quantum level. This ensures that the spectrum considered is fundamental and that the need for N=2 supergravity is essential to the SLED picture. However, to obtain an explicit solution in the SLED framework one has to find a model in which 1-loop contributions of order  $M^2 m_{sb}^2$  will vanish. Work is still underway on that subject.

### 2.4.3 *Hidden fine tuning*

An explicit model of the SLED scenario will have to achieve the self-tuning and the quantum cancellation needed for a solution to the cosmological constant problem without any fine-tuning argument. We saw earlier that it is possible in the SLED proposal to write down an explicit self-tuned solution to the bulk equations of motions which includes the gravitational effects of the brane. This was the Salam-Sezgin model (its bosonic part). In this concrete example, the solution included two branes located at poles of a sphere. However, the tension of the these branes was required

to be positive and precisely equal. This thus seems to be a hidden fine-tuning of the parameters of the specific theory. Is it a worry for our SLED proposal? Since we don't expect to know what the physics at the micro-scale  $M$  is, the answer will be no, provided that a specific constraint on the tensions imposed in the short distance theory remains imposed as we renormalize down to long distance. In that case, the explicit form of a good SLED model will be deferred until we get a better understanding of the physics at the energy  $M$ . Ref [11] argues that constraints like the equality of the tensions should indeed be stable against integrating out the scales between  $M$  and  $1/r$ . In brief, their argument is that all the degrees of freedom that are integrated out at the scale  $1/r$  are of very short wavelength compared to the size  $r$  of the extra dimensions in the SLED scenario, even for the electron since  $r \sim 10 \mu\text{m}$ . These degrees of freedom must thus be considered as local operators such that those which propagate in the bulk will be too localized to completely cross the internal space. They will thus be blind to topological effects and will then have no influence on the topological constraints imposed at the scale  $M$ . The SLED proposal is therefore preserved from fine-tuning. However, much work has still to be done on the understanding of this physics at high energy scales before we can obtain explicit examples of models within the SLED framework that are free of any fine-tuning.

#### 2.4.4 *Astrophysical bounds*

We have seen that in order to yield a solution to the cosmological constant problem, the SLED scenario predicts very restrictive range of values allowable for the size  $r$  of the extra dimensions. In fact, an order of magnitude smaller for  $r$  would destroy the explanation of the observed Dark Energy. This strong falsificability of the scenario assures that experimental tests would be decisive. This contributes to the scientific power of the theory. However, it is now well-known, since the first LED proposals, that astrophysics already put bounds on the possible values of  $r$  [24, 25]. The question is then to see if these bounds already rule out the SLED scenario.

The strongest limit on the size of two large extra dimensions comes from the requirement that emission of Kaluza Klein modes must not provide a too efficient

energy-loss mechanism for supernova cooling [12, 25]. This process has been studied in detail for the special case of the radiation of gravitons into the bulk and has yielded a limit of  $M_D > 8.9$  TeV, where  $M_D$  is the gravitational scale. However, in the SLED scenario we expect many more gravitational degrees of freedom in the bulk, therefore increasing the current limit on  $M_D$  by a factor depending on the number of bulk modes. Following ref [12] we can evaluate the SLED bound on  $M_D$  to be:

$$M_D > \left( \frac{32 + 16N_g + 8N_m}{9} \right)^{1/4} 8.9\text{TeV} \quad (2.26)$$

where  $N_g$  and  $N_m$  count the number of gauge and matter multiplets in the bulk. This formula has been obtained by counting the number of spin states for each field in the typical N=2 gauge or matter supermultiplets. In the Salam-Sezgin model the number of matter and gauge multiplets required for anomaly cancellation are related by the condition  $N_m = N_g + 244$ , and therefore even if  $N_g = 0$ , we will have  $M_D > 34$  TeV and so  $r < 0.67 \mu\text{m}$ , which is too small to properly describe the observed Dark Energy. This is why it is expected [12] that ungauged solutions with no chiral matter multiplet could provide good explicit models for the SLED scenario.

Other astrophysical bounds that increase the limit on  $M_D$  were considered in LED proposals. The non-observance of Kaluza Klein modes decaying into photons after having been produced in supernova or in early Universe is one such example. However, all these bounds are completely model-dependent and models can be built where they will not be considered as important limits. This will be the case if, for example, the KK modes decay into light modes on other branes. Of course this argument is a kind of evasion, but “it is worth the cost if the resulting theory can make progress on the much more difficult cosmological constant problem” ([12]). This indicates again that a good knowledge of the microphysics is needed in order to achieve a complete explicit model within the SLED framework.

\*\*\*

We have just seen that few problems are still to be solved before building a concrete model in the SLED framework. These difficulties are all related to the fact that

some important ingredients are missing on our understanding of the physics at and above the TEV scale. This is, after all, why the LHC is being built. These difficulties, in their present state, do not put into question the general SLED proposal but only to its specific realizations in an explicit model. The fact that SLED explains why the electron and other known physics don't contribute too much to the cosmological constant is an enormous improvement in our understanding of nature which should eclipse the few difficulties in building explicit models. Whether or not this point of view on these problems is too optimistic for the SLED realization of a solution to the cosmological constant problem is to be seen in the near future. Our interests in this proposal is for its low energy phenomenology. For this reason we won't be concerned by the physics at the microscopic scales, and a general effective theory (which approximate the exact microscopic theory) including all the fundamental features stressed in section 2.2 will provide all the relevant physical predictions that could be made at this scale. This is what concerns this thesis.

## 2.5 *Conclusion on this chapter*

This chapter has presented the SLED scenario which constitutes the theoretical framework and the fundamental motivation for the physics analysis that will be presented in the following chapters. What is important to remember from this proposal is that it provides all the fundamental ingredients necessary and sufficient to solve the cosmological constant problem. More than that, it offers a radically new way by which supersymmetry can be realized at low-energy. The rich phenomenological implications of this proposal are all likely to be decisively tested (and possibly ruled out) in the next few years. This falsifiability thus ensures a strong scientific value to this scenario. Finally, we saw that even if we don't have a concrete SLED model so far, it is sufficient and justified for collider phenomenology to write down a low-energy effective field theory that contains every fundamental generic feature of the SLED scenario and to use it for physical predictions. This ensures that our work will be relevant, highly motivated and original.

In the following, we will write down the most general low-energy Lagrangian that couples the Standard Model brane fields to the effective bulk fields from the 4D point of view and develop the physical predictions for the case of two large extra dimensions. Although there is a huge number of bulk fields that can appear close to the TeV scale in 4D experiments, we will concentrate our analysis on only one type of these degrees of freedom, one that has been fundamental in the development of our SLED scenario (in particular when we talked about the cancellation of the brane tension with the bulk curvature): scalar particles. In the next chapter we will see what these scalars could be, how they could generically couple to Standard Model particles and what the predictions on particle physics observables are. In particular we will identify how the production of such a scalar at the LHC can compete with the prediction for graviton production, therefore providing a clear signal of the SLED rather than simply the LED scenario (along with what has been said in section 2.3.2). This will be followed by a specific experimental analysis at ATLAS.

### *3.1 Low-Energy bulk scalar coupling*

In this chapter we will show how bulk scalars can emerge from SLED scenario and how they can couple to Standard Model particles. The aim of the first section is thus to derive an effective Lagrangian (ie a Lagrangian that describes the physics at colliders energies and which constitutes a low energy approximation of a theory valid in a broader context (we will be more explicit about effective theory in section 3.1.2)) from which all our physical predictions will be made. Again, we do not intend to provide a detailed and complete explanation of how scalars emerge from a N=2 6D supergravity and how they couple to brane particles, but only to give an insight on the concepts and mechanisms involved in such a demonstration. This is sufficient since the low-energy effective approximation which will be used for our physical predictions will be blind to the specific details of any higher-energy model. A much more complicated but accurate explanation could be found in [13].

#### *3.1.1 Four-dimensional extended SUSY*

For the purpose of studying the phenomenology of SLED, in particular the direct production of bulk scalars in colliders, we need to identify the effective 4D theory which governs this physics at the LHC energy scale. It is thus natural to adopt a 4D point of view in our effective theory emerging from the SLED scenario. Now, in order to solve the cosmological constant problem, we have seen in chapter 1 that SLED theory involves a supersymmetric gravitational sector in 6 dimensions. From the four-

dimensional perspective, this means that the graviton supermultiplet is necessarily a representation of an extended supersymmetry. It will thus be suitable for us to identify our bulk scalar states from this four-dimensional extended SUSY.

Note that we are not saying here that there are supersymmetries in the usual 4D space (ie on the 3-brane). On the contrary, as we explained in section 2.3.3, in the SLED scenario supersymmetry is badly broken on our brane, and we don't expect at collider energies to see the superpartners of ordinary particles. What we really mean by "four-dimensional extended SUSY" is that bulk SUSY appears differently from our brane point of view than from the six-dimensional one. Bulk particles which are part of the 6D graviton supermultiplet will thus appear to a 4D observer as the members of an extended graviton supermultiplet. In this respect, it must be noted that our interest, here, is with genuine bulk scalars, and not bulk modes that *appear* as scalars in our 4D perspective. The first case necessarily implies supersymmetry in the bulk (since bulk scalars are superpartners of the graviton) while the second case does not require this symmetry. For example, 4D scalars (graviscalars) can arise as components of the higher-dimensional metric. Although many of the results that will be obtained in the next chapters can also apply to such states, we will not focus on the study of their properties because they don't provide a test of the SLED scenario. According to [32], the production rate of the Kaluza-Klein modes of such graviscalar particles is much less important than its spin-2 counterpart in most processes. Between the two types of scalars that can be seen by a 4D observer it is therefore the production of a bulk scalar that will be expected to compete with graviton production, justifying our concentration on such a particle.

Also note that we will work with an extended SUSY because it will be easier to count the relevant bulk states associated by supersymmetry to a spin 2 particle and include them in an effective 4D Lagrangian (we will explain that in section 3.1.2) using 4D arguments, than to compute the Lagrangian for the high energy N=2, 6D supergravity.

First, we demonstrate with a simple example that every supersymmetry transfor-

mations in 6 dimensions will appear as an extended supersymmetry in 4 dimensions. Consider, as our academic example, the following Lagrangian in a six-dimensional Minkowski space for a gauge field  $A_a$  with  $a = 0\dots 5$  and a chiral spinor  $\lambda$  (we will follow [37] and its notation):

$$L = \text{tr}\left(-\frac{1}{4}F_{ab}F^{ab} + \frac{1}{2}i\bar{\lambda}\Gamma^a \overleftrightarrow{\nabla}_a \lambda\right) \quad (3.1)$$

where

$$\nabla_a \lambda = \partial_a \lambda + i[A_a, \lambda] \quad (3.2)$$

$F_{ab}$  is the usual field strength and  $\Gamma$  are the 6D  $\gamma$  matrices. This is the straightforward generalization of the corresponding 4D case for which the index  $a$  only runs from 0 to 3. We must however understand that here the spinors are in a higher-dimensional representation of the six-dimensional Lorentz group. The algebra and properties of the Dirac  $\Gamma_a$  matrices can provide an irreducible representation for such spinors [30, 37]. Among other things, it tells us that the dimension of the irreducible representation is given by:

$$\begin{aligned} n &= 2^{d/2} && \text{for even dimension } d \\ n &= 2^{(d-1)/2} && \text{for odd dimension } d \end{aligned}$$

Thus, in our 6D case the spinors will have 8 components. A particular representation for the Dirac matrices is given by [37]:

$$\begin{aligned} \Gamma_\mu &= \begin{pmatrix} 0 & \gamma_\mu \\ \gamma_\mu & 0 \end{pmatrix} && \text{for } \mu = 0, \dots, 3 \\ \Gamma_5 &= \begin{pmatrix} 0 & \gamma_5 \\ \gamma_5 & 0 \end{pmatrix} && \Gamma_6 = \begin{pmatrix} 0 & -\mathbf{1} \\ \mathbf{1} & 0 \end{pmatrix} \\ \Gamma_7 &= \Gamma_0 \dots \Gamma_6 = \begin{pmatrix} -\mathbf{1} & 0 \\ 0 & \mathbf{1} \end{pmatrix} && \beta = \Gamma_0 \end{aligned}$$

where  $\Gamma_7$  is the 6D equivalent of  $\gamma_5$  and  $\beta$  is the matrix for which  $\bar{\psi} \equiv \psi^\dagger \beta$  (in this notation there is no  $\Gamma_4$ ).

We can verify that the Lagrangian of equation 3.1 is invariant under the supersymmetric transformations:

$$\delta A_a = i\bar{\zeta}\Gamma_a\lambda - i\bar{\lambda}\Gamma_a\zeta \quad (3.3)$$

$$\delta\lambda = -\frac{1}{2}\Sigma^{ab}\zeta F_{ab} \quad (3.4)$$

where  $\zeta$  is the spinor infinitesimal parameter of a supersymmetric transformation (a ‘‘fermionic number’’ which anticommutes with everything fermionic, satisfying Grassmann’s algebraic rules, but which commutes with everything bosonic) and  $\Sigma^{ab}$  are matrices (which can be expressed in a Dirac matrix basis) which provide a representation of the six-dimensional infinitesimal Lorentz transformation  $\Lambda$  on the spinors space:  $\delta\psi = \frac{1}{4}i\Lambda^{ab}\Sigma_{ab}\psi$ . All this describes our supersymmetric theory in 6 dimensions.

Now, we take the 4-dimension point of view. For this, we have first to make explicit in the Lagrangian the independent extra dimensional degrees of freedom. Using the Dirac matrix representation given above, and writing our chiral spinor in term of an unconstrained complex 4-spinor  $\chi$  as:

$$\lambda = \begin{pmatrix} \chi \\ 0 \end{pmatrix} \quad (3.5)$$

we can make the substitution in the two terms of equation 3.1 on  $a$  and get:

$$-\frac{1}{4}F_{ab}F^{ab} = -\frac{1}{4}F_{\mu\nu}F^{\mu\nu} + \frac{1}{2}\nabla_\mu A_4\nabla^\mu A_4 + \frac{1}{2}\nabla_\mu A_5\nabla^\mu A_5 + \frac{1}{2}[A_5 \cdot A_6]^2 + \dots$$

and

$$\frac{i}{2}\bar{\lambda}\Gamma^a\overleftrightarrow{\nabla}_a\lambda = \frac{i}{2}\bar{\chi}\gamma_\mu\overleftrightarrow{\nabla}_\mu\chi - \frac{i}{2}\bar{\chi}\gamma_5\overleftrightarrow{\nabla}_4\chi - \frac{i}{2}\bar{\chi}\overleftrightarrow{\nabla}_5\chi$$

where the ellipse (...) corresponds to the terms that involve  $\partial_4$  or  $\partial_5$ . We didn’t write them explicitly because to pass from a 6D theory to a 4D one, we have to eliminate the dependence on  $x^4$  and  $x^5$ . We do so by using what is called the *trivial dimensional reduction* [37], ie by taking  $\partial_4 = \partial_5 = 0$ . The Lagrangian of equation 3.1 will then depend only on the four-dimensional coordinates  $x^\mu$ . With the identifications

$\chi = \frac{1}{\sqrt{2}}(\lambda_1 - i\lambda_2)$ ,  $A_4 = N$  and  $A_5 = M$ , we have that our 6D supersymmetric Lagrangian become:

$$L = \text{tr}\left[-\frac{1}{4}F_{\mu\nu}F^{\mu\nu} + \frac{1}{2}i\bar{\lambda}_i\gamma^\mu\nabla_\mu\lambda_i + \frac{1}{2}\nabla_\mu M\nabla^\mu M + \frac{1}{2}\nabla_\mu N\nabla^\mu N - i\bar{\lambda}_2[\lambda_1, M] - i\bar{\lambda}_2[\lambda_1, N] + \frac{1}{2}[M, N]^2\right]$$

We see from this Lagrangian that the spin of the fields range from 0 to 1, with two different and independent spin- $\frac{1}{2}$  particles:  $A_\mu$ , which composes the tensor  $F_{\mu\nu}$  is the spin-1 particle; the two fermions  $\lambda_1$  and  $\lambda_2$  have spin- $\frac{1}{2}$ ; and  $M$  and  $N$  are the two real components of a complex scalar). It corresponds in fact into the superposition of a gauge multiplet and a chiral multiplet (with the auxiliary fields eliminated) and is invariant under the following set of transformations:

$$\begin{aligned}\delta A_\mu &= i\bar{\zeta}_i\gamma_\mu\lambda_i \\ \delta M &= \epsilon_{ij}\bar{\zeta}_i\lambda_j \\ \delta N &= \epsilon_{ij}\bar{\zeta}_i\gamma_5\lambda_j \\ \delta\lambda_i &= -\frac{1}{2}i\sigma^{\mu\nu}\zeta_i F_{\mu\nu} + i\epsilon_{ij}\gamma^\mu\nabla_\mu(M + \gamma_5 N)\zeta_j - i\gamma_5\zeta_i[M, N]\end{aligned}$$

which correspond precisely to the transformations of a superalgebra with N=2 generators.

We thus see that starting with a simple supersymmetric theory in six dimensions and eliminating the two extra spatial coordinates to take a four-dimensional perspective, automatically yields a theory with two supersymmetry generators. This is what we call an *extended supersymmetry*. Here we took a simple theory and didn't pay much attention to the gauge group of the supermultiplet. However, even if the algebra is more complicated, as is the case with gravity, the principle of extending the number of supersymmetry generators by adopting a 4D point of view when starting from a higher-dimensional theory remains the same.

One would probably also have noticed that the way in which we have eliminated the two extra dimensions in our example was trivial and much easier than what actually happens in the SLED scenario. In fact, since in SLED the extra dimensions

are compactified on a radius  $r \sim \frac{1}{m}$ , to obtain a sensible theory in four dimensions from a six-dimensional one, we need to assume that all the fields are periodic in  $x^4$  and  $x^5$  with periods  $1/m$  and  $1/m'$  and then to Fourier decompose them as following:

$$N(x^\mu, x^4, x^5) = \sum_{nn'} \exp(-in'm'x^4 - inmx^5) N_{nn'}(x^\mu) \quad (3.6)$$

where  $N_{nn'}(x^\mu)$  is called the  $nn'$  Kaluza-Klein mode of the N field. Note, as we mentioned in sections 2.3 and 2.2.2, that the KK modes correspond to 4D fields (describing states when applied on  $|0\rangle$ ) with a definite value of the quantized bulk momenta, as we can easily verify by an application of  $P_5 = -i\partial_5$  on  $N(x^\mu, x^4, x^5)$  (recall that  $c = \hbar = 1$ ). Substituting the corresponding Fourier development of each 6D field in the Lagrangian will eliminate all the  $\partial_4$  and  $\partial_5$  acting on the exponential of equation 3.6. It is when we evaluate this Lagrangian at the position of the brane in the bulk space (by substituting  $x^4$  and  $x^5$  by 0, for example) that we finally get a completely four-dimensional theory. This procedure is more complicated than directly substituting  $\partial_4$  and  $\partial_5$  by 0. We can however argue (see [37]), that this will not have any effect on the fundamental result that we obtained from the trivial dimensional reduction: every mode will form an extended supermultiplet. Because terms like  $\partial_a N \partial^a N$  will be reduced to  $\partial_\mu N_{nn'} \partial^\mu N_{nn'} + (n'^2 m'^2 + n^2 m^2) N_{nn'}^2$  (with  $n$  and  $n'$  running from 0) by this mechanism of quantization of the extra dimensional component of momentum, every Kaluza-Klein mode will appear as a massive copy of a massless 0-mode 4D field, member of the extended supermultiplet, the mass being defined as:  $M_{nn'} = \sqrt{n^2 m^2 + n'^2 m'^2}$ . The appearance of such an infinite tower of identical supermultiplets of different mass is the only thing that will differ from the trivial dimensional reduction approach.

In our SLED scenario,  $m = m' \sim v \sim 10^{-3}$  eV. Each mode will therefore be separated by a mass splitting much smaller than any detector resolution and the complete KK tower associated to a 6D field will look like a particle of continuous mass, in our 4D point of view. We conclude from all of this that we can correctly describe the SLED bulk spectrum at low-energy in four-dimensions, provided that we consider an extension of the bulk supersymmetry and that these bulk states are

considered as continuously massive particles. What we now have to do is to examine the 4D spectrum to prove that we can indeed expect scalars.

To identify the states associated with the fields of a supermultiplet for a given extended supersymmetry, we will refer only to general properties of supersymmetric transformations and their action on physical states. The results will be applicable to any SUSY theory, regardless of the exact structure and other symmetries of a specific theory. However, the way we will present things will suppose massless supermultiplets and one-particle states. Fortunately, this is not a restriction for us since the mass of the graviton, from which we expect a scalar superpartner, is zero.

It is well known that supersymmetry transformations are generated by quantum operators  $Q$  which change the fermionic states into bosonic ones and vice versa, ie:

$$Q|\text{fermion}\rangle = |\text{boson}\rangle ; \quad Q|\text{boson}\rangle = |\text{fermion}\rangle \quad (3.7)$$

Which particular bosons and fermions are related to each other by the action of such  $Q$  and how properties other than the statistics of the states are modified by that operation depends on the supersymmetric model under study. However, since for now we are only interested in the spin, and hence in the statistical connection between states related by supersymmetry, we can indeed expect to find results valid for any supersymmetric theory, and in particular for SLED.

In an extended supersymmetry, there are  $N$  operators  $Q$  that each generate a different supersymmetric transformation. This means that bosons can be associated to other bosons by successive actions of  $Q$ s:

$$Q_2 Q_1 |\text{boson}\rangle = Q_2 |\text{fermion}\rangle = |\text{boson}'\rangle . \quad (3.8)$$

The question is whether there is a way to connect a spin-2 boson to a spin-0 one by means of supersymmetric transformations. If we can show that the answer is positive on a completely general basis, we will then prove that every SLED model predicts the existence of bulk scalars that must hence be included in an 4D Lagrangian.

In quantum field theory, states are defined from the irreducible representation of the Lorentz transformation on the Hilbert space. Massless states are thus labeled

by their 4-momentum  $p^\mu$  and their helicity  $\lambda$ . We want to know how the helicity operator will act on a particle state which has been modified by the application of a supersymmetric operator. Note that it will be easier, in order to follow the literature, to work with the Pauli-Lubanski vector [37, 22, 38]:

$$W_\mu = -\frac{1}{2}\epsilon^{\mu\nu\rho\sigma} P_\nu J_{\rho\sigma} \quad (3.9)$$

where  $P_\mu$  and  $J_{\mu\nu}$  are the generators of the Poincaré group (that describe translations, rotations and Lorentz transformations), rather than directly with the helicity operator. The results will however be completely equivalent. In fact, considering the standard frame for a massless one-particle state  $p_\mu = (E, 0, 0, E)$ , we have  $W_\mu|p, \lambda \rangle = \lambda p_\mu|p, \lambda \rangle$ . For  $\mu = 0$  we find that  $W_0$  is proportional to the helicity of the state. Now in order to find how this operator acts on states on which a SUSY transformation has previously been applied, we need to know the fundamental structure of any such transformation, structure which is provided by the supersymmetric algebra, ie the commutator of the  $Q$  generators with other generators of Lorentz transformations. Since the supersymmetry algebra obeys the following commutator relations:

$$[Q, P_\mu] = 0 \quad (3.10)$$

$$[Q, J_{\mu\nu}] = \frac{1}{2}\sigma_{\mu\nu}Q \quad (3.11)$$

where  $\sigma_{\mu\nu} \equiv \frac{1}{4}(\sigma_\mu \bar{\sigma}_\nu - \sigma_\nu \bar{\sigma}_\mu)$ ,  $\bar{\sigma}_\mu \equiv (\mathbf{1}, -\vec{\sigma})$  and  $\vec{\sigma}$  are the Pauli matrices, we have:

$$W_0(Q|p, \lambda \rangle) = QW_0|p, \lambda \rangle + [W_0, Q]|p, \lambda \rangle = (\lambda - \frac{1}{2})E(Q|p, \lambda \rangle) \quad (3.12)$$

In other words:

$$Q|p, \lambda \rangle \propto |p, \lambda - \frac{1}{2} \rangle \quad (3.13)$$

which means that a supersymmetry transformation change by  $\frac{1}{2}$  the helicity of a state, in agreement with our definition of equation 3.7. If we apply  $N$  different supersymmetry generators on a state of helicity  $\lambda_0$ , we will have:

$$Q_1 Q_2 \dots Q_N |p, \lambda_0 \rangle = |p, \lambda_0 - \frac{N}{2} \rangle. \quad (3.14)$$

Because the  $\{Q_i, Q_i\}$  ( $i = 1 \dots N$ ) anticommutator of the supersymmetry algebra is null, any further application of  $Q$ s on the above expression will give 0.

For the intermediate states of helicity number between  $\lambda$  and  $\lambda - \frac{N}{2}$ , since the  $Q_i$  operators are all different and that only a number  $n < N$  of such operators are needed to produce those states, we expect more than one state with such an intermediate helicity in the extended supermultiplet. The combination of the application of the various  $Q$  operators will then yield the following spectrum:

$$\begin{array}{ccccccc} \text{helicity:} & \lambda_0 & \lambda_0 - \frac{1}{2} & \lambda_0 - 1 & \dots & \lambda_0 - \frac{N}{2} \\ \text{number of states:} & \binom{N}{0} = 1 & \binom{N}{1} = N & \binom{N}{2} = \frac{N(N-1)}{2} & \dots & \binom{N}{N} = 1. \end{array}$$

Normally, a spectrum of states derived from a Lorentz-covariant field theory will exhibit CPT symmetry [37, 39]. This implies that for every state with helicity  $\lambda$  there should be a parity reflected state which has helicity  $-\lambda$ . However, spectra obtained by successive applications of SUSY operators on a reference state will not generally have this property. For example, for  $N = 1$  and  $\lambda_0 = \frac{1}{2}$  we will only have one state of helicity  $\frac{1}{2}$  and one of 0 helicity. The spectrum of a Lorentz-covariant field theory can therefore contain these states only in conjunction with those of the CPT conjugate multiplet with  $\lambda_0 = 0$  such that the smallest  $N = 1$  multiplet for the massless case is:

$$\begin{array}{cccc} \text{helicity:} & -\frac{1}{2} & 0 & \frac{1}{2} \\ \text{number of states:} & 1 & 2 & 1 \end{array}$$

This is the case, for example, of the massless Wess-Zumino model [37, 30]. In table 3.1 we give the very general particles content of the various extended supersymmetric theories for highest spin 2 and zero mass, ie for supergravity multiplet.

We see from this table 3.1 that we need  $N \geq 4$  in order to have scalar particles associated to the graviton by supersymmetry transformations. We know, from chapter 1 (see section 2.2.2), that the SLED scenario consist of a N=2 6D supergravity theory, and we have seen at the beginning of this section that every 6D supersymmetry transformations will be extended to two supersymmetry generators after dimensional

$\lambda$	Number of supersymmetries					
	N=1	N=2	N=3	N=4	N=5	N=6
2	1	1	1	1	1	1
$\frac{3}{2}$	1	2	3	4	5	6
1		1	3	6	10	15+1
$\frac{1}{2}$			1	4	10+1	20+6
0				1+1	5+5	15+15
$-\frac{1}{2}$			1	4	1+10	6+20
-1		1	3	6	10	1+15
$-\frac{3}{2}$	1	2	3	4	5	6
-2	1	1	1	1	1	1

Table 3.1: Number of states for each helicity value  $\lambda$  associated to a spin-2 graviton by a N-extended supersymmetry

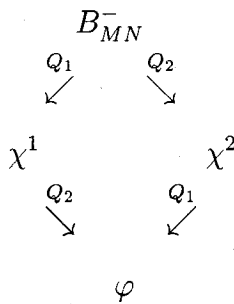
reduction. We can thus conclude that, from a 4D point of view, the SLED scenario possesses N=4 supersymmetry and hence predicts the existence of bulk scalars.

If we had worked out this analysis directly at high energy in the 6D case with two supersymmetry generators (SLED scenario), following our spin state counting, we would have expected a spin-2 particle (the graviton), two spin- $\frac{3}{2}$  ones (gravitino) and a spin-1 particle. This would exhibit the following scheme for the action of supersymmetry operators on graviton field [40]:

$$\begin{array}{ccc}
 & g_{MN} & \\
 Q_1 \swarrow & & \searrow Q_2 \\
 \psi_M^1 & & \psi_M^2 \\
 Q_2 \swarrow & & \searrow Q_1 \\
 & B_{MN}^+ &
 \end{array}$$

where  $g_{MN}$  is the graviton,  $\psi_M^i$  are the gravitinos and  $B_{MN}^+$  is the anti-symmetric 2-form potential associated with the spin-1 graviton's superpartner, equivalent to

the  $F_{\mu\nu}$  describing a photon field<sup>1</sup>. We see here that we don't explicitly obtain a scalar field. However, it has been shown in [36, 13] that this theory is one of a class that cannot be described by manifestly Lorentz-invariant action and which therefore does not have Lorentz-covariant Green's functions (from which physical predictions are made). To restore this Lorentz invariance, we have to introduce a new field corresponding to a new spin-1 particle<sup>2</sup>. Applying the supersymmetric operators to this field would yield the following scheme [40]:



where  $B_{MN}^-$  is the 2-form potential that is related to the anti-self-dual field strength,  $\chi^i$  are the spin- $\frac{1}{2}$  fermions and  $\varphi$  is a scalar. The full spectrum of the 6D N=2 supergravity thus corresponds to what has been presented for SLED in the section 2.4.1 above. We clearly confirm here that the SLED proposal predicts the existence of a bulk scalar. Moreover, as was explained in sections 2.3.2 and 2.4.1, we need other supermultiplets in the bulk space (in order to cancel anomalies) that involve superpartners of spin-1 and spin- $\frac{1}{2}$  particles as well as possibly other fields on other branes and fields associated to string oscillation modes. All this will imply a certain number of bulk scalar fields.

Since we don't have an explicit SLED model in the high-energy sector, we cannot say exactly how many scalars there will be in the bulk, which symmetries they will

<sup>1</sup>In the general 6D N=2 supergravity with other possible gauge transformations, this anti-symmetric 2-form potential appears in the graviton supermultiplet as a self-dual (ie for which  $*F = F$ , where  $*$  is the Hodge-star operator) third-rank field strength  $G_{MNP}$ . The detail of this is beyond the scope of the present work. You can however see references [36, 13] for completeness

<sup>2</sup>To be more precise, we must add a new anti-symmetric tensor multiplet containing an anti-self-dual ( $*F = -F$ ) field strength that couple to supergravity. Again a complete discussion on that is provided by [36, 13]

satisfy and what will be their exact coupling to the different bulk and brane fields. This is not an issue for us since we just want to make approximate predictions at low energy. What is important here is that SLED predicts the existence of at least one bulk scalar field that would be seen, in 4D, as a continuously massive particle. We will thus call  $\phi$  such a generic bulk scalar field that will be included in a 4D low-energy Lagrangian with undetermined coupling constants explicitly written as  $a, b, c, \dots$ , depending on which particle they couple to. Our physical predictions will thus be completely general and applicable to any such possible bulk scalar. We want to study the range of observability for such couplings. To do this we have first to see how the interaction Lagrangian could be written.

### 3.1.2 *Coupling of bulk scalar with SM fields*

First, we will be more explicit about what we mean by a low-energy approximation of an interacting Lagrangian and by free parameter coupling constants. To this end, suppose that at the microscopic level we have an explicit, consistent, complete and exact SLED model with given couplings between bulk and brane modes. The bulk scalar coupling constants to Standard Model particles would then be read directly from the action. However, since we are interested in evaluating physical predictions at low-energy scales, we would have to evolve these known couplings from the high-energy sector down to the experimental energies by integrating out all the model's heavy or invisible degrees of freedom following the Wilson flow [39, 41]. It is thus only the effective coupling of this low-energy theory that is probed in experiments. The new effective Lagrangian obtained by this procedure however involves an infinite expansion of terms in powers of mass and replacing the various degrees of freedom that have been integrated out [39, 41]. This power series thus consists in the complete development of the exact microphysics theory in terms of low-energy local operators. This description is only valid at energies lower than a cut-off scale  $\Lambda$  at which the convergence radius of the series becomes infinite, ie at which the theory cannot be anymore expressed in terms of low energy concepts. In the SLED scenario, this scale correspond to the fundamental D-dimensional Planck scale  $M_D$  related to the string

scale where the various degrees of freedom cannot be described by local operators but must rather be described in terms of strings. Now, for energies much lower than  $\Lambda$ , we can approximate the exact series by a finite sum obtained by dropping higher mass-dimension terms. The error on such approximation is generically evaluated by the factor  $(\frac{E}{\Lambda})^n$  where  $-n$  is the power of mass of the coupling constant of the higher-dimensional interaction terms. Since in SLED  $\Lambda = M_D \sim 10$  TeV, and LHC's typical energies at the parton level are  $E \sim 0.1-1$  TeV and since the cross sections are, by definition, proportional to the square of this factor ( $\sigma \sim \langle \mathcal{L} \rangle^2$ ), we will have a sufficiently good precision in our physical predictions if we keep terms for which  $n \leq 2$  (which corresponds to dimension 6 interaction terms in the Lagrangian). Note that for certain processes we will have to evaluate the limiting cases for which our  $n \leq 6$  approximation hold. We will come back on this later.

Among other things, this approximation procedure substitutes high energy coupling through loops diagrams by effective direct coupling of local operators. This is particularly helpful for us. In fact, the SLED scenario predicts, in order to achieve the self-tuned solution to the cosmological constant problem as stated in section 2.2.2, that there is no dilaton-brane coupling (the coupling constant is set to 0) at the classical level because of the scale invariance<sup>1</sup> presupposed by this mechanism ([11, 13]). However, this does not prevent brane fields from coupling to other bulk fields (if that was not the case, then it would be impossible to have a SLED signal from colliders) like the graviton which, in turn, can couple to the dilaton. This means that dilaton and brane fields can, in the SLED scenario, couple through loop diagrams at the microscopic scale. Thus, in passing to the low-energy limit, even in the extreme (and unlikely) case where no other bulk scalars than the dilaton are present, after having integrated out heavy degrees of freedom (including heavy quantum correc-

<sup>1</sup>A scale transformation can be represented as a change in the spacetime coordinates of a field:  $\phi(x) \rightarrow e^{-\sigma} \phi(xe^{-\sigma})$ . If the quantum field theory under consideration is coupled to gravity, then the symmetric energy-momentum tensor  $\Theta^{\mu\nu}$  identified as the source of the gravitational field will be related to the classical conserved current  $D^\mu$  of the scale transformation by the relation  $\partial_\mu D^\mu = \Theta^\mu_\mu = 0$ , which thus provide a constrain on the possible coupling with this gravitational source [39, 42]

tions as loops of graviton, etc) these high-energy loop couplings will appear as direct contact interaction. The resulting low-energy effective 4D Lagrangian with explicit direct couplings between brane fields and bulk scalar will thus yield the low-energy spectrum of our theory.

In the absence of an explicit microscopic model, we can use the very general approach of effective field theory ([39, 41]) which does not require any explicit knowledge of a high energy theory to write down directly the low-energy couplings. To achieve this, one only needs to identify the symmetries that must be respected as well as the spectrum allowed (by experimental constraints) at this energy scale and then write down the most general Lagrangian density involving the lowest-dimensional interactions ( $n \leq 2$ ) which are consistent with this spectrum and these symmetries. This procedure however requires that the coupling constants be fixed by experiment. Since experimental results are not yet available, we will have to leave the coupling constant as free parameter for our physical predictions. Our work will then consist in evaluating the possible range of coupling values at which the LHC experiment will be sensitive. Hence, for our low-energy effective 4D theory involving a spectrum consisting in Standard Model particles and continuously massive bulk scalars we must select the possible interactions that will dominate at the LHC energies and which are allowed by symmetries.

The strength of these couplings will not be completely free, however. In fact, in our general effective theory framework, the coupling constants of the 4D interacting terms of dimensions more than 4 in power of mass are suppressed by inverse powers of a cutoff mass scale  $\Lambda$ . This is intimately related to the fundamental microscopic theory underlying this low-energy approximation. Because a real bulk scalar is part of a gravitational supermultiplet, it should share the universal and gravitational strength coupling of the graviton which is defined to be  $\mathcal{O}\left(\frac{1}{M_D^{2+n}}\right)$  where  $M_D$  is the fundamental  $4+n$ -dimensional Planck scale. This will thus set the mass scale dependence of our effective interactions. It is the absence of supersymmetry on the brane that will cause the bulk-brane couplings to be more complicated than this universal coupling. Bulk

scalars will thus couple to brane modes through effective interactions that respect all the low-energy symmetries, with couplings suppressed by some powers of the  $M_D$  scale predicted by the SLED scenario. This is what will govern the phenomenological properties of the bulk scalars.

Now, we have to consider the various symmetries and determine which interacting terms between bulk scalars and Standard Model fields have the lowest dimension of mass. The first symmetries that we have to consider are the bulk symmetries. We have just seen that it is possible to forbid classical brane-bulk scalar couplings because of scale invariance [11, 13, 44]. In more general grounds, every bulk scalar that has a shift symmetry defined as  $\phi \rightarrow \phi + \epsilon + \dots$  will be an exact 6D Goldstone boson (massless scalar particle that becomes interaction free in the 0 momentum limit) and will thus decouple from the brane modes (because they will be eaten by other bulk modes). However we argue that even if such symmetries preclude classical brane-bulk scalar interactions, such interactions will be generated by loops, and will therefore appear as effective interactions at low-energy. These symmetries will thus not be considered for our low-energy effective theory. Is it also the case for all the other possible gauge symmetries of a 6D high energy theory that apply to bulk scalars? The answer is yes. Our effective Lagrangian must only display the symmetries that are present at low-energy, ie the Standard Model ones. In fact, since we include these scalars in a low-energy Lagrangian that is defined well below the scale that breaks the fundamental symmetries of nature (electroweak symmetry, supersymmetry, etc), we can always choose a specific gauge that will reduce bulk scalars to fields having only one degree of freedom. This is how the Higgs field is handled in the Standard Model. Since we leave our couplings free to remain general, and since other possible internal symmetries of bulk scalars commute with the electroweak gauge group, we can generically consider that at low energy our effective bulk scalar is a singlet in any given symmetry [33]. Our concern is therefore to write down a Lagrangian that couples such bulk scalars by gauge invariant terms to Standard Model fields. Of course, our 4D effective Lagrangian must also be Lorentz-invariant. Note that an

explicit 6D model at the microscopic level will be complicated by the fact that one will also have to consider how the Standard Model fields behave under the other possible symmetries of the exact theory. This is however beyond the scope of our work.

Finally, for phenomenological purpose, we will concentrate on the implications of real bulk scalar production, rather than calculate the consequences of its virtual exchange. We do so for the same reason as in the case of virtual exchange of gravitons [17] and bulk vectors [33]: their virtual exchange cannot be distinguished from the effects of local interactions produced by other kinds of high-energy physics (such as the exchange of massive string modes) [18]. For this reason, and since the allowed terms involving many bulk scalar fields will be of too high mass dimension for our expected precision ( $n \leq 2$ ), we will concentrate on trilinear interactions involving only a single higher-dimensional scalar and two Standard Model particles. We may now write down the most general lowest-dimensional interactions which are consistent with the assumed low-energy particle content and the SM symmetries of the theory and that will explicitly be used for our physical predictions. This is given by the following Lagrangian density:

$$\begin{aligned}
\mathcal{L}_{\text{EFF}} = & \partial_M \phi(x, y) \partial^M \phi(x, y) \\
& - \delta^2(y) \left[ \sum_Q \bar{\Psi}_Q^i(x) (\bar{g}_{ij} + i(\bar{g}_5)_{ij} \gamma_5) \Psi_Q^j(x) \right. \\
& + \bar{c}_g G_a^{\mu\nu}(x) G_{\mu\nu}^a(x) + \bar{b}_g \epsilon^{\mu\nu\lambda\rho} G_{\mu\nu}^a(x) G_{\lambda\rho}^a(x) \\
& + \bar{c}_\gamma F^{\mu\nu}(x) F_{\mu\nu}(x) + \bar{b}_\gamma \epsilon^{\mu\nu\lambda\rho} F_{\mu\nu}(x) F_{\lambda\rho}(x) \\
& \left. + a H^\dagger(x) H(x) \right] \phi(x), \tag{3.15}
\end{aligned}$$

with  $M = 0, \dots, 5$ ,  $a$  a dimensionless coupling and  $\bar{g}_{ij}$ ,  $(\bar{g}_5)_{ij}$ ,  $\bar{c}_g$ ,  $\bar{b}_g$ ,  $\bar{c}_\gamma$  and  $\bar{b}_\gamma$  are arbitrary dimensionful coupling parameters. The indices  $i, j = 1, 2, 3$  here label the Standard Model's three generations. In these expressions, the coordinates  $x^\mu$  describe the 4 dimensions parallel to the Standard Model brane and  $y^m$  similarly

describe the  $n$  transverse dimensions. The brane itself is assumed to be located at the position  $y^m = 0$  in these extra dimensions.  $F_{\mu\nu}$  denotes the usual electromagnetic field strength defined as  $F_{\mu\nu} = \partial_\mu A_\nu - \partial_\nu A_\mu$ ,  $A$  being the photon field, and  $G_{\mu\nu}^a$  is the non-Abelian gluon field strength,  $G_{\mu\nu}^a = \partial_\mu G_\nu^a - \partial_\nu G_\mu^a + g_3 f^{abc} G_\mu^b G_\nu^c$ , with  $g_3$  denoting the QCD coupling constant. Finally,  $\Psi_Q$  generically denotes any of the Standard-Model fermion mass eigenstates, whose electric charge is denoted by  $Q$ .

Before continuing with this effective Lagrangian and computing explicit physical predictions concerning direct production of bulk scalars at the LHC (and evaluating how they compete with direct graviton production) several comments concerning these effective interactions bear emphasis:

- In a  $4 + n$ -dimensional theory, the Lagrangian density describing the theory must be of dimensions  $4 + n$  in power of mass in order to yield a dimensionless action  $S = \int d^{4+n}x \mathcal{L}$ . Since each derivative is of dimension 1, the kinetic term  $\partial_M \phi \partial^M \phi$  of the Lagrangian density tells us that the scalar field will have a dimension of  $1 + \frac{n}{2}$ . The dimensional reduction from the  $(4 + n)$ D point of view to the 4D perspective will not change this dimensional analysis, as can be seen from equation 3.6. Therefore, for two extra dimensions ( $n = 2$  in the SLED proposal) the couplings to the QED and QCD sectors in equation 3.15 involve terms of dimensions 5 or 6 (as required for our expected precision, see discussion at beginning of this section), while the lowest-dimensional interaction with the Higgs sector ( $HH\phi$ ) will be a term of dimension 4 and will hence not be suppressed by a mass scale. In what follows it will be convenient to define dimensionless couplings for the QCD sector also by scaling out the appropriate power of the reduced Planck mass in  $D$  dimensions,<sup>1</sup> according to  $g_{ij} = \bar{g}_{ij} \bar{M}_D^{n/2}$ ,  $c_g = \bar{c}_g \bar{M}_D^{1+n/2}$  and so on. It should be kept in mind when doing so, however, that the fermion interactions are not  $SU_L(2) \times U_Y(1)$  invariant and so the size to be expected for the couplings  $\bar{g}_{ij}$  and  $(\bar{g}_5)_{ij}$  depends strongly on the way in which the electroweak gauge group is broken in the underlying theory which produces

<sup>1</sup>More precisely,  $\bar{M}_D$  is the reduced Planck mass in  $D = 4 + n$  dimensions, defined in terms of the  $D$ -dimensional Newton's constant by  $8\pi G_D = \bar{M}_D^{2-D}$ .

them. In particular, if the new physics is not involved in electroweak symmetry breaking then there is a natural suppression of the fermionic dimensionless couplings,  $g_{ij} \sim v/\overline{M}_D$ , where  $v = 246$  GeV. (If the relevant dimensionless couplings of the underlying model are similar in size to Standard Model Yukawa couplings, then this suppression can be even smaller, although they need not be this small in all explicit models.) In principle, if the extra-dimensional physics were itself the sector which broke the electroweak gauge group, even the suppression by powers of  $v/\overline{M}_D$  might not be present, although in this case the new-physics scale cannot be very large compared to  $v$ .

- Even if, as we have just mentioned, the fermion interaction of eq. 3.15 appears not to be invariant under electroweak gauge transformations, we can still use it for relevant physical predictions at the LHC because it simply tells us that we have already replaced an explicit factor of the Standard Model Higgs field with its vacuum expectation value,  $v = 246$  GeV, and rotated to a fermion mass eigen-basis. The resulting couplings,  $g_{ij}$  and  $(g_5)_{ij}$ , can in principle be off-diagonal and so involve flavor-changing neutral currents, but we will assume these not to arise since they would be strongly constrained, if present.

However, this substitution has not been explicitly done for the coupling to the Higgs sector. For this case, in unitary gauge, we have  $H = \begin{pmatrix} 0 \\ v+h(x) \end{pmatrix}$  where  $v$  is, as always, the expectation value which breaks the electroweak gauge group, and, in the absence of bulk-brane couplings,  $h(x)$  is the physical scalar field. In terms of this, the coupling to the bulk field becomes

$$\mathcal{L}_{\text{Higgs}} = -a(v + h(x))^2 \phi(x), \quad (3.16)$$

We see that three separate terms are implied for the coupling between the bulk scalar,  $\phi$ , and the Higgs scalar,  $h$ : (a) a linear potential for  $\phi$  of the form  $a v^2 \phi$ ; (b) a bulk-brane mixing term of the form  $a v h \phi$ ; and (c) a trilinear coupling of the form  $a h^2 \phi$ . We ignore the first of these since it acts to shift the ground state of  $\phi$  away from the value determined by the bulk scalar potential, and none of our results depend on this value in any case.

The second type of interactions implies a mixing between  $h$  and the various Kaluza-Klein modes of the bulk scalar,  $\phi$ . This mixing is removed by diagonalizing the resulting scalar mass matrix, which for small  $a$  leads to an  $O(a)$  overlap between the physical Higgs state and the bulk KK modes. The physics of this mixing is very similar to previously studied graviscalar mixing with brane modes, and leads to a non-negligible invisible width [6, 32, 8] for the Higgs particle. We do not further explore this width in detail, although its implications would be important to understand once the Higgs is discovered and its properties are being explored in detail. In this work we will focus on the trilinear  $h^2\phi$  interaction, the last term of our effective Lagrangian 3.15.

- As mentioned before, the interactions written above are of lowest-dimension allowed, given only a gauge singlet extra-dimensional scalar and the Standard Model particle content. As such, these interactions may be expected to dominate at energies low compared to the basic interaction scale  $\overline{M}_D$ . This effective theory must simply be regarded as the leading term of an expansion in inverse powers of  $\overline{M}_D$  and must be expected to break down once physical energies approach this scale. Since it will be possible (but rare) for the LHC to produce collisions at this energy (center of mass energy in the proton-proton system will be of 14 TeV) we will later have to evaluate what validity range of the physical predictions will come out from this effective Lagrangian. We postpone this discussion to section 3.2.3.

Note however that this need not to be the case for the coupling to the Higgs sector since its effective coupling constant involves a *non-negative* power of mass. For this reason, we will treat separately the phenomenological analysis of the bulk scalar coupling to the hadronic sector and its coupling to the Higgs sector. Also note that this dimensionless coupling to Higgs is a special case of the SLED scenario where we have only two extra dimensions. We will thus restrict to  $n = 2$  in our phenomenological analysis of the  $hh\phi$  interaction. For the hadronic case, the suppression will also be weaker for the SLED scenario, as can be seen from the dependence of the coupling constant on  $M_D$  (see first bullet following equation 3.15). However, since there is a

dependence on  $M_D$ , it will be interesting, phenomenologically, to remain general and make our physical predictions for a general number  $n$  of extra dimensions. We must nevertheless keep in mind that it is indeed the  $n = 2$  case which is the best motivated scenario, even if other possibilities are consistent with any other LED proposals. Finally, note that because our physical predictions will be made for a hadronic collider (LHC), partonic interactions and the Higgs interaction will dominate (the Higgs one because it is unsuppressed by the scale  $M_D$ ). We will thus ignore the interactions with photons or with  $W$  and  $Z$  bosons.

- In order for our physical predictions to be reliable for energies below the cut-off scale  $M_D$  the dimensionless coupling  $c$  and  $g$  that we have just defined must reasonably be of  $\mathcal{O}(1)$  or less. For example, suppose that the energies probed in an experiment are one order of magnitude smaller than the fundamental scale  $M_D$ . Then, our physical predictions will be expected to be good within a few percent (since the cross section is proportional to the square of the coupling constant). In the opposite case where the dimensionless coupling is of  $\mathcal{O}(10)$ , this will be equivalent to a rescaling of the fundamental scale by an order of magnitude. We will then have  $E \sim M_D$  and thus our physical predictions will break down. Therefore, theoretically, we expect  $c, g \lesssim 1$ . This must also be the case for the dimensionless coupling constant  $a$  of the  $hh\phi$  interaction in order for the theory to be perturbative. Upper limits on the values of dimensionless coupling constants will be lower, however, in particular models where the low-energy effective scalar coupling derives exclusively from high energy loops terms. A representative size for such couplings as generated by one loop in 6 dimensions might then be set by loop-counting factors, like  $a, c, g \sim N/(4\pi)^3$  with  $N$  denoting the number of particle species circulating in the loop. For the simplest 6D supergravities [46]  $N$  is typically  $\mathcal{O}(10 - 20)$ , while for chiral 6D supergravities the requirements of anomaly cancellation can imply  $N \gtrsim \mathcal{O}(1000)$ . Depending on the number of fields which contribute, an estimate for the loop-induced coupling could well be  $a, c, g \sim \mathcal{O}(0.01 - 0.1)$ . We shall see that couplings at the upper end of this range might be observable at the LHC.

- One might imagine writing other interactions having the same dimension as those given above, such as derivative couplings to the fermions of the form

$$\Delta\mathcal{L} \propto \overline{M}_D^{-1-n/2} \delta^n(y) \bar{\Psi}(x) \gamma^\mu \Psi(x) \partial_\mu \phi(x, y). \quad (3.17)$$

We do not include these terms explicitly because they are not independent, since they can be rewritten into the form given above by performing a field redefinition. (The possibility of doing so can be seen by integrating by parts, and using the equations of motion for the fermions to trade the derivative for a fermion mass. For more details about such redundant operators, see for instance ref. [41].) Seen in this light these derivative couplings are expected to be small, since they imply that the dimensionless couplings  $g_{ij}$  and  $(g_5)_{ij}$  are proportional to the corresponding Standard Model Yukawa couplings.

- The factor  $\delta^n(y)$  in eq. 3.15 expresses explicitly the broken translation invariance of the bulk due to the presence of the brane. Consequently momentum transverse to the brane is not conserved, allowing bulk particles to be emitted into the extra dimensions even if all of the initial particles of the interaction were themselves confined to the brane. Physically, the unbalanced transverse momentum is absorbed by the recoil of the brane itself, with no energy cost because of the brane's enormous mass.

### 3.2 Bulk scalar production at LHC

The effective Lagrangian of equation 3.15 can be used to compute the cross sections at tree-level for production of bulk scalars in  $p - p$  collisions at the Large Hadron Collider (LHC). We shall restrict our attention to hadronic production mechanisms and to bulk scalars radiated by a Higgs boson since these processes are expected to dominate at LHC energies, and so might be expected to give the clearest signal. As we mentioned in the previous section, we will treat these two cases separately in the following.

### 3.2.1 Parton-level cross section of the hadronic processes

Because of our interest in the study of direct bulk scalar production accompanied by a quark or gluon, we want to compute the cross section for the relevant processes which are:  $qq \rightarrow g\phi$ ,  $qg \rightarrow q\phi$  and  $gg \rightarrow g\phi$ . The physical signal which such a reaction would produce is a well defined jet plus missing energy as the bulk scalar escape into the extra dimensions. To evaluate these cross sections, we must first obtain the Feynman rules for the  $\bar{q}q\phi$ ,  $gg\phi$  and  $ggg\phi$  vertices which follow from the effective Lagrangian of eq. (3.15). Of course we will also use the Standard Model vertices and propagators as given in [39]. We can derive our new Feynman rules by either of two methods: the canonical method and the path integral one. The canonical method consists in computing the first order matrix element of the effective Lagrangian ([39, 30]). For example, if we want to find the  $\bar{q}q\phi$  vertex, we need to compute  $\langle \phi | \bar{\Psi}(g + ig_5\gamma_5)\Psi\phi | q\bar{q} \rangle$  where the fields and the states are defined in terms of the ladder operators  $a_q$  (or  $b_q$  and  $d_q$ ) and  $a_q^\dagger$  as:

- $\langle \phi(l) | = \langle 0 | a_l$
- $|q(p, \sigma, c)\bar{q}(k, \sigma', c') \rangle = a_{p,\sigma,c}^\dagger b_{k,\sigma',c'} |0 \rangle$
- $\psi(x) = \sum_{c,\sigma} \int \frac{d^3k}{(2\pi)^{3/2}} [a_{k,\sigma,c} u(k, \sigma, c) e^{ik \cdot x} + \dots]$
- $\phi(x) = \int \frac{d^3k'}{(2\pi)^{3/2}} [d_{k'} e^{ik' \cdot x} + c.c.]$
- $[a_{k,\sigma,c}, a_{k',\sigma',c'}^\dagger] = \delta(k - k') \delta_{\sigma\sigma'} \delta_{cc'}$

where  $|q(p, \sigma, c) \rangle$  denote a quark state,  $\sigma$  is the spin index and  $c$  is the color one. Of course, which particles are in the initial state and which are in the final state is arbitrary. This will fix the momentum flow convention used in the vertex. In this example, the quark momentum points towards the vertex while the anti-quark and the scalar come out of the vertex.

Alternatively we can calculate these vertices by the path integral formulation of quantum field theory. This requires to expand the exponential of the action  $S$ , which

weights the contribution of each quantum path to the Green function, following

$$\langle T\phi(x_1)\phi(x_2) \rangle \propto \int \mathcal{D}\phi \phi(x_1)\phi(x_2) \exp[iS] \quad (3.18)$$

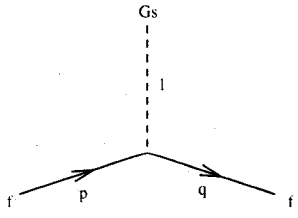
and to read directly the coefficient of the appropriate first order interaction terms [39, 30, 47]. This can be directly achieved by computing the functional derivative of the action as a function of the fields involved in the relevant vertices. Let us take, for example, the  $gg\phi$  vertex. It will be given by the evaluation of:

$$V_{\mu\nu}^a = \frac{(2\pi)^{12}}{(2\pi)^4 \delta^4(p+q+l)} i \frac{\delta^3 S_3}{\delta \tilde{G}_\mu^a(p) \delta \tilde{G}_\nu^b(q) \delta \tilde{\phi}(l)} \quad (3.19)$$

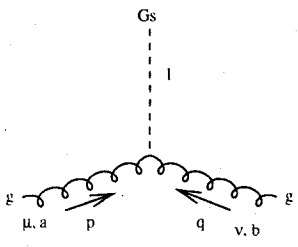
where:

- $S_3 = \int d^4x [-G_{\mu\nu}^a (\bar{c}_g G_a^{\mu\nu} + \bar{b}_g \tilde{G}_a^{\mu\nu}) \phi]$
- $G_{\mu\nu}^a(x) = \partial_\mu G_\nu^a(x) - \partial_\nu G_\mu^a(x) + g_3 f^{abc} G_\mu^b(x) G_\nu^c(x)$
- $G_\nu^a(x) = \int \frac{d^4k}{(2\pi)^4} \tilde{G}_\mu^a(k) \exp^{-ik \cdot x}$
- $\frac{\delta \tilde{G}_\alpha^a(k')}{\delta \tilde{G}_\beta^b(k)} = \delta^4(k - k') \delta_{\alpha\beta} \delta_{ab}$

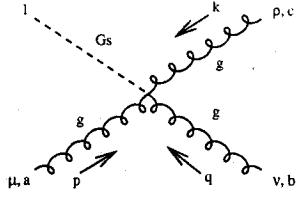
with  $G_\nu^a(x)$  being the gluon fields and  $a$  the color index. Using these methods, we obtain the following Feynman rules for the relevant vertices:



$$= -i(\bar{g} + i\bar{g}_5 \gamma_5)$$



$$= 4i[\bar{c}(p \cdot q) g_{\mu\nu} - \bar{c} p_\nu q_\mu + \bar{b} \epsilon_{\mu\nu\alpha\beta} p^\alpha q^\beta] \delta_{ab}$$



$$= 4g_3 f^{abc} [\bar{c} g_{\mu\nu} (p_\rho - q_\rho) + \bar{c} g_{\mu\rho} (k_\nu - p_\nu) + \bar{c} g_{\nu\rho} (q_\mu - k_\mu) + \bar{b} \epsilon_{\alpha\mu\nu\rho} (p^\alpha + q^\alpha + k^\alpha)]$$

We can now use these Feynman rules to compute the matrix elements of the relevant processes. Before computing the differential cross sections, we must, however, rethink the phase space element. In fact, we argued earlier that the sum over the finely-spaced Kaluza-Klein massive states of the bulk scalar field can be replaced by an equivalent integral over the continuous mass of a single bulk scalar. This can be understood as an approximation when the length scales associated with the extra dimensions are much larger than the wavelengths of the partons involved in the experimental processes such that the quantization of the higher-dimensional bulk scalar momentum vector is not important. This mass is thus related to the approximately continuous extra dimensional bulk scalar momentum and we will then have a new phase-space factor, multiplying the usual 4D one.

It is convenient to divide the higher-dimensional bulk scalar momentum vector,  $\ell_{4+n}^M$  with  $M = 0, \dots, 3+n$ , into its continuous 4-dimensional components parallel to the brane,  $\ell^\mu$  with  $\mu = 0, \dots, 3$ , and its quantized  $n$ -dimensional bulk components,  $L^m$  with  $m = 4, \dots, 3+n$  such that  $\ell_{4+n} = \{\ell^\mu, L^m\}$ . If  $\phi$  has a D-dimensional mass  $\mu_\phi$ , the total squared-momentum for a bulk scalar of mass  $\mu_\phi$  will then be given by  $\ell_{4+n}^2 = \ell^\mu \ell_\mu + L^m L_m = -\mu_\phi^2$ , which we write as  $\ell^2 = -M^2$ , where  $M$  is the effective 4-dimensional mass due to the particle's motion in the extra dimensions. Note that we recognize here the metric  $\eta = (-1, 1, 1, 1)$ .

We now have to determine a typical value for  $\mu_\phi$  because it will correspond to the lower limit for the integration over  $M$ . In the high-energy theory, the bulk scalar is related to the graviton by supersymmetry. We thus expect, since the graviton is massless, that the bulk scalar will have a zero mass also. However, since SUSY is broken in the bulk, the mass splitting between the graviton and its superpartners must be of

the order of the supersymmetry breaking scale. For the SLED scenario, we explained in chapter 1 that this symmetry breaking scale must have a magnitude equivalent to the cosmological constant in the bulk, ie  $m_{sb} \sim v$ , which is extremely small. We will thus consider in later applications that, consistently with the SLED scenario,  $\mu_\phi = 0$ . Generalization of our results to arbitrary  $\mu_\phi$  is nevertheless straightforward. The corresponding integration measure is then:

$$\frac{d^n L}{(2\pi)^n} = \frac{(L^2)^{(n-2)/2}}{2(2\pi)^n} dL^2 d\Omega_n. \quad (3.20)$$

After integration over the angular degrees of freedom,  $\Omega_n$ , the final phase-space measure used for the bulk scalar bulk momentum becomes:

$$\int_{\Omega_n} \frac{d^n L}{(2\pi)^n} = \frac{(M^2)^{(n-2)/2} dM^2}{2\Gamma(\frac{n}{2})(2\pi)^{n/2}}. \quad (3.21)$$

From the above phase-space factor and Feynman rules, we can now obtain the parton-level differential cross sections for the processes  $q\bar{q} \rightarrow g\phi$ ,  $qg \rightarrow q\phi$  and  $g\bar{g} \rightarrow g\phi$  for which the contributing Feynman graphs are given in figure 3.1. The results are the following:

The quark-annihilation channel is obtained by evaluating graphs (a) through (c), which give:

$$\begin{aligned} \frac{d\sigma(q\bar{q} \rightarrow g\phi)}{d\hat{t} d\hat{u} dM^2} &= \frac{\alpha_s (2\pi)^{n/2} (M^2)^{(n-2)/2}}{18\Gamma(\frac{n}{2}) M_D^n \hat{s}^2} \left[ \frac{(g^2 + g_5^2)}{(2\pi)^{2n/(2+n)}} \left( \frac{2M^2 \hat{s} + (\hat{u} + \hat{t})^2}{\hat{u}\hat{t}} \right) \right. \\ &\quad \left. + \frac{4(c^2 + b^2)}{M_D^2} \left( \frac{\hat{t}^2 + \hat{u}^2}{\hat{s}} \right) \right] \delta(\hat{s} + \hat{t} + \hat{u} + M^2). \end{aligned} \quad (3.22)$$

Notice that helicity conservation precludes graph (c) interfering with graphs (a) and (b) in the limit where parton masses are neglected (as we assume).

The quark-gluon scattering contribution is similarly obtained by evaluating the graphs (d), (e) and (f), yielding

$$\begin{aligned} \frac{d\sigma(qg \rightarrow q\phi)}{d\hat{t} d\hat{u} dM^2} &= - \frac{\alpha_s (2\pi)^{n/2} (M^2)^{(n-2)/2}}{48\Gamma(\frac{n}{2}) M_D^n \hat{s}^2} \left[ \frac{(g^2 + g_5^2)}{(2\pi)^{2n/(2+n)}} \left( \frac{\hat{u}^2 + M^4}{\hat{s}\hat{t}} \right) \right. \\ &\quad \left. + \frac{4(c^2 + b^2)}{M_D^2} \left( \frac{\hat{t}^2 + \hat{s}^2}{\hat{u}} \right) \right] \delta(\hat{s} + \hat{t} + \hat{u} + M^2). \end{aligned} \quad (3.23)$$

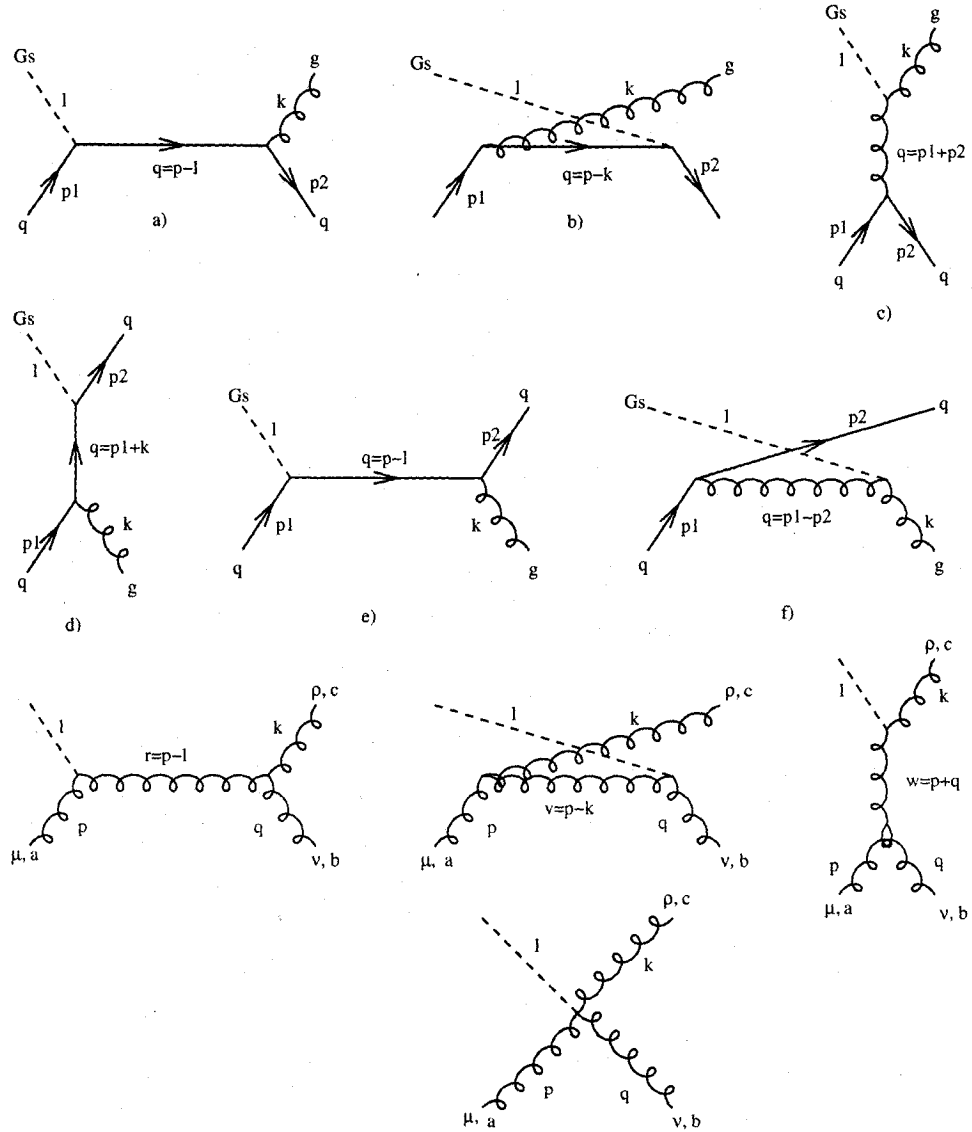


Figure 3.1: The parton-level Feynman graphs which contribute to bulk scalar production with an associated jet in proton-proton scattering.

As before, the neglect of parton masses ensures the non-interference of graph (f) with graphs (d) and (e). It is also important to notice here that when we square the amplitude and sum (average) over final (initial) spins we must *not* make the ‘‘Feynman gauge’’ replacement  $\sum_{\text{spins}} \epsilon^\mu(p, \lambda) \epsilon^{*\nu}(p, \lambda) \rightarrow -g^{\mu\nu}$  as is commonly done in QED. This replacement introduces unwanted longitudinal components into the polarization vector and, unlike the case of QED, these components do not vanish unless there is only one external gluon [48]. One way to obtain the correct, gauge-invariant, cross section is to use the appropriate projection operators for the transverse polarization states in the scattering process:

$$\sum_{\text{spins}} \epsilon^\mu(p, \lambda) \epsilon^{*\nu}(p, \lambda) = -g^{\mu\nu} + \frac{2}{\hat{s}}(p^\mu q^\nu + p^\nu q^\mu) \quad (3.24)$$

where  $q^\mu$  is the 4-momentum of the other particle that accompanies the gluon in the initial or the final state.

Evaluating the last four gluon fusion graphs gives<sup>1</sup>

$$\begin{aligned} \frac{d\sigma(gg \rightarrow g\phi)}{d\hat{t} d\hat{u} dM^2} &= \frac{3 \alpha_s (2\pi)^{n/2} (M^2)^{(n-2)/2}}{16 \Gamma(\frac{n}{2}) \hat{s}^3 \hat{t} \hat{u}} \left( \frac{(c^2 + b^2)}{M_D^{n+2}} \right) [(\hat{u} + \hat{t})^4 + (\hat{u} + \hat{s})^4 + (\hat{t} + \hat{s})^4 \\ &+ 12 \hat{s} \hat{t} \hat{u} M^2] \delta(\hat{s} + \hat{t} + \hat{u} + M^2). \end{aligned} \quad (3.25)$$

The mass scale  $M_D$  used here is related to the scale  $\overline{M}_D$  defined earlier by  $M_D^{n+2} = (2\pi)^n \overline{M}_D^{n+2}$ . Notice that both the expressions for the gluon-fusion and quark-annihilation processes are invariant under the exchange  $\hat{t} \leftrightarrow \hat{u}$ , as is expected on general grounds from the charge-conjugation invariance.

Note finally that since these expressions depend only on the dimensionless coupling combinations  $g^2 + g_5^2$  and  $c^2 + b^2$ , in what follows we set  $g_5 = b = 0$  and choose  $c \geq 0$  and  $g \geq 0$  without loss of generality.

<sup>1</sup>I am indebted to Peter Osland and Sherif Elgammal for drawing my attention to an error in my first evaluation of these graphs. I founded what the error was and it turned out to be negligible in its effects on my numerical results.

### 3.2.2 Proton-Proton Cross Sections of the hadronic processes

The cross section for proton-proton collisions is obtained from the parton-level results just calculated in the usual way, ie by convoluting with the parton distribution functions,  $f_i(x, Q^2)$ . For our later analysis we compute the cross section for the process  $pp \rightarrow \phi + \text{jet}$ , which has the form:

$$\sigma = \sum_{ij} \int dx_1 dx_2 d\hat{t} dM^2 f_i(x_1, Q^2) f_j(x_2, Q^2) \left. \frac{d\sigma(ij \rightarrow \phi X)}{d\hat{t} dM^2} \right|_{\hat{s}=x_1 x_2 E_{cm}}, \quad (3.26)$$

where the sum on  $i, j$  runs over the types of partons available in the proton and  $X$  corresponds to an energetic quark or gluon. Because we do not have analytic expression for these parton distribution functions, we perform the above integrals numerically using Monte Carlo techniques, as in the PYTHIA generator [49]. This works as follows. We first implement our calculated differential cross sections in the generator and then we perform the phase-space integration using the following constraints:

- We require the final jet transverse momentum to satisfy  $P_T^2 > P_{cut}^2$ , where  $P_{cut}$  ( $= E_{T,jet}^{min}$ ), is a minimum value which we specify below. Using the kinematical relation  $P_T^2 = \hat{t} \hat{u} / \hat{s}$ , where  $\hat{u} = M^2 - \hat{t} - \hat{s}$ , the following integration limits for  $\hat{t}$  are obtained:  $t_{min} < \hat{t} < t_{max}$ , where

$$t_{min} = \frac{1}{2} \left[ (M^2 - \hat{s}) - \sqrt{(M^2 - \hat{s})^2 - 4P_{cut}^2 \hat{s}} \right]$$

and  $t_{max} = \frac{1}{2} \left[ (M^2 - \hat{s}) + \sqrt{(M^2 - \hat{s})^2 - 4P_{cut}^2 \hat{s}} \right]. \quad (3.27)$

- Energy-momentum conservation implies the following upper limit for  $M^2$

$$0 \leq M^2 \leq M_{max}^2 = \hat{s} - 2\sqrt{\hat{s}} P_{cut}. \quad (3.28)$$

- Finally, the integration limits on the parton energy fractions are:

$$x_{min} \equiv \sqrt{\frac{\hat{s}_{min}}{s}} = \frac{2P_{cut}}{\sqrt{s}} \leq x_1, x_2 \leq 1, \quad (3.29)$$

where as usual  $s$  denotes the invariant initial energy of the proton-proton collision.

From this, we generate events randomly over the total phase-space volume and we assign weights to them using the differential cross section evaluated at the selected phase-space element. The events are then accepted or rejected proportionately to these weights by PYTHIA, which also performs the relevant hadronizations. After repeating this procedure a sufficient number of times, PYTHIA will sum the results and thus provide the numerical evaluation of the cross section. We have checked our numerical integration by recomputing the total cross section for graviton production, using the parton-level differential cross sections computed by Giudice *et al* [6], and by comparing it with their results. Figure 3.2 shows the agreement of both results.

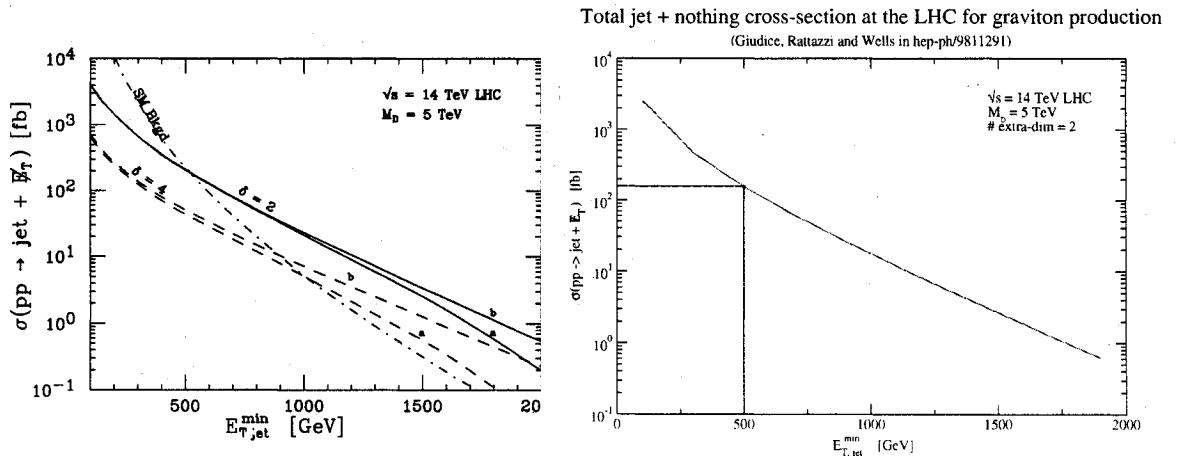


Figure 3.2: Comparison of the graviton cross section computed by Giudice *et al.* (left) and the one obtained by our numerical integration (right). We see that these results are consistent

### 3.2.3 Validity of the Low-Energy Approximation

As discussed above, our expressions for the parton-level reaction cross sections are only valid for parton energies well below the cut-off scale  $M_D$ . But since we can only specify the initial proton energies (and phase-space cut-offs like  $P_{cut}$ ), we cannot know for sure whether the numerical integration includes parton reactions which carry energies which are too large. If so, our calculation becomes unreliable in that part of phase space for which the probability of very-energetic parton processes cannot be neglected. In this section we define a proton-level criterion for estimating the extent to which high-energy parton processes pollute our calculations in various parts of

phase space. Our goal in so doing is to be able to choose upper limits for quantities like  $P_{cut}$  which minimize this pollution.

In order to do so, we compare in Fig. 3.3 the total proton-proton cross section,  $\sigma$ , calculated in the following two ways [6, 50]:

1. We calculate using the above parton cross sections for all possible parton energies.
2. We calculate using the above parton cross sections only if  $\sqrt{\hat{s}} < M_D$ , and set the parton-level cross-section to 0 if  $\sqrt{\hat{s}} > M_D$ .

The bottom panel of Fig. 3.3 shows this comparison when only the quark-bulk scalar couplings,  $g, g_5$ , are nonzero. The top panel shows the result assuming that only the gluon-bulk scalar couplings,  $c, b$ , do not vanish. The various curves plot  $\sigma$  against  $E_{T,jet}^{min} = P_{cut}$  for different choices for  $\hat{s}_{max}$  (with the effective dimensionful couplings  $\bar{g}$  and  $\bar{c}$  held fixed at some arbitrary reference value). When the two curves start to deviate, high-energy parton contributions are significant and we do not trust our calculation.

We use these curves to define the maximum value of  $P_{cut}$  which we may trust, given a value for  $M_D$  (and so also for the effective bulk scalar couplings). Quantitatively, we fix  $P_{cut}$  by demanding that the curves not differ by more than 10%. As is clear from the figure, the value of  $P_{cut}$  which is obtained in this way is smaller for the gluon-bulk scalar couplings ( $g = g_5 = 0$ ) than for the quark-bulk scalar couplings ( $c = b = 0$ ), and we use the lower of the two in the following calculations.

Notice that these two plots also indicate that for numerically equal couplings, the gluon-bulk scalar couplings dominate the cross-section at high energy, while the low-energy regime obtains bigger contributions from the quark-bulk scalar interactions. This is as expected from the effective Lagrangian, since the gluon terms involve an additional derivative (and so an additional power of  $E/M_D$  in cross sections) relative to the quark terms.

For fixed  $P_{cut}$ , we ask how large the effective bulk scalar couplings may be without introducing more than a 10% error into our calculations. This is illustrated in

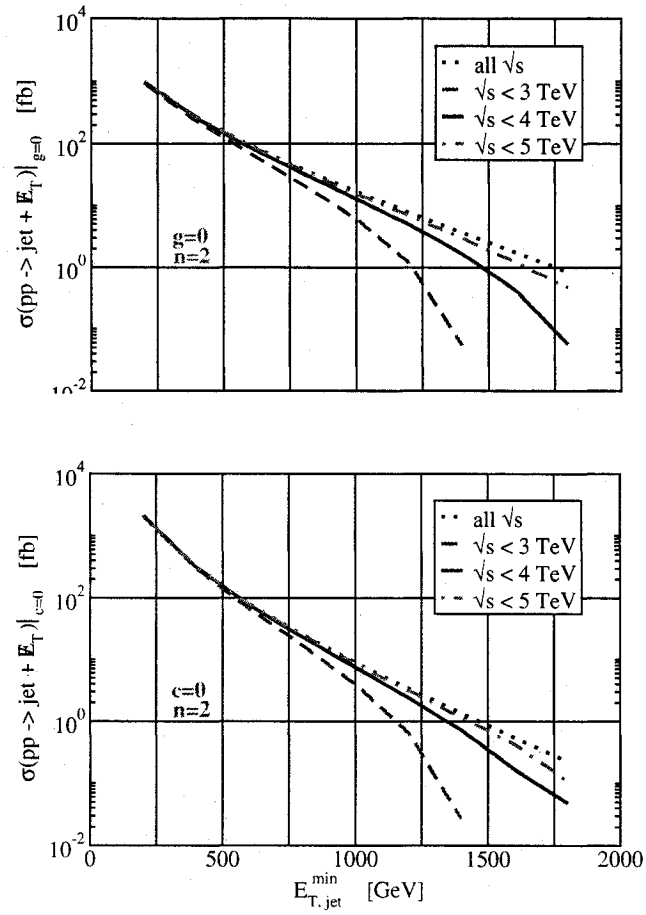


Figure 3.3: Total jet + nothing cross section for bulk scalar production at LHC to evaluate the validity limit of the phase space volume when: top) only the bulk scalar-gluons coupling is present; bottom) only the bulk scalar-fermions coupling is present. The curves are normalized to the cross section for graviton production at a value of  $E_{T,jet}^{\min}$  of 500 GeV.

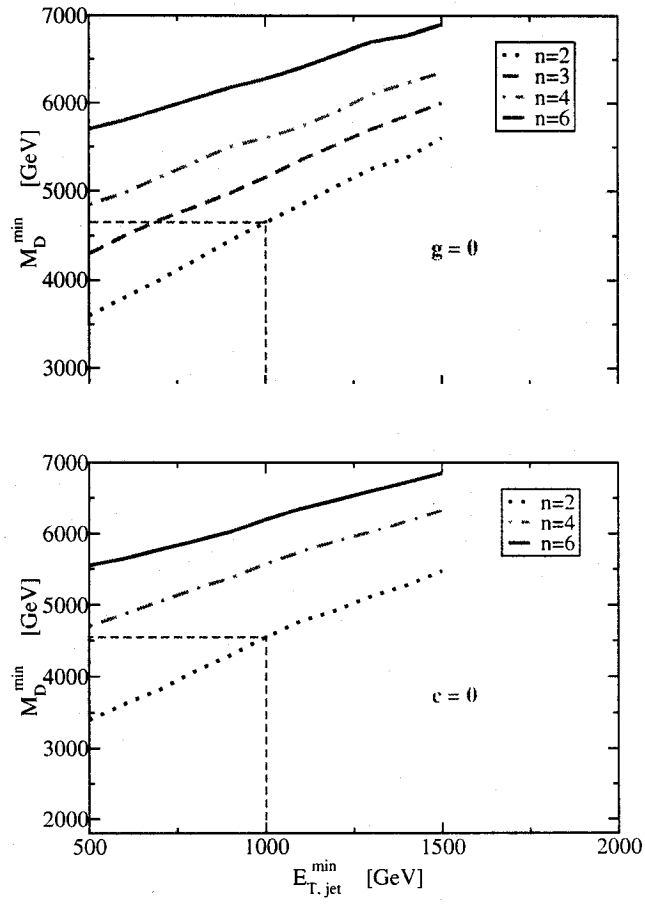


Figure 3.4: Evaluation of the minimum  $(4+n)$ -dimensional Planck scale for which the effective model is valid, at the 90% level, given a cut  $E_{T,jet}^{\min}$ , as explained in the text

Figs. 3.4, which show the smallest value of  $M_D$  which is permitted given a choice for  $E_{T,jet}^{min} = P_{cut}$ . This lower bound on  $M_D$  amounts to choosing an upper bound for the effective dimensional couplings,  $\bar{g}$  and  $\bar{c}$ .

In what follows we calculate the proton-proton cross sections assuming a value for  $P_{cut}$ , and so the condition  $M_D > M_D^{min}$  determines the domain of validity of our calculations. As discussed above, we determine  $M_D^{min}$  using gluon-bulk scalar couplings, since this is the stronger requirement. From this we find the minimum values for  $\bar{g}$  and  $\bar{c}$  for which a bulk scalar signal would be observable above the statistical Standard Model background at the  $5\sigma$  level.

### 3.2.4 $h - \phi$ production at colliders

Using the methods that we described in the last section, we can here compute the cross section at the tree-level for the production of bulk scalars radiated by a Higgs boson in  $p-p$  collisions at the LHC. Note however that since the effective coupling of  $\phi$  to Higgs is dimensionless, the following process is likely to dominate and that we also don't need to worry about the validity range of our results. Since Higgs production at the LHC is dominated by gluon fusion, our interest at the parton level is in the reaction  $gg \rightarrow H\phi$ , where both final-state particles are on shell. For most values of the Higgs mass, its dominant decays are either hadronic (the  $b\bar{b}$  decay dominates for Higgs mass smaller than  $\sim 130$  GeV) or involve jets in the final state ( $\sim 67\%$  of the electroweak gauge bosons decay in quarks), but such decay channels can be easy to miss because of the strong QCD background at LHC. Consequently, we choose instead to study the more rare, but cleaner,  $h \rightarrow \gamma\gamma$  channel. Figure 3.5 shows that for a SM Higgs boson of about 120 GeV, the branching ratio  $h \rightarrow \gamma\gamma$  is much smaller than other decay channels but, as we can see on figure 3.6, it has nevertheless high significance. It is extremely important to probe this mass region since this is the most likely region, according to the LEP measurements of Electro-Weak parameters [51]. The physical signal which bulk-scalar emission would produce in this channel is then two photons plus missing energy, as the scalar  $\phi$  escapes into the extra dimensions. [51]

The Feynman rule for the  $hh\phi$  vertex which follow from the effective Lagrangian

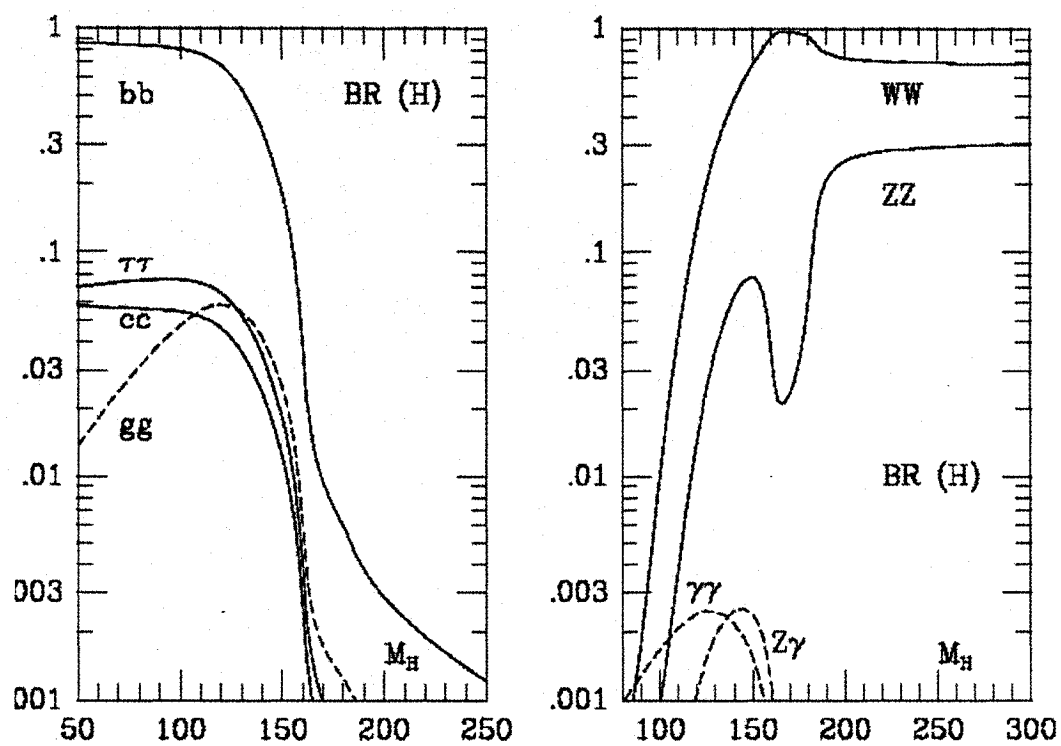


Figure 3.5: Branching ratio for the various decay channels of the Higgs boson in function of the mass of this particle.

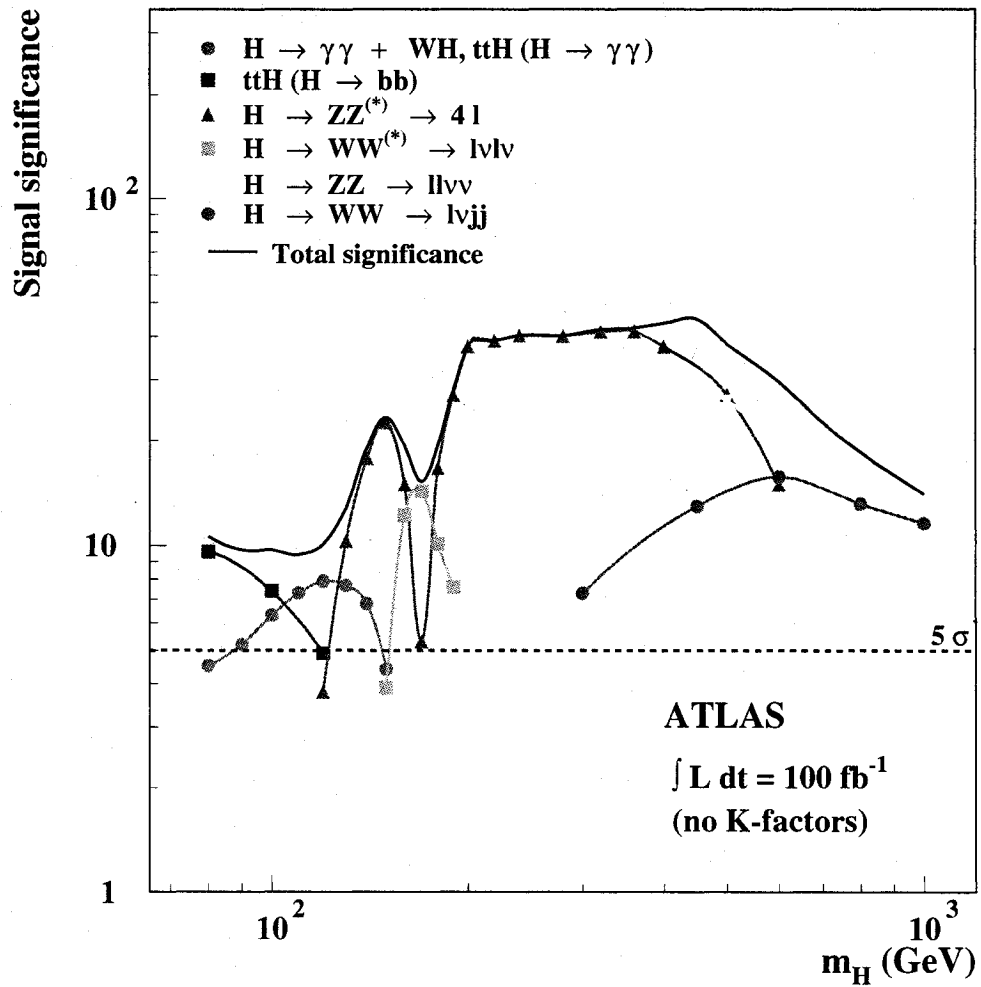
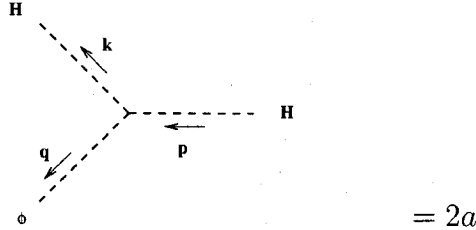


Figure 3.6: ATLAS sensitivity for the discovery of a Standard Model Higgs boson for each individual decay channels in function of the mass of this particle. This assume an integrated luminosity of 100 fb<sup>-1</sup> and a statistical significance computed as  $\frac{\text{signal}}{\sqrt{\text{bkg}}}$ . This figure is taken from [52]

of equation 3.15 can be evaluated using the method and the normalization of the canonical approach described above in section 3.2.1. In this case, it will be given by:



Here again we consider that the extra-dimensional phase-space factor of the bulk scalar momentum is given by equation 3.20. However, since here we explicitly restrain our phenomenological analysis to the  $n = 2$  extra dimensional SLED scenario, we can directly evaluate this equation for  $n = 2$  and we obtain:

$$\int_{\Omega_2} \frac{d^2 L}{(2\pi)^2} = \frac{dM_\phi^2}{4\pi}. \quad (3.30)$$

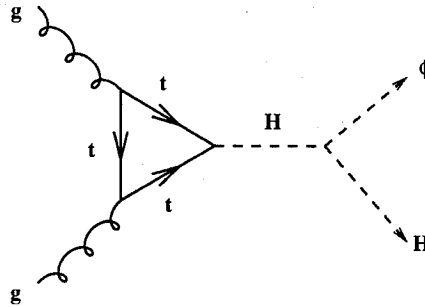


Figure 3.7: Parton-level Feynman graphs which dominate the Higgs/bulk-scalar production at the LHC.

The dominant amplitude at the parton-level is obtained by evaluating the Feynman graph of Fig. 3.7. Other graphs having the bulk scalar emitted by other particles give contributions which are suppressed relative to Fig. 3.7 by powers of external momenta divided by  $M_D$ . In fact, the most dangerous such graph is the Box diagram of figure 3.8, because a priori it could be divergent enough to dominate (ie higher momentum would, in that case, contribute significantly to the amplitude). Let us

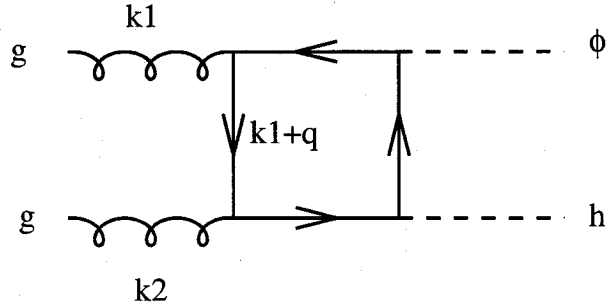


Figure 3.8: Parton-level Feynman graphs which could contribute to the Higgs/bulk scalar production at the LHC. We argued in the text that this contribution is too weak to be considered in this first analysis.

evaluate how divergent it is. If we evaluate the superficial degree of divergence of this graph, we will count four powers of momenta in the numerator due to the potentially divergent 4-momentum integral of the loop  $\int d^4q$  and four powers of momenta in the denominator due to the four fermionic propagators running in this loop. This evaluation would then predict a logarithmic divergence [39]. However, since the two gluons are taken to be on-shell (external), gauge invariance will reduce this divergence. The Ward identity (which is the diagrammatic expression of the conservation of the electric current, which, in turn, is a consequence of gauge invariance) requires that if we replace any external polarization vector  $\epsilon^\mu(k)$  by its 4-momentum  $k^\mu$ , the amplitude will vanish [39, 30]. This condition will be satisfied for the box diagram only if its amplitude is proportional to  $g^{\mu\nu}k_1^\sigma - g^{\mu\sigma}k_1^\nu$ , with a similar factor for the other gluon propagator. Each of these factors involve one power of the external momentum that can thus be “extracted from the loop”. This will appear mathematically in specific calculations after dimensional regularization. However, we can see this on more general ground [39]. If we expand this amplitude in a Taylor series about low external momentum ( $k=0$ ), we will have:

$$A = A_0 + A_1^\mu k_\mu + A_2 k^2 + \dots \quad \text{where} \quad (3.31)$$

$$A_n = \frac{1}{n!} \frac{d^n}{dk^n} A|_{k=0} \quad (3.32)$$

Thus, the Ward identity requires that all terms with less than two powers of momentum  $k$  in the Taylor series of this amplitude must vanish. Now since the amplitude

is integrated on the virtual momenta but is expanded on the external momenta, we can apply the derivative on the integrand with  $\frac{d}{dk} \frac{1}{(k+q)^2} = -\frac{1}{(k+q)^3}$ . We see that terms with higher  $n$  are less divergent. By requiring that the first two terms of this expansion be 0, this gauge invariance condition is equivalent to adding two powers of momentum to the denominator of the loop. The first non vanishing term has therefore  $4-4-2=-2$  degrees of divergence and hence this amplitude is finite and the leading term is proportional to the inverse cutoff squared of the theory ie  $\sim \frac{1}{M_D^2}$ . Therefore, we don't expect higher momentum than the external ones to contribute significantly to this amplitude. Moreover, since the fermion-bulk scalar vertex involves a coupling constant proportional to  $\frac{1}{M_D}$ , as we saw in section 3.1.2, we will have an overall suppression of the amplitude by a total of 3 powers of external momenta divided by  $M_D$ , as announced. This is consistent with the effective approach for which at low energy we would substitute this box diagram by a contact vertex coming from the effective interaction term  $\bar{\psi}\psi\phi h$  which is of dimension 7 and is thus suppressed by  $\left(\frac{E}{M_D}\right)^3$ , where  $E$  is the external energy scale. It is thus enough for the precision level of our analysis to restrict to the graph of Fig. 3.7.

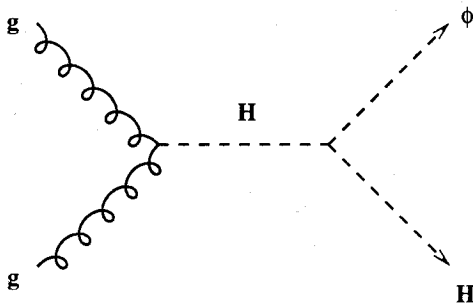


Figure 3.9: Effective parton-level Feynman graph for the direct production of Higgs/bulk-scalar production at the LHC.

In evaluating this graph we use the full momentum-dependent expression for the effective Higgs-gluon vertex which is obtained by evaluating the fermion sub-loop, along the lines of refs. [53]. Similarly to the box diagram case, gauge invariance requires that the amplitude of the graph of Fig. 3.7 be proportional to the momentum of each of the external gluon. Since, for on-shell gluons, there is only one combination

of 4-momenta that is non-zero and which has the appropriate tensor structure [39, 54], this amplitude is equal to the one of graph of Fig. 3.9 (the  $ggh$  vertex is the same as the  $gg\phi$  vertex given in section 3.2.1) up to invariant  $q^2$ -dependent functions which are obtained by the exact evaluation of the loop of Fig. 3.7 and which are given by the following form factor :

$$V_{ggh} = \frac{\alpha_s}{12\pi v} \mathcal{F} \left( \frac{m_t^2}{Q^2} \right), \quad (3.33)$$

with  $Q^2 = -q^2$  and  $q^\mu$  the 4-momentum carried by the virtual Higgs. Following the conventions of ref. [54], this form factor will be given by

$$\mathcal{F}(r) = 3[2r + r(4r - 1)f(r)] \quad (3.34)$$

where

$$f(r) = \begin{cases} -2 \left[ \arcsin \left( \frac{1}{2\sqrt{r}} \right) \right]^2 & \text{if } r > \frac{1}{4}; \\ \frac{1}{2} \left[ \ln \left( \frac{\eta_+}{\eta_-} \right) \right]^2 - \frac{\pi^2}{2} + i\pi \ln \left( \frac{\eta_+}{\eta_-} \right) & \text{if } r < \frac{1}{4}; \end{cases} \quad (3.35)$$

and  $\eta_\pm = \frac{1}{2} \pm \sqrt{\frac{1}{4} - r}$ . Note that it suffices to keep only the contribution of the top-quark loop.

The form factor  $\mathcal{F}(r)$  defined by the above expressions has the following well-known properties [53]. It vanishes for small  $r$ , ensuring the negligible contributions of all low-mass quarks in the loop. For large  $r$  it behaves as  $\mathcal{F}(r) = 1 + O(1/r)$ . For intervening values of  $r$ ,  $\mathcal{F}(r)$  grows to a maximum for  $r = O(1)$ , falling off on either side towards the two asymptotic limiting forms.<sup>1</sup>

The differential parton-level cross-section obtained in this way is therefore given by:

$$\frac{d\sigma}{d\hat{t} dM_\phi^2}(gg \rightarrow h\phi) = \left( \frac{a^2 \alpha_s^2}{144v^2} \right) \frac{|\mathcal{F}|^2}{(\hat{s} - m_h^2)^2}. \quad (3.36)$$

where  $\mathcal{F} = \mathcal{F}(m_t^2/\hat{s})$ ,  $m_h$  is the Higgs mass and  $M_\phi$  is the effective bulk-scalar mass as defined above. The quantities  $\hat{s}$  and  $\hat{t}$  denote the usual parton-level Mandelstam kin-

<sup>1</sup>Because of the small rise in  $\mathcal{F}(r)$  for  $m_t^2 < Q^2 < 4m_t^2$ , we find that use of the asymptotic expression  $\mathcal{F} \approx 1$  underestimates the size of the cross section by roughly 20%.

matic variables. As usual, the integrated cross section grows like  $M_\phi^2$ , and so is dominated by the highest bulk-scalar masses, reflecting the enormous extra-dimensional phase space which is available for such states.

The cross section for proton-proton collisions is obtained from this parton-level result in the usual way, by convoluting with the parton distribution functions,  $f_i(x, Q^2)$ . Since we are interested in the production of a real Higgs that decays into two photons for our later analysis, when performing these steps we compute the cross section for the missing-energy process  $pp \rightarrow \phi + h \rightarrow \gamma\gamma \cancel{E}_T$ . The result takes the following form:

$$\sigma(pp \rightarrow h\phi) = \int dx_1 dx_2 d\hat{t} dM_\phi^2 \left[ f_g(x_1, Q^2) f_g(x_2, Q^2) \left( \frac{d\sigma(gg \rightarrow h\phi)}{d\hat{t} dM_\phi^2} \right)_{\hat{s}} \right], \quad (3.37)$$

where  $\hat{s}$  is related to the  $pp$  center-of-mass energy,  $E_{cm}$ , by  $\hat{s} = x_1 x_2 E_{cm}^2$ . Finally, we obtain the cross section for  $pp \rightarrow \gamma\gamma \cancel{E}_T$  by multiplying the above expression by the appropriate branching ratio,  $B = B(h \rightarrow \gamma\gamma)$ . As we did in section 3.2.2, the numerical value for the total proton-proton cross section will be provided by the PYTHIA generator in which we have implemented this process.

When performing the phase-space integrations we use the following constraints:

- We require the transverse momentum of the final Higgs particle to satisfy  $P_T^2 > P_{cut}^2$ , where  $P_{cut}$  is a minimum value which can be chosen at generation level. (We set  $P_{cut} = 0$  in the analysis below.) This implies that the variable  $\hat{t}$  must lie in the range  $t_- \leq \hat{t} \leq t_+$ , with

$$t_{\pm} = \frac{1}{2} \left[ (m_h^2 + M_\phi^2 - \hat{s}) \pm \sqrt{(m_h^2 + M_\phi^2 - \hat{s})^2 - 4(m_h^2 M_\phi^2 + P_{cut}^2 \hat{s})} \right]. \quad (3.38)$$

- Energy-momentum conservation implies the following upper limit for  $M_\phi^2$

$$0 \leq M_\phi^2 \leq M_{max}^2 = \hat{s} + m_h^2 - 2\sqrt{\hat{s}(m_h^2 + P_{cut}^2)}. \quad (3.39)$$

- The parton energy fractions,  $x_i$ , lie in the range  $x_{min} \leq x \leq 1$ , with:

$$x_{min} = \frac{\hat{s}_{min}}{s} = \frac{P_{cut}^2 + \sqrt{P_{cut}^2 + m_h^2}}{s}, \quad (3.40)$$

and, as usual,  $s$  denotes the Mandelstam initial-energy invariant for the full proton-proton collision.

Higgs mass (GeV)	80	90	100	110	120	130	140	150
Cross-section (pb)	34.2	27.4	22.5	18.8	15.9	13.6	11.8	10.3
Branching ratio (%)	0.086	0.119	0.148	0.190	0.220	0.222	0.193	0.138
$\sigma \times B$ (fb)	29.4	32.6	35.6	34.9	30.2	22.7	14.2	5.9
SM $pp \rightarrow h$ (pb)	46.5	38.0	31.8	26.7	23.0	20.0	17.4	15.8
Mass resolution (GeV)	1.11	1.20	1.31	1.37	1.43	1.55	1.66	1.74

Table 3.2: Cross-sections for the signal process  $pp \rightarrow h\phi$  using the coupling value  $a = 0.5$ , and for  $pp \rightarrow hX$  as a function of the Higgs mass. Also shown are the branching ratio for Higgs decay into two photons and the mass resolutions ( $\sigma_H$ ) at high luminosity in ATLAS.

Table 3.2 shows the various pieces of the total cross section for  $pp \rightarrow h\phi \rightarrow \gamma\gamma \cancel{E}_T$  as a function of Higgs mass in the range 80 GeV – 150 GeV. The first row of the table gives the total cross-section for  $pp \rightarrow h\phi$  (in pb); the second row gives the branching ratio for the decay channel  $h \rightarrow \gamma\gamma$  (in percent), and the third row multiplies these to give the cross section for  $pp \rightarrow h\phi \rightarrow \gamma\gamma\phi$  (in fb). For comparison, the last two rows give the cross section for the Standard Model process  $pp \rightarrow hX$ , as well as the Higgs mass resolution in the ATLAS detector, for the process  $h \rightarrow \gamma\gamma$ , at high luminosity (as computed by the ATLAS collaboration in ref. [52]). For this table, the bulk-scalar process effective coupling constant,  $a$ , was set to 0.5, so as to yield a  $pp \rightarrow h\phi$  production cross section which is comparable to the SM process  $pp \rightarrow hX$ . This gives a rough indication of what size effective couplings might be observable, and so motivates the more detailed calculations which we will next describe.

\*\*\*

This concludes our theoretical analysis. In this chapter we first explained how and why the SLED scenario predicts interactions between bulk scalars and Standard Model particles at low energy. We deduced that such states are likely to be directly produced at the LHC. We then explained that the most general effective Lagrangian

that would be used to describe such direct production of bulk scalars at LHC is that of equation 3.15. Afterwards, we used this effective Lagrangian to compute the Feynman rules, and then the total proton-proton cross section for various processes of interest. This constitutes our physical predictions. We can now use the results of these calculations to study phenomenologically the signature of bulk scalar particles at the LHC and more particularly to evaluate the sensitivity of the ATLAS detector to couplings involved in the various processes presented above. However, before diving into such an analysis, it is worth to first give a quick overview of the LHC and the ATLAS detector.

---

---

## LHC AND ATLAS DETECTOR

---

---

In this chapter, we explain the experimental context in which the simulations and measurements are carried out. In high energy physics, it is the accelerators and the detectors that define the appropriate experimental framework. Accelerators fix the physical processes that can be produced and thus analyzed, while detectors determine what can be measured at a given precision. Now, physics beyond the Standard Model and, more precisely, tests of the SLED scenario require high energies and luminosity since the typical mass of the particles involved are high and the cross sections are low (recall that the number of events expected to be measured in one year is proportional to the product of the cross section and the luminosity integrated over one year). This imposes strong constraints on the design of a suitable experimental setup. These constraints are not exclusive to the SLED scenario, but are common to many scenarios beyond the Standard Model such as MSSM, technicolor, new gauge interactions or quarks and leptons compositeness. This physics has driven the design of the Large Hadron Collider (LHC) which therefore offers the possibility to study a SLED signal such as the production of bulk scalars presented in the previous chapter. Moreover, the need to accommodate the very large spectrum of possible physics signatures has guided the optimization of the design of the “general purpose” ATLAS detector [52]. ATLAS has thus the potential to greatly improve our understanding of fundamental physics, or at least to constraint new theories. In this chapter, we will briefly describe the LHC and the properties of the most important components of ATLAS detector.

## 4.1 LHC

The LHC is a proton-proton collider currently under construction in a 27 km circular tunnel at the European particle physics laboratory (CERN) near Geneva (see Fig 4.1)<sup>1</sup>. The machine will accelerate 2 beams of protons to energies of 7.0 TeV each and will collide them head-on in their center of mass to maximize the energy available to create new particles. It will also be able to accelerate heavy ions (Pb-Pb) that will be used in specific experiments. The 1250 TeV of center of mass energy that they expect for these heavy ions collisions will be a factor 30 higher than the Relativistic Heavy Ion Collider (RHIC) at Brookhaven National Laboratory. Four experiments (see Fig. 4.2) are planned to exploit the LHC physics opportunity. ATLAS and CMS (Compact Muon Solenoid) are two multi-purpose detectors designed to optimize the search for all the physics accessible at the LHC. ALICE (A LHC Ion Collider Experiment) is devoted to the study of heavy ion collisions. Finally, LHC-B is optimized to study B meson physics.



Figure 4.1: Picture of the LHC location in the Geneva area.

The LHC itself is the last step of an acceleration chain. The injector complex (see Fig. 4.3) indeed consists of a 50 MeV linac, a 1.4 GeV PSB (Proton Synchrotron

---

<sup>1</sup>All the figures and numbers presented in this chapter come from reference [52]. Many documents and PhD thesis made within the ATLAS Collaboration also provide clear summaries of the LHC and ATLAS detector design and performance [55]

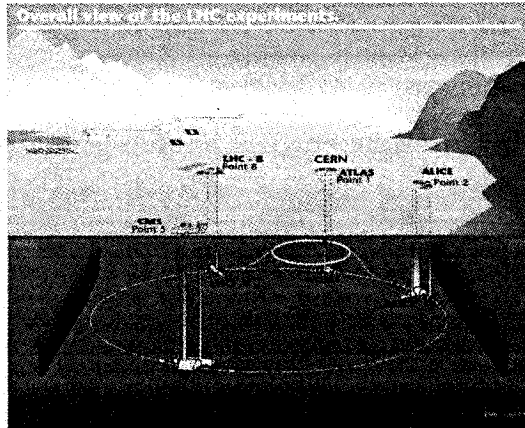


Figure 4.2: Picture of the four experiments on the underground LHC ring.

Booster), a 26 GeV PS and a 450 GeV SPS (Super Proton Synchrotron). These accelerators have already existed for some time, but have undergone a major upgrade in the last few years due to the demanding requirements of the LHC. It is expected that the first detectable collisions will be produced by 2007.

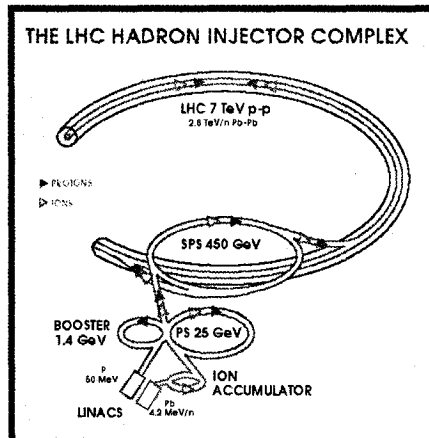


Figure 4.3: Picture of the LHC injector complex and of the main LHC ring.

Since the LHC will collide beams of like-charge protons, two separate beam-lines are necessary to allow the two proton beams to circulate in opposite directions. Two opposite magnetic guide fields are therefore needed to accelerate the colliding protons. However, due to space restriction in the LEP tunnel in which the LHC is being built, CERN has decided to use a magnet design that combines the two field guides into a

single magnet as shown in figure 4.4, rather than to have two separate ones. In order to meet the LHC energy requirement, the 14.2 meter dipole magnets needed to bend the proton beams must be superconducting (cooled with superfluid helium). This will yield a 8.33 Tesla field strength. In all, 1232 dipole magnets will be required for the LHC. Bending the proton beams to constrain them to a circular path is one thing; focusing these beams is another. In fact, natural divergences of the originally injected beams, small asymmetry in the fields and magnet alignment can cause spreading of the beam. This would reduce the luminosity which is proportional to the inverse cross-sectional area of the beams. To cure this, quadrupole magnets are used. They will act as magnetic focal lenses. Note that in counterpart, beam particles circulating in the synchrotron will not travel in ideal circular orbits, but will wander in and out of the circular path, in both the horizontal and vertical planes. This is called betatron oscillations [56]. At the LHC, this focusing will be achieved by 392 superconducting 3.1 meter quadrupole magnets of 6.86 Tesla.

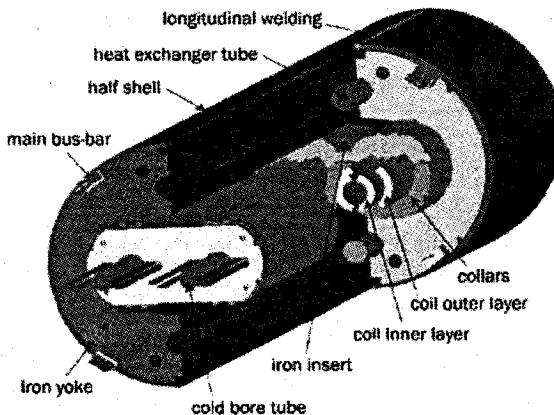


Figure 4.4: The cross section of an LHC standard two-in-one dipole in its cryostat.

As mentioned before, because new physics has generally low cross section compared to well-known Standard Model processes and because it is easier to detect leptonic decays of gauge bosons (which have small branching ratios), to suppress the high QCD backgrounds of proton collisions, the machine must work at very high luminosity. For the LHC, we expect a nominal luminosity of  $\mathcal{L} = 10^{34} \text{cm}^{-2} \text{s}^{-1}$  which corresponds,

when integrated over one year ( $\sim 10^7$ s), to  $100 \text{ fb}^{-1}$ . With a QCD cross section of  $\sim 100 \text{ mb}$ , this will produce about 23 collisions every 25 ns. In order to maintain such a luminosity, the longitudinal spread of a bunch of particles (bunch length) must be kept short. In fact, short bunch lengths keep degradation in luminosity caused by beam crossing angle to a minimum. Such short bunches will be obtained with RF cavities operating at 400 MHz. Since, as it is the case for the B field, RF frequency must be increased and synchronized (hence the name synchrotron!) as particle velocities increase, the voltage needed to operate these cavities will rise from of 8 MV at injection to 16 MV at collision. Note that each beam will have a separate RF system consisting of eight superconducting such cavities. Table 4.1 summarizes the LHC performance parameters.

Properties	Parameters value
Total CMS energy	14.0 TeV
Luminosity	$10^{34} \text{ cm}^{-2} \text{ s}^{-1}$
Circulating current	0.54 A
Time between collisions	25 ns
Bunches per beam	2835
Particles per bunch	$10^{11}$
Bunch length	7.5 cm
Bunch width	$15.9 \mu\text{m}$
Energy loss per turn	6.7 keV
Bending B field strength	8.33 T
Dipole magnet temperature	1.9 K

Table 4.1: Some parameters of the LHC

## 4.2 ATLAS

The ATLAS detector, as mentioned above, is designed to exploit the full physics potential of the LHC. For this reason, and in order for this general-purpose detector to perform well in the high luminosity environment provided by the LHC, very general constraints have been taken under consideration while designing and constructing it.

We summarize these requirements as follow:

- It must have a very good electromagnetic calorimeter for the identification of electrons and photons.
- The calorimeters must be hermetic for the jets, thus providing a good estimate of the transverse missing energy of an event.
- The tracking system must provide an efficient trajectography at high luminosity in order to permit a good measurement of the particle momenta and to allow for good reconstruction of leptons and photons. This is also important for b-quark tagging.
- It must be able to measure the momentum of muons independently of the tracker.
- It needs a large pseudorapidity ( $\eta$ ) acceptance.
- It must trigger and detect particles of low momenta.
- Because of the small bunch separation, the detector must use fast readout to avoid sampling events from several different simultaneous bunch-crossings (this will be the source of a noise called pile-up).
- Because of the high luminosity, it must be built with radiation-hard materials.

All these points are important for our SLED analysis, especially the second one since missing energy is the fundamental signal of any LED theory. These factors can be expressed more quantitatively as performance criteria, which we summarize

in table 4.2 and 4.3. The rest of the section is devoted to the description of the most important sub-detector parts (shown on figure 4.5), designed according to these requirements. This description will be a quick overview. One can find a detailed review of the design and performances of the ATLAS detector in the ATLAS Technical Proposal [52].

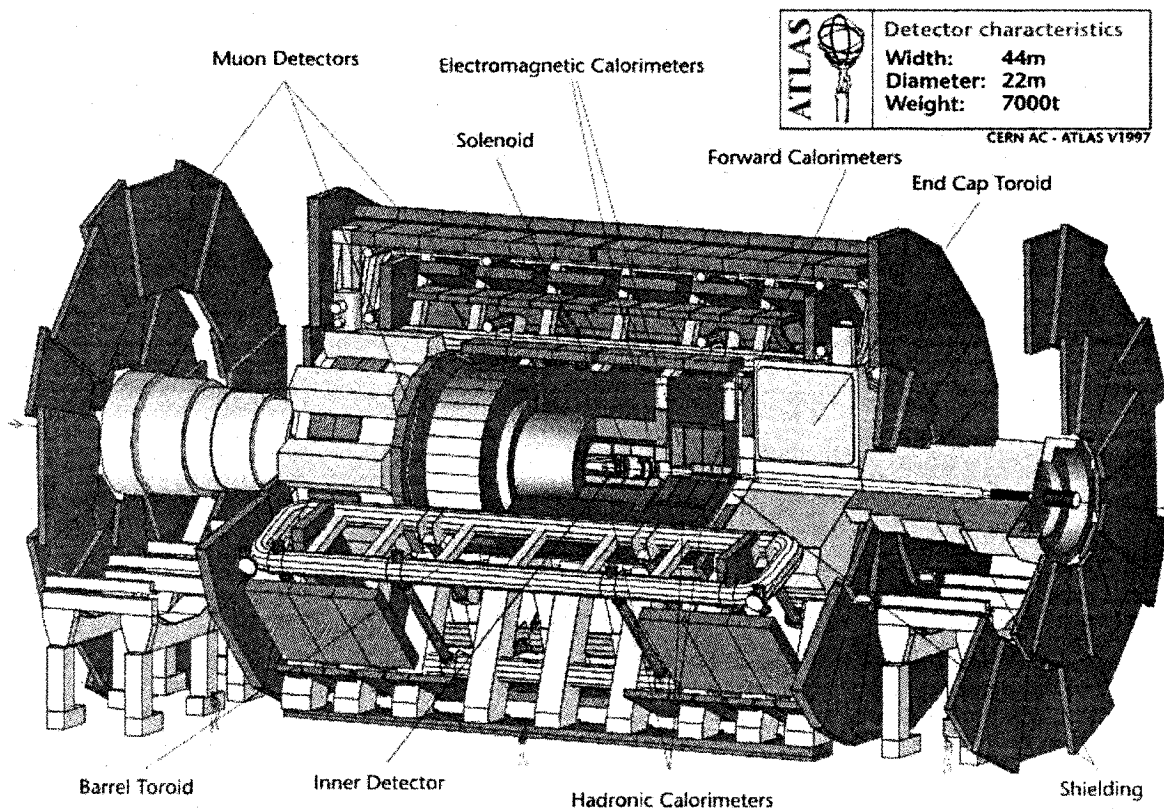


Figure 4.5: A cut-away view of the ATLAS detector.

#### 4.2.1 Transverse momentum observables

To understand the detector description that will follow, we first need to define the coordinate system and the terminology used in the general design of the entire detector. By convention, the beam direction defines the  $z$ -axis, and the  $x$ - $y$  plane is the plane transverse to the beam direction. The positive  $x$ -axis is defined as pointing from the interaction point to the center of the LHC ring, while the  $y$ -axis is pointing upwards. Since, the ATLAS detector has an approximate cylindrical symmetry, it is often more

Detector components	Characteristics and resolution ( $\sigma_E/E$ )	Coverage in $\eta$ (measured)	Granularity ( $\Delta\eta \times \Delta\phi$ )
EM calorimeter:			
Barrel	$10\%/\sqrt{E} \oplus 0.7\%$	$ \eta  < 1.475$	$\sim 0.003 \times 0.1$
End-cap		$1.375 <  \eta  < 3.2$	$\sim 0.004 \times 0.1$
Presampler	<ul style="list-style-type: none"> <li>•separate <math>\gamma</math>-<math>\pi^0</math> and <math>\gamma</math>-jet</li> <li>•b-tagging</li> <li>•measure direction of b</li> </ul>	$ \eta  < 1.8$	$\sim 0.025 \times 0.1$
Hadronic Cal.:			
Barrel	$50\%/\sqrt{E} \oplus 3\%$	$ \eta  < 1.7$	$\sim 0.1 \times 0.1$
End-cap		$1.5 <  \eta  < 3.2$	$\sim 0.1 \times 0.1$
Forward Cal.	$50\%/\sqrt{E} \oplus 3\%$	$3.1 <  \eta  < 4.9$	$\sim 0.2 \times 0.2$

Table 4.2: Performance objectives for the ATLAS calorimetry. Here, the granularity is defined in terms of the pseudorapidity  $\eta$  and the azimuthal angle  $\phi$ . Note that the numbers that are quote here are indicative. For example, the granularity change in the EM end-cap detector with decreasing  $\eta$  because of the geometry of that sub-detector.

System	Position	Area (m <sup>2</sup> )	Coverage in $\eta$ (measured)	Resolution ( $\sigma(\mu\text{m})$ )	Channels (10 <sup>6</sup> )
Pixel	1 removable barrel layer	0.2	$ \eta  < 2.5$	$R\text{-}\phi = 12, z = 66$	16
	2 barrel layers	1.4	$ \eta  < 1.7$	$R\text{-}\phi = 12, z = 66$	81
	4 end-cap disks on each side	0.7	$1.7 <  \eta  < 2.5$	$R\text{-}\phi = 12, z = 77$	43
Silicon Strips	4 barrel layers	34.4	$ \eta  < 1.4$	$R\text{-}\phi = 16, z = 580$	3.2
	9 end-cap wheels on each side	26.7	$1.4 <  \eta  < 2.5$	$R\text{-}\phi = 16, z = 580$	3.0
TRT	axial barrel straws		$ \eta  < 0.7$	170 (per straw)	0.1
	radial end-cap straws		$0.7 <  \eta  < 2.5$	170 (per straw)	0.32

Table 4.3: Performance objectives for the ATLAS inner detector. Here, the granularity is defined in terms of the transverse distance  $R$  to the beam-pipe in the pseudorapidity-azimuthal angle space (for any  $\phi$ ).

convenient to use a cylindrical coordinates system  $\{R, \phi, z\}$ , where  $z$  is defined as above,  $\phi$  is the azimuthal angle and  $R$  is the transverse distance to the beam-pipe. Rather than working with the polar angle we generally use the pseudorapidity variable defined as:

$$\eta = -\ln\left(\tan\frac{\theta}{2}\right) \quad (4.1)$$

which has the advantage that in the ultra-relativistic limit, ie in the limit where the particles can be considered massless, it is equivalent to the rapidity

$$y = \frac{1}{2} \ln\left[\frac{E + p_z}{E - p_z}\right] \quad (4.2)$$

The difference in rapidity of two Lorentz vectors is invariant under Lorentz boost along the  $z$  direction. Thus, quantities such as  $d\sigma/dy$  are independent of the boost of the scattering system in the  $z$  direction. Such a variable is then very useful for the description of processes in hadronic colliders because, in these experiments, the initial  $z$ -momenta of the primary partons are unknown. It is convenient to describe the momentum of the final state particles in terms of the transverse momentum  $p_T$ ,

the pseudorapidity  $\eta$  and the azimuthal angle  $\phi$ . Sometimes we will use directly the variable  $\eta$  and sometimes we will rather refer to the  $\eta$  ( $\theta$ ) -dependent variable  $R \equiv \sqrt{\eta^2 + \phi^2}$  as mentioned before.

Note that some particles, such as neutrinos and SLED particles, have a vanishingly small probability to interact with the detector. In principle the presence of such “invisible” particles can be inferred from an apparent non-conservation in the momentum of the observed ones. However, since we don’t know the initial  $p_z$  momentum of the system, we cannot deduce the  $p_z$  momentum of these undetectable particles. This is a particularly important example which shows that it is better to use observable variables that are independent of the boost in the  $z$  direction. In such cases, we will refer to the missing transverse momentum (or energy). To minimize the background for events where  $\cancel{E}_T$  is present as a distinguishing feature, we need a maximum coverage of the detector. As we have seen in the above performance tables, ATLAS provides a coverage angle up to  $|\eta| = 5$  which correspond to a polar angle of  $0.19^\circ$ . Particles emitted in more forward angles escape in the beam pipe. They are thus nearly longitudinal. Since we are interested in the transverse variables, this will not be of great importance for us except for very high energy jets. ATLAS therefore provides an approximately complete coverage.

#### 4.2.2 *The ATLAS Inner Detector*

The task of the inner detector is to reconstruct the tracks and vertices of charged particles with high efficiency and to provide a measurement of their momenta. It will also contribute to the identification of electrons, photons and muons and supply an important extra signature for short-lived particle decay vertices. It finally has a role to play in the tagging of b-jets, which is important in the b and top physics studies. It should therefore make many precise measurements of the positions of these particles along their tracks. In order to easily reconstruct tracks from these points, the individual active elements must detect particles with high efficiency, yet with a minimal probability of registering an error. In addition, they must have high granularity with a low average occupancy, so that a particular hit pattern can be

efficiently reconstructed into tracks. All this derives from the performance criteria of table 4.3.

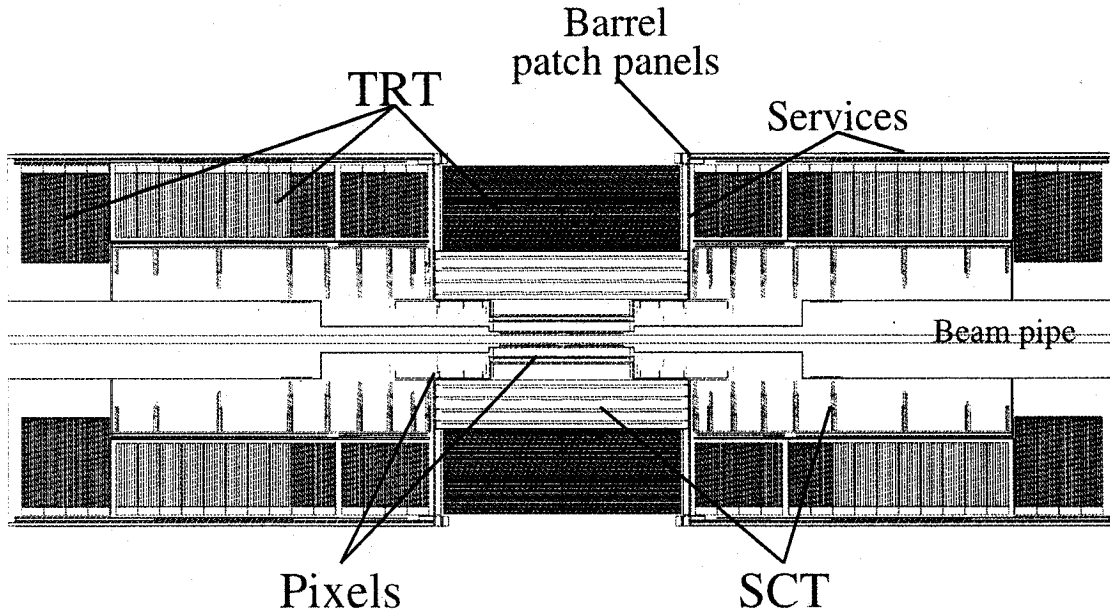


Figure 4.6: Cut-away view of the ATLAS inner detector.

To meet these requirements, the design of the inner detector combines three different subsystems, as shown on figure 4.6, inside a 2 Tesla solenoidal B field directed along the beam axis (to bend the tracks of charged particles according to their momenta in the transverse direction). These are, from the innermost layer out:

- the pixel detector: high-precision and very fine granularity (140 M channels) layers of silicon detectors nearest the interaction point;
- the semiconductor tracker (SCT): 4 double layers of silicon microstrip precision detectors;
- the transition radiation tracker (TRT): a gas filled straw tube tracker which contains a wire under high voltage thus creating a radial electric field in which the particles ionized in the gas by the so detected charged particle will drift to be collected at the wire.

The pixel and SCT subsystems allow the track origins to be reconstructed and secondary decays to be found, while the TRT gives an excellent pattern recognition from a continuous measurement of the tracks and allows the electrons to be identified by their characteristic transition radiation. The combined system gives a momentum resolution of about 30% for track with a  $p_T$  of 500 GeV (recall that the curvature radius of a particle moving in an orthogonal B field is proportional to the momentum of this particle. Using this curvature to measure the momentum, the precision is therefore poorer for higher momentum tracks). This is supplemented by the energy measurement in the calorimeters. The curvature measurement also ensures an identification of the charge sign for particles of higher energy, allowing detailed measurements of vector boson decays, for example. Finally, these measurements allow 50% of b-jets to be identified while reducing the background from light-quark jets by a factor  $> 70$ .

Note that this design faces two constraints. First, the number of precision layers is a compromise between the competing demands of precise track-finding and accurate energy measurement. In fact, each additional layer increases the material between the interaction point and the calorimeter and so degrades the calorimeter performance. Second, the components must be able to tolerate and operate in the high-radiation environment. These complementary technologies therefore give an excellent performance for physics channels of interest.

### 4.2.3 *ATLAS calorimetry*

ATLAS calorimeters are designed to provide fast signals used to decide whether to read out the detector or not (known as triggering) and to provide precision energy measurements of electrons, photons, jets and missing transverse energy. Another design requirement is the ability to separate different types of particles based on the shape and the structure of the showers developed in the calorimeter. In fact, high energy electrons and photons incident upon matter initiate particles cascade from pair production ( $\gamma \rightarrow e^+e^-$ ) and bremsstrahlung ( $e \rightarrow e\gamma$ ) due to the electric field of the matter nucleons close to which they pass. This will develop a shower. Having a

shape characterized longitudinally by the radiation length ( $X_0$ ) of the material and by narrow transverse profiles. Similarly, particle cascades are produced when high energy hadrons interact with dense material, where multiplication occurs through a succession of inelastic hadronic-nuclear interactions. Such showers will involve a larger lateral spread than the purely electromagnetic case. Because of this difference between the electronic and hadronic calorimetry, two different systems using different types of calorimetry technology are used in ATLAS: liquid argon calorimeters and scintillating plates. The various ATLAS calorimeters are presented in the figure 4.7

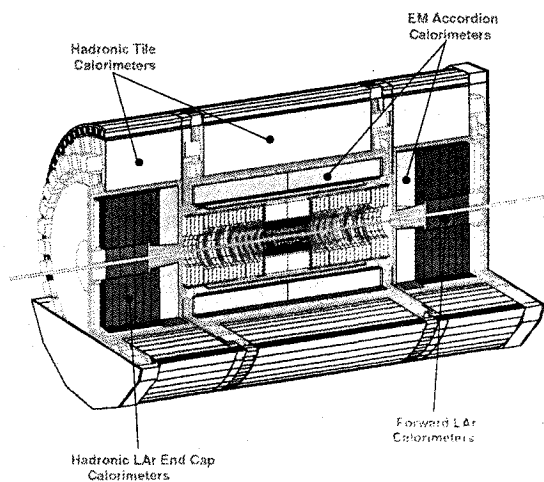


Figure 4.7: Cut-away view of the ATLAS calorimetry.

The electromagnetic calorimeter uses lead as an absorber and liquid argon as active material. The lead plates are bent into an “accordion” shape which allows readout towers to point toward the interaction region. A major advantage of this design is that it allows calorimeter readout with minimal dead space (ie. it is hermetic!). This sub-detector is divided into three longitudinal sections. The first one serves as a pre-sampler. It is used for discrimination between gammas and narrow hadronic jets. In fact, since the shower from photons tend to start farther (after the first pair production interaction) jets constitute an important background, when misidentified, to the

study of the process  $h \rightarrow \gamma\gamma$ , for example, of great interests for our analysis. The complete EM calorimeter allows to find the interaction point by providing information needed to reconstruct the directions of photons.

The hadronic barrel calorimeter uses iron as absorber while the active material is constituted of plastic scintillating tiles aligned with the particles direction. This design allows hadronic showers to be measured (sampled) in a homogeneous manner. However, the hadronic end-cap calorimeter uses a different technology than the one used for the hadronic barrel because radiation damage would severely degrade the scintillators. It thus uses parallel plate copper and liquid argon technology. This also contains the absorption of hadronic shower in a limited volume.

Finally, a forward calorimeter will be installed to reduce the uncertainty on missing transverse energy and to provide better detection of jets in the forward region. This ensures good coverage in  $|\eta|$  from 3 to 5. This subdetector, composed of three longitudinal sections, uses a structure of rods and tubes to create very thin cylindrical gaps filled with liquid argon. The first section is made of copper, but the two others are made of a very dense material to contain the showers longitudinally and laterally: tungsten. Considering the entire calorimetry at ATLAS, it is estimated that the overall missing transverse energy resolution will be  $\frac{\sigma}{\cancel{E}_T} \approx \frac{0.48}{\sqrt{\sum E_T/\text{GeV}}}$ , where the sum is taken over the transverse energy in all the calorimeters. Other specifications of the calorimeters are summarized in table 4.2

#### 4.2.4 ATLAS Muon system

The quality of the muon measurements has been one of the guiding design criterion for the ATLAS experiment. In fact, high momentum final state muons are among the most promising and robust signatures of physics at the LHC [52]. On this basis, ATLAS has decided to use a high resolution muon spectrometer, independent of the inner detector, which can provide muon momentum measurements over a wide range of transverse momenta (from 5 GeV to  $\sim 1$  TeV) and a good angular coverage ( $|\eta| < 2.5$ ). It also has a fundamental role to play in the triggering. This system uses three layers of MDT chambers (Monitored Drift Tubes) to achieve precision

measurements of muon tracks in the central region ( $|\eta| < 1.5$ ) and CSC proportional chambers (Cathode Strip Chambers) in end-cap regions. There are separate sets of chambers employed for triggering. All this is set in a magnetic field of 4 Teslas generated by 8 superconducting coils of 25 meters long each.

#### 4.2.5 Trigger

In total, the ATLAS detector has more than  $10^8$  electronic channels. This would amount to an output of about 40 terabytes of data per second, the storage of which would be clearly unmanageable. Most of the information will come from QCD noise, due to high energy proton collisions, which is not of much interest in the search for new physics. Efficient event selection will therefore be extremely important. We require a rejection factor of nearly  $10^7$  while, at the same time, maintaining good efficiency for rare new physics phenomena. This is the capital task of a trigger system.

The ATLAS trigger system is based on three levels of selection. Figure 4.8 presents the architecture scheme of such a trigger system. Each subsequent level faces a lower event rate, and so can afford a higher level of sophistication per event. These levels are:

- Level 1:

The level 1 works for each proton-proton collision, ie at a rate of 40 MHz. It makes use of information coming from muon chambers and calorimeters. It must take a decision within  $2 \mu\text{s}$ . During that time, events will be kept in “pipeline” memory. This trigger level is expected to reduce the rate of potentially interesting events to 100 kHz.

- Level 2:

The level 2 trigger must reduce the acceptance from 100 to 1 KHz. It will organize the information in “Region Of Interest” (ROI) and will select events which have jets and electrons. It must process the data within 10 ms.

- Level 3:

The third and last level, also called the “event filter”, will provide a complete

event reconstruction in 1 second. The output rate expected will be of about 100 Hz.

This will leave us with still 1 Petabyte (a million of Gigabytes) of raw data each year. A powerful grid network is under study to analyze and store this enormous quantity of information.

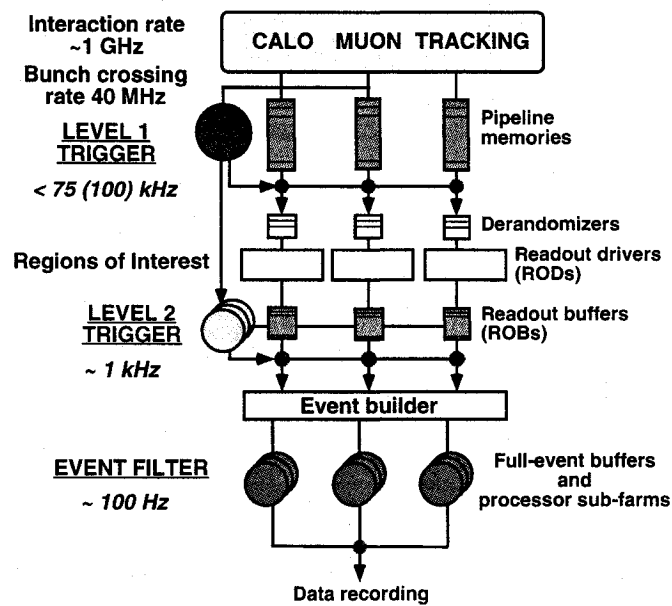


Figure 4.8: Architecture of the three level trigger system of ATLAS.

## PHENOMENOLOGICAL ANALYSIS

So far, we have calculated the total cross section for the production of a bulk scalar in association with a jet, or in association with a Higgs boson that further disintegrates in two photons. We have then seen that the experimental signal for such processes is jets plus missing transverse energy or two photons plus missing transverse energy. However, in both cases, these cross sections were given as functions of free parameters: gluon-scalar dimensionless coupling  $c$ , fermion-scalar dimensionless coupling  $g$ , fundamental Planck scale  $M_D$  and dimensionless Higgs-scalar coupling  $a$ . If we knew the theoretical value of these parameters, we would be able to say whether or not we expect such signals at the LHC. But in our analysis we preferred to stay as general as possible, not favoring any given model (remember that in the SLED proposal, no explicit complete model exists, nor the specific properties of the bulk scalar predicted). Our phenomenological task is thus to use the general physical predictions computed in chapter 2 to determine the ATLAS sensitivity to each of the free parameters controlling the interaction of a generic effective bulk scalar with Standard Model particles. This will therefore permit to evaluate the parameter space in which SLED predictions can be reliably tested at the LHC by these channels. If, later on, one provides us with a specific model of a bulk scalar interacting with Standard Model modes, our analysis will then allow to determine if this particular theory is testable or not at ATLAS.

Now, since we don't have real experimental data yet, how can we determine the sensitivity of ATLAS to any physical process? The approach will be a "phenomenological analysis" which consists in simulating the signal of interest in the ATLAS

experimental environment and finding observable criteria that would allow one to distinguish this signal from all the anticipated background events. Given a specific criterion for claiming a discovery, we can determine for what values of the free theoretical parameters such discovery will be possible.

We saw in the previous chapter that the LHC and ATLAS detector are designed (and under construction) and that the expected performance has been evaluated. To make these predictions, the ATLAS designers have made use of well known models of interactions of particles with matter to simulate, given the chosen detector design, the signals in ATLAS of all the known particles at various energies and angles. Here we will take as input particles produced in our processes of interest, and account for detector effects in the simulation of our processes. Of course, we will also simulate the background events in such a way that our phenomenological analysis will be a true estimate of what the real experiment will be.

Before studying the processes  $pp \rightarrow \text{jet} + \cancel{E}_T$  and  $pp \rightarrow \gamma\gamma + \cancel{E}_T$  in detail, let us state more technically what our simulation procedure involves.

## 5.1 Simulations

The complete simulation procedure is performed in three specific steps. The first one is the *generation*. This step has been described in chapter 2. We have seen there that it consists in using Monte Carlo techniques to randomly choose points in the phase space volume specified by the integration limits computed analytically and in evaluating, for each of the selected points, the differential cross section of the process (defining weights) and the 4-vectors describing this event. The generator program, PYTHIA in our case, will then accept or reject events according to their respective weights. The generating step provides us with a set of four-vectors and of particle labels that correspond to the theoretical final state. This will be the input of the detector simulation, as we mentioned above. Note that a generator like PYTHIA does not only compute the total cross section (numerical integration) and sort events according to their weight but it also [49]:

- computes the structure functions used in the numerical integration;
- produces the Initial State Radiation (ISR) and Final State Radiation (FSR),
- performs hadronization and fragmentation processes,
- decays short-lived unstable final state particles (Higgs, etc),
- provides statistics on generation and events history.

We properly assigned parton flavors to each event according to the **CTEQ 5L** parton distribution function [58] evaluated at the renormalization scale  $Q^2 = \frac{1}{2}M_\phi^2 + p_T^2$  in the case of the jets +  $\cancel{E}_T$  analysis and  $Q^2 = \frac{1}{2}(m_h^2 + M_\phi^2) + p_T^2$  for the the  $\gamma\gamma$  +  $\cancel{E}_T$  one. We then applied the appropriate color flow between the partons following the “Les Houches accord” [workshop on physics at TeV colliders, Les Houches 2001]. This is essential, if PYTHIA is to perform properly the hadronization.

The second step is the *simulation* itself. It consists in passing the PYTHIA generator output to a fast ATLAS detector simulator code that will, among other things, account for most important detector effects and provide [59]:

- jet reconstruction in the calorimeter;
- momentum/energy smearing for leptons and photons;
- magnetic field effects;
- missing transverse energy due to the detector resolution;
- list of reconstructed charged tracks;
- definition of isolated leptons and photons;
- response to the triggering.

Although a complete and full ATLAS simulation using GEANT 4 exists, it requires enormous computing time and the reconstruction algorithms are not yet complete and

debugged. For the sake of our analysis, we are not very sensitive to a detailed account of detector effects. We use a fast simulation program of the ATLAS detector, called ATLFAST [59], to carry out the enumerated tasks.

The last step is the *reconstruction*. We can see from the enumeration above that ATLFAST performs this step to a large extent. Another program, called ATLFAST-B, completes the job by providing useful routines which:

- randomly simulates b-tagging of jets labelled by ATLFAST;
- gives a  $p_T$  dependent recalibration of jet energies;
- randomly simulates  $\tau$ -tagging and  $\tau$ -veto.

However the efficiencies for rejection of  $\gamma$ /jet,  $\gamma$ /lepton and jet/lepton are not yet implemented and must be introduced by hand in any analysis.

We are now ready to summarize our detailed analysis and their results.

## 5.2 *jet+bulk scalar signal*

The first thing to do before starting the complete analysis<sup>1</sup> on the sensitivity limits of ATLAS to the free parameters of our effective theory is to quickly check if there are at least few relevant values of these free parameters that can provide a possible signal protruding out of the backgrounds. These values will then serve as a reference case for running the programs. To this end, a useful choice would be a set of couplings for which the low-energy approximation applies (see sect. 3.2.3) and for which the proton-proton cross section would be of the same size as the cross section required for a  $5\sigma$  discovery of the graviton production (as evaluated by[50]). The reference dimensionless effective couplings, when  $P_{cut} = 500$  GeV,  $M_D = 5$  TeV and for  $n = 2$  extra dimensions, have been evaluated to be  $g \simeq 0.70$  or  $c \simeq 0.41$ . These couplings are reasonable from the point of view of the effective theory because the  $g$  and  $c$  obtained

---

<sup>1</sup>The analysis and the results that I will present in this section have been published in [43]. A full simulation analysis based on my work has been done by Ola Oye and have been published as an ATLAS note [57]. Its results confirm my analysis.

in this way are smaller than unity. Notice that the existence of such couplings shows that there exist scenarios for which the bulk scalar production would be as important as graviton production, proving therefore that they can compete.

Note finally that the following analysis is independent of this choice of reference values. This will become evident later on.

### 5.2.1 Standard Model Backgrounds

As we mentioned before, if bulk scalars are produced in association with a jet in proton collisions, the events can be found by searching for a jet plus missing energy:  $pp \rightarrow \text{jet} + \cancel{E}_T$ . The Standard Model background to this process originates from events having neutrinos in the final state. The principal backgrounds of this type and their cross-section in the phase space regions  $E_{T,\text{jet}}^{\text{min}} > 500$  GeV and  $E_{T,\text{jet}}^{\text{min}} > 1000$  GeV are given, following ref. [50], in Table 5.1. For comparison, the bulk scalar production cross section using our reference couplings — 2 extra dimensions,  $M_D = 5$  TeV,  $E_{T,\text{jet}}^{\text{min}} = 500$  GeV and  $(c, g) = (0.41, 0.70)$  — is  $\sigma = 156$  fb.

Processes	cross-section (fb)	
	500 GeV	1000 GeV
$pp \rightarrow \text{jet} + Z(\rightarrow \nu\nu)$	278	6.21
$pp \rightarrow \text{jet} + W(\rightarrow e\nu_e)$	364	8.57
$pp \rightarrow \text{jet} + W(\rightarrow \mu\nu_\mu)$	364	8.51
$pp \rightarrow \text{jet} + W(\rightarrow \tau\nu_\tau)$	363	8.50

Table 5.1: S.M. backgrounds to the bulk scalar production at ATLAS and their cross section for different phase space volume.

### 5.2.2 Analysis

We now determine a set of experimental cuts which will allow us to find the minimum values of  $g$  and  $c$  for which a  $5\sigma$  discovery is possible. These cuts will apply to jets and leptons. In the ATLAS detector, leptons are detected if they are emitted in the range of pseudorapidity  $-2.5 < \eta < 2.5$ . Because, in general, a particle (a cluster in the

E.M. calorimeter) will hit many detector cells, leptons will be defined as isolated if the energy deposited by other particles in a cone of radius  $\Delta R = \sqrt{(\Delta\phi)^2 + (\Delta\eta)^2} < 0.4$  is less than 10 GeV. For jet reconstruction, we also use a cone algorithm with a cone radius  $\Delta R = \sqrt{(\Delta\phi)^2 + (\Delta\eta)^2} = 0.4$ . With these conditions of reconstruction, we impose the following two cuts:

As a first cut we require:

**Cut 1:** No isolated lepton (electron or muon) with  $p_T > 6$  GeV is allowed in the event.

This eliminates most of the  $W \rightarrow e\nu_e$  and  $W \rightarrow \mu\nu_\mu$  events, leaving only those for which the leptons are not properly reconstructed in the detector. It does not eliminate events like  $W \rightarrow \tau\nu_\tau$  in which the  $\tau$  decays hadronically. However, in this case we expect to also have an energetic low-multiplicity jet which is opposite, in the azimuthal plane, to the principal jet. We see in Fig. 5.1 that a cut on the difference in azimuthal angles between the two most energetic jets can eliminate a significant fraction of this  $\tau$  background.

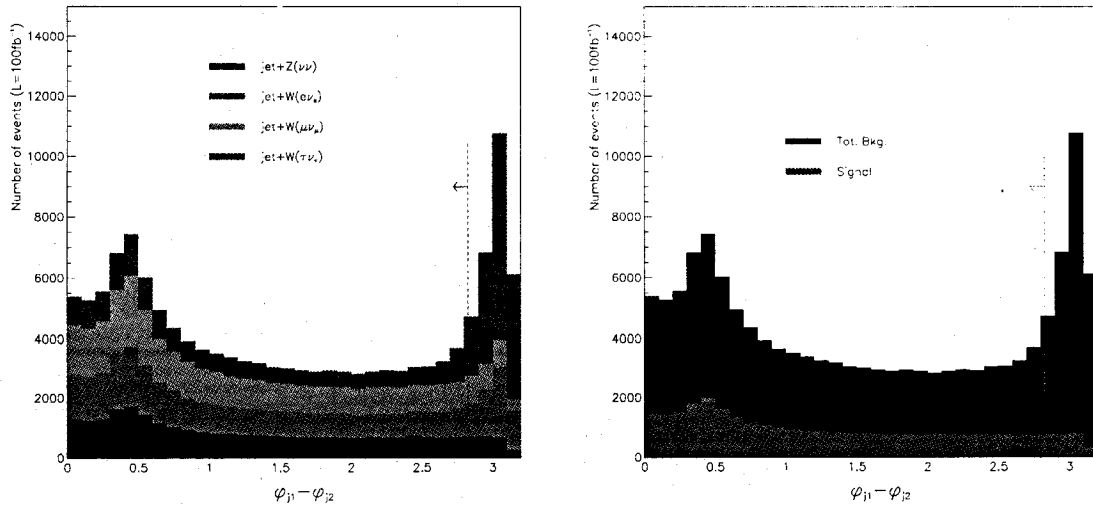


Figure 5.1: Distribution of the difference in the azimuthal angle between the two most energetic jets of an event for: (top) each of the backgrounds; (bottom) the signal and the total background on top of it.

We therefore impose the second cut:

**Cut 2:** We keep only events for which  $|\varphi_{j_1} - \varphi_{j_2}| < 2.285$  radians.

This cut is chosen to maximize the significance of the remaining signal as can be seen on figure 5

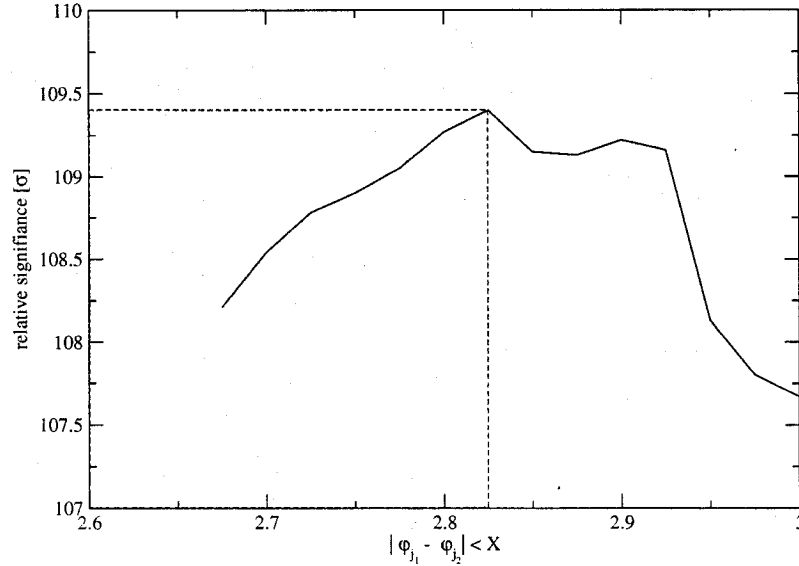


Figure 5.2: Significance of the signal for different values of cut 2

Fig. 5.3 shows the relative contribution of each process to the total background. After the above cuts have been applied, the most important background remaining is  $pp \rightarrow \text{jet}Z \rightarrow \text{jet} \nu\nu$ . Table 5.2 makes this more explicit, by breaking down the background and comparing the number of events to those of the signal after each cut is applied in succession, assuming an integrated luminosity of  $100 \text{ fb}^{-1}$ — which corresponds to one year’s running at the nominal LHC luminosity. We therefore expect a total of 36700 background events to remain after cuts.

Is this good enough? We estimate the number of signal events required for a  $5\sigma$  discovery using the following significance criterion:

$$\frac{S}{\sqrt{S+B}} > 5, \quad (5.1)$$

where  $S$  and  $B$  are respectively the number of signal and background events. For this level of background, we have a  $5\sigma$  discovery if more than 970 bulk scalar events are

Processes	$E_T^{min} > 500\text{GeV}$	# events after cut 1	# events after cut 2
jet+Z( $\rightarrow \nu\nu$ )	27760	27100	24940
jet+W( $\rightarrow e\nu_e$ )	36420	5224	1430
jet+W( $\rightarrow \mu\nu_\mu$ )	36370	957	866
jet+W( $\rightarrow \tau\nu_\tau$ )	36330	24600	9459
jet+bulk scalar	30960	30090	27720

Table 5.2: Number of signal ( $M_D = 5\text{ TeV}$ ,  $n = 2$ ,  $g = 0.70$  and  $c = 0.41$ ) and background events that survive each cut for an integrated luminosity of  $100\text{ fb}^{-1}$ . The cuts are defined in the text. Remember finally that the value of the coupling constants has each been chosen for rough comparison with the graviton production and are independent of the  $5\sigma$  reach of the bulk scalar production.

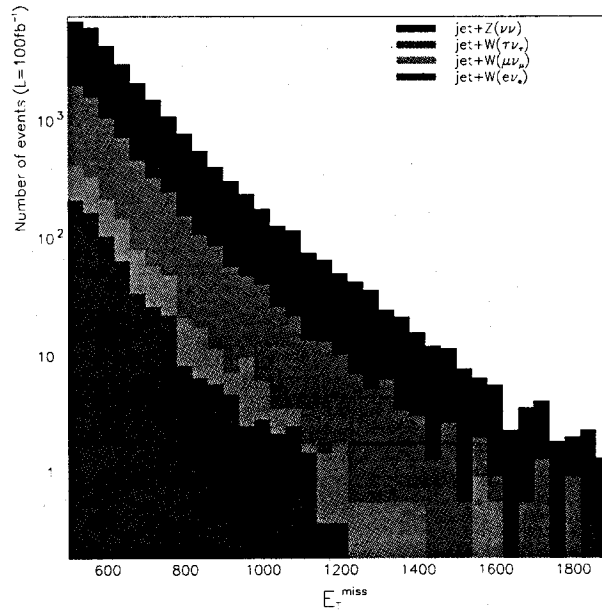


Figure 5.3: Contributions of different processes to the total background after application of the cuts, for an integrated luminosity of  $100\text{ fb}^{-1}$ .

detected, *i.e.* if the total cross section for the process is:  $\sigma(pp \rightarrow \text{jet} + \phi) > 10.9 \text{ fb}$ . In terms of the effective couplings ( $\bar{g}$  and  $\bar{c}$ ) this corresponds for  $n = 2$  to:

$$\bar{g} > 0.18 \text{ TeV}^{-1} \quad \text{if} \quad \bar{c} = 0, \quad (5.2)$$

or

$$\bar{c} > 3.2 \times 10^{-2} \text{ TeV}^{-2} \quad \text{if} \quad \bar{g} = 0. \quad (5.3)$$

Fig. 5.4 plots the number of events as a function of missing energy, for two choices of couplings. The choice in the bottom panel corresponds to the  $5\sigma$  discovery limit, and shows that the discovery would be due to an excess of events in the distribution of missing transverse energy at high energies.

Notice that the cross section required for discovery is determined by the background rate and so is the same for any choice for  $n$ , the number of extra-dimensions. In fact, as can be seen in eq. 3.25, the  $\hat{t}$  and  $\hat{u}$  dependence of the cross section does not depend on the number of extra dimensions. Only the effective coupling constants and the energy dependence depend on  $n$ , through the overall factor  $(M^2)^{(n-2)/2}$ . Since the angular distribution depends only on  $\hat{t}$  and  $\hat{u}$ , cut 2 has the same effect for all possible  $n$  (as does cut 1). Note finally that this also means that these numbers are independent of the reference coupling values that we use for running our simulation, as announced earlier. Let us now see what this analysis implies.

### 5.2.3 Results

We now turn to the central question: what range of effective couplings is likely to be detectable at the LHC? The following results will consider different possibilities for the number  $n$  of extra dimensions and will thus apply for a general LED scenario with supersymmetry in the bulk. We must however keep in mind that it is only  $n = 2$  that provides a framework in which we can build a solution to the cosmological constant problem. We will, in any case, see that the case  $n = 2$  yields a stronger signal, and therefore SLED will constitute a good motivation for testing our predictions. Let us first discuss about the free coupling constants  $g$  and  $c$ .

We have seen that any determination of the reach of the LHC must be made relative to a choice for  $E_{T,jet}^{min} = P_{cut}$ , since this plays a role in the reliability of the entire theoretical calculation. From Fig. 3.4 we see that the choice  $E_{T,jet}^{min} = 500$  GeV implies that the cross-section is sensitive to high-energy parton processes at less than the 10% level, provided  $M_D \geq M_D^{min}$ , where  $M_D^{min} = 3.60, 4.30, 4.85$  and  $5.70$  TeV for  $n = 2, 3, 4$  and  $6$  extra dimensions respectively. Given the value for  $M_D^{min}$  we then determine what values of dimensionless couplings produce an observably large cross section (*i.e.*  $\sigma > 10.9$  fb).

In fact, suppose  $(\bar{g}_{obs}^{(n)}, \bar{c}_{obs}^{(n)})$  are a pair of dimensionful couplings which each by itself produces a  $5\sigma$  signal (in  $n$  extra-dimensions) above the Standard Model background. Remembering how we defined the dimensionless free  $g$  and  $c$  couplings at section 3.1.2

we then have that the LHC can detect couplings which lie in the intervals

$$1 \gtrsim g > \bar{g}_{obs}^{(n)} (\overline{M}_D^{min})^{n/2} \quad \text{if } c = 0$$

or

$$1 \gtrsim c > \bar{c}_{obs}^{(n)} (\overline{M}_D^{min})^{1+n/2} \quad \text{if } g = 0.$$

The upper limit in these inequalities expresses the theoretical criterion that the calculation only makes sense for experimental energies below the cut-off scale  $M_D^{min}$ .

Fig. 5.5 shows the couplings which are accessible if both  $c$  and  $g$  are simultaneously nonzero. The shaded regions indicate the range of couplings which are too small to have detectable effects for various choices of the dimension  $n$ . The potentially observationally-interesting couplings are those which lie outside the ellipses, but inside the box defined by  $c < 1$  and  $g < 1$ . (Recall that, since only  $c^2$  and  $g^2$  enter into the cross sections, these plots should be interpreted as constraints on  $|c|$  and  $|g|$ .) So, if a particular SLED model ( $n = 2$ ) predicts values of couplings in these ranges, for example if such a model predicts  $g = 0.62$  and  $c = 0.15$ , our result says that ATLAS will be able to test the SLED hypothesis since this point in parameter space is outside the  $n = 2$  excluded region of our graph).

The constraints on the couplings depend on the number of dimensions  $n$ , fewer dimensions allowing better reach. If  $n = 2$ , couplings outside the innermost region are potentially detectable. For  $n = 3$  detectable couplings must lie outside the next-to-innermost region. Detection for the case  $n=4$  is unlikely for the dimensionless constant  $g$  in the limit of small  $c$ , but is possible if  $c$  is also nonzero. For more than 6 extra dimensions, detection of any signal is unlikely since the minimum value of coupling needed for a discovery when  $n = 6$  is  $(c, g) = (0.9, 3.3)$ . Any coupling in this region is far enough from the limits of validity of the calculation to be reliable. The  $n = 2$  requirement of SLED therefore encourages us since we are sensitive to a large range of parameters for a bulk scalar at LHC.

An alternative way of expressing the potential ATLAS reach for a bulk scalar

signal is in terms of the value of the fundamental Planck scale to which the detector might be sensitive. It is bounded on the low side by the requirement that the effective theory be a good approximation, and on the high side by the condition that the signal be detectable. Defining the effective upper limit by

$$M_D^{max} = (2\pi)^{\frac{n}{n+2}} \times \min \left[ \left( \bar{g}_{obs}^{(n)} \right)^{-2/n}, \left( \bar{c}_{obs}^{(n)} \right)^{-2/(n+2)} \right], \quad (5.4)$$

there are prospects for detection when  $M_D^{min} \lesssim M_D^{max}$ . Table 5.3 summarizes these results, with  $M_D^{max}$  calculated using the worst case:  $c = 0$ .

ndim	$M_D^{min}$ (TeV)	$M_D^{max}$ (TeV)
2	3.2	14.00
3	3.8	6.45
4	4.4	1.45

Table 5.3: Sensitivity of the ATLAS detector to the fundamental Planck scale  $M_D$  through the discovery of a bulk scalar signal, for  $c = 0$  and for an integrated luminosity of  $100 \text{ fb}^{-1}$ . For  $n \geq 4$ , observation of a signal is not possible.

In the more optimistic limit  $g = 0$ , the maximum value of the fundamental Planck mass to which the ATLAS detector is sensitive increases from 6.45 to 9.50 TeV when  $n = 3$ , and from 1.45 to 7.55 when  $n = 4$ . These results are summarized in Table 5.4. We find again that  $n = 6$  is the limiting case since for  $g = 0$ , we have  $M_D^{max} = 5.8 \text{ TeV} \approx M_D^{min} = 5.7 \text{ TeV}$ . From these two tables we also verify that SLED is testable with ATLAS. As we mentioned in chapter 1 that it requires  $M_D \gtrsim 10 \text{ TeV}$ , and we see here that ATLAS is sensitive to bulk scalars up to  $M_D \sim 14 \text{ TeV}$ .

A comparison of these results with those obtained from graviton emission [50] is also instructive, although some care must be taken in so doing because the graviton results were obtained using a more restrictive phase-space cut ( $E_T^{min} > 1 \text{ TeV}$ ), a different criterion for defining the validity region of the model and with a more conservative statistical estimator ( $S > \sqrt{7B}$ ). Tables 5.5 and 5.6 compare the sensitivity of ATLAS to  $M_D$  as computed using bulk scalar and graviton production, using these

ndim	$M_D^{min}$ (TeV)	$M_D^{max}$ (TeV)
2	3.60	14.10
3	4.30	9.50
4	4.85	7.55
6	5.70	5.80

Table 5.4: Sensitivity of the ATLAS detector to the fundamental Planck scale  $M_D$  through the discovery of a bulk scalar signal, for  $g = 0$  and for an integrated luminosity of  $100 \text{ fb}^{-1}$ . For  $n \leq 6$ , observation of a signal is possible.

more conservative criteria. The two tables differ in their choice of either  $g = 0$  or  $c = 0$ .

Table 5.5 also shows the existing non-accelerator limits on  $M_D$ , taken from ref. [60] (see also [33]). Unlike the situation for gravitons (which couple universally) these astrophysical bounds are more model-dependent when applied to bulk scalars because they relate the couplings of KK modes to electrons and photons, and so need not directly apply to the gluon and quark couplings of most interest for colliders.

c=0	Graviton		Bulk Scalar		limit from Astrophysics	
	$M_D^{min}$	$M_D^{max}$	$M_D^{min}$	$M_D^{max}$	$M_D^{min}$ (A)	$M_D^{min}$ (B)
n=2	$\sim 4.0$ TeV	7.5 TeV	4.35 TeV	5.45 TeV	O(90) TeV	$\sim 10$ TeV
n=3	$\sim 4.5$	5.9	4.85	3.65	5.0	0.8
n=4	$\sim 5.0$	5.3	5.35	3.20	$\lesssim 4$	$\lesssim 1$

Table 5.5: With  $c=0$ : comparison of the sensitivity of ATLAS to  $M_D$  for bulk scalar and graviton signals under the conditions  $E_T^{min} > 1 \text{ TeV}$ ,  $\frac{S}{\sqrt{7B}}$  and with indirect constraints from cosmology. The integrated luminosity is  $100 \text{ fb}^{-1}$ . For  $n \geq 3$ , observation of a bulk scalar signal is not possible since  $M_D^{min} > M_D^{max}$ . For the cosmology bounds, Scenario A means limits to neutron star heating by KK-decays, while scenario B corresponds to bounds from the cooling of SN1987A by KK-modes emission.

We see that the scenario where  $g \rightarrow 0$  gives the best case for detection, competitive with the graviton result, and that accelerator experiments are most sensitive to lower  $n$ . Although these tables indicate that for quark couplings the limits obtained may

g=0	Graviton		Bulk Scalar	
	$M_D^{min}$	$M_D^{max}$	$M_D^{min}$	$M_D^{max}$
n=2	~4.0 TeV	7.5 TeV	4.65 TeV	10.20 TeV
n=3	~4.5	5.9	5.15	7.75
n=4	~5.0	5.3	5.60	6.50

Table 5.6: With  $g=0$ : comparison of the sensitivity of ATLAS to  $M_D$  for bulk scalar and graviton signals under the conditions  $E_T^{min} > 1\text{TeV}$ ,  $\frac{S}{\sqrt{7B}}$  and with indirect constraints from cosmology. The integrated luminosity is  $100 \text{ fb}^{-1}$ . For  $n \leq 4$ , observation of a bulk scalar signal is possible.

be lower than the non-accelerator bounds, this is not alarming for SLED because of the model-dependence discussed above (see also sect. 2.4.4 for a discussion on this).

The difference between the cases  $c = 0$  and  $g = 0$  shows that ATLAS is likely to be only weakly sensitive to the bulk scalar Yukawa couplings (especially keeping in mind these are naturally expected to be at most of order  $v/\overline{M}_D$ , as explained in chapter 2), and a discovery is more likely to come from gluon-bulk scalar couplings. However, once a signal is seen we are unlikely to be able to decide directly on the relative importance between  $g$  and  $c$ . Therefore, even if the discovery of a significant bulk scalar signal at ATLAS should turn out to be possible, it may be impossible to completely determine its couplings.

#### 5.2.4 Graviton-Bulk Scalar Confusion

Should a missing-energy signal be seen at the LHC, how does one tell if it is due to gravitons or bulk scalars? We do not yet see a way to do so, despite the difference in their spins, for the following reasons:

- The bulk scalar production cross-section has an energy dependence which is similar to the graviton one, precluding the use of  $P_{T,jet}, \cancel{E}_T$  or any other function of energy to discriminate the two.
- Parton-level discriminants are not likely to be of practical use, because the center of mass energy of the hard scattering is not known in a  $pp$  collider such

as the LHC. Furthermore, the final state we consider consists of a single jet and missing transverse energy, so it is not possible to reconstruct the longitudinal component of momentum of the system of interacting partons, nor the angular distribution in the center of mass, nor the forward-backward asymmetry. Even if this were possible, we have checked that the discrimination between the shapes of the bulk scalar and graviton differential cross sections is difficult even at the purely theoretical parton level. Only gluon fusion processes lead to a small difference.

It is therefore important to find a way to prove or disprove the SLED scenario. If we adopt the LED perspective, we have the freedom to choose the value of the fundamental Planck scale  $M_D$ . The model is unproductive in this regard because nothing in the theory favors a specific value of  $M_D$  and if, after the test of experiment, we do not find a LED signal, we will have the freedom to say that  $M_D$  is beyond the scope of this particular experiment, making it impossible, therefore, to falsify the theory. This is a real disadvantage. In fact, nothing, a priori, precludes the possibility of bulk supersymmetries. On the contrary, since LED is a string inspired theory and that string theories are supersymmetric, we can indeed expect that the bulk space would also be supersymmetric. If it is the case, there is a strong possibility for bulk scalar or other bulk degrees of freedom to couple to brane particles similarly to the graviton. Since, as we just mentioned, we cannot distinguish the graviton from other bulk fields, considering only the possibility of such couplings is sufficient to prevent us from making any conclusion about the value of  $M_D$ , even if we detect a signal.

On the other hand, the SLED proposal allows a limited range of values for  $M_D$ . Thus, even if we cannot distinguish the graviton from a bulk scalar, we can predict the production rate for the graviton for  $n = 2$  and an excess in the number of measured events will thus be due to other bulk particles. We can therefore clearly predict and test properties of SLED models but not those of LED alone (for which we can just say if there is a signal or not).

### 5.2.5 *Summary and Conclusions on the jet+ $\cancel{E}_T$ signal*

We have computed the rate for the production of extra-dimensional scalars in  $pp$  collisions. Such particles arise in virtually all supersymmetric higher-dimensional theories. We saw however that all our general predictions are better motivated in the more predictive SLED scenario. Moreover, we saw that this scenario allows for the widest range of discovery for a bulk scalar with the ATLAS detector. We find that the cross sections for the reaction  $pp \rightarrow \phi + \text{jet}$  are similar in size and shape to those for graviton production, although the competing non-accelerator constraints on the couplings can differ because bulk scalars need not couple universally (unlike gravitons). We used simulation codes tailored to the ATLAS detector, and conclude that ATLAS can be sensitive to bulk scalar couplings, provided there are less than 6 extra dimensions. The sensitivity improves with fewer dimensions and is maximal for SLED predictions (specification of LED possibilities). Nontrivial windows of opportunity can be consistent with all bounds, therefore providing SLED with real possibilities of testing.

Generically,  $pp$  collisions are more sensitive to bulk scalar couplings to gluons than they are to couplings to quarks. Both couplings are considered in our analysis, and we find that observable quark couplings often push the limits of validity of the effective-field-theory description.

We are now ready to study a bulk scalar signal emitted from a Higgs.

## 5.3 *Higgs+bulk scalar signal*

There is another free parameter of our theory, mentioned at the beginning of this chapter, for which we want to fix the sensitivity range of the ATLAS detector: the dimensionless coupling  $a$  of a Higgs particle to a bulk scalar. This is a clear signal of SLED that does not exist for the graviton and that must dominate the previous signal. It is therefore of great importance to study it for establishing a test of this proposal. We will also see in the following analysis<sup>1</sup> that such a signal could be of great help

<sup>1</sup>The analysis and the results that I will present in this section have been published in [44]

in finding the Higgs boson itself. We will thus devote the rest of the chapter to this important SLED channel. Note that because the  $hh\phi$  coupling is dimensionless when  $n = 2$ , this analysis differs from the previous one not only for the processes considered but also because it does not depend on the scale  $M_D$ .

### 5.3.1 Standard Model Backgrounds

Since the bulk scalar,  $\phi$ , radiated by the Higgs would quickly escape into the extra dimensions, it should escape detection. The observed process is therefore  $pp \rightarrow \gamma\gamma$  with missing energy in the final state, and some backgrounds are the usual ones for the process  $pp \rightarrow h \rightarrow \gamma\gamma$ . As discussed in [52] these come in two types. First, there is an irreducible background consisting of genuine photon pairs produced by the Born process ( $q\bar{q} \rightarrow \gamma\gamma$ ), by the box diagram process ( $gg \rightarrow \gamma\gamma$ ) and by quark bremsstrahlung ( $qg \rightarrow q\gamma \rightarrow q\gamma\gamma$ ) as we can see on figure 5.6. Second there is also the reducible background — consisting of QCD jet-jet or  $\gamma$ -jet events — in which one or both jets are misidentified as photons [52]. These two sources of background are comparable in size, even though the reducible backgrounds have huge cross-sections compared to the irreducible ones. This is because there are compensating large rejection factors, thanks to the efficient photon/jet discrimination which is expected for ATLAS. These rejection factors have been evaluated to be  $2 \times 10^7$  or  $8 \times 10^3$  respectively, for jet-jet and  $\gamma$ -jet backgrounds. Once this rejection efficiency is included, the reducible background events number about 20% of the expected number of irreducible background events.

To the above backgrounds, we add processes with much lower cross sections, but which include neutrinos in the final state. In particular, we consider the associated production processes  $Zh \rightarrow \nu\bar{\nu}\gamma\gamma$ ,  $Wh \rightarrow \ell\nu\gamma\gamma$  and  $t\bar{t}h \rightarrow WWb\bar{b}$  where at least one of the Ws decay leptonically, with  $h \rightarrow \gamma\gamma$ . These backgrounds will be the most difficult one to eliminate, but their small production rate will preclude them from contributing significantly to the total background. Note however, that these events can themselves be considered as a significant SM signal for the SM Higgs search with

the ATLAS detector at the LHC<sup>1</sup>. We also take into account the processes  $Z\gamma\gamma$ ,  $Z \rightarrow \nu\bar{\nu}$  and  $W\gamma\gamma$ ,  $W \rightarrow \ell\nu$  which can also mimic the signal. All the backgrounds were generated with PYTHIA. For the cases of  $Z\gamma\gamma$  and  $W\gamma\gamma$ , we simulated the processes  $Z\gamma$  and  $W\gamma$ , with the second  $\gamma$  arising from initial or final state radiation. A  $p_T$  cut of 35 GeV was applied in these cases.

Processes	cross-section (pb)	Number of events
$pp \rightarrow \gamma\gamma$ (Born)	56.2	$5.62 \times 10^6$
$pp \rightarrow \gamma\gamma$ (box)	49.0	$4.90 \times 10^6$
$pp \rightarrow \text{jet}+\text{jet}$	$4.9 \times 10^8$	$2.50 \times 10^6$
$pp \rightarrow \text{jet}+\gamma$	$1.2 \times 10^5$	$1.50 \times 10^6$
$pp \rightarrow h \rightarrow \gamma\gamma$	$4.63 \times 10^{-2}$	4630
$pp \rightarrow Zh, Wh, t\bar{t}h$ $Z \rightarrow \nu\bar{\nu}, W \rightarrow \ell\nu, h \rightarrow \gamma\gamma$	$2.5 \times 10^{-3}$	250
$pp \rightarrow Z\gamma; Z \rightarrow \nu\bar{\nu}$	3.3	$3.3 \times 10^5$
$pp \rightarrow W\gamma; W \rightarrow \ell\nu$	5.6	$5.6 \times 10^5$

Table 5.7: SM backgrounds to the production of bulk scalars in association with the Higgs at ATLAS, their cross section (for an  $E_T^{\text{cut}}$  of 23 GeV) and the total number of events expected at ATLAS for an integrated luminosity of  $100 \text{ fb}^{-1}$  (after application of rejection factors).

Table 5.7 shows the cross-sections and the total number of events expected after the application of the above-mentioned rejection factors, for each background process. The table assumes an integrated luminosity of  $100 \text{ fb}^{-1}$ . Notice that a further reduction factor of around 80% for each photon must also be applied in addition due to the expected reconstruction efficiency of photons. Finally, following ref. [52], we incorporate the quark bremsstrahlung process in the simulation by scaling the two other irreducible backgrounds by 50% of the combined Born plus box contribution, after having applied isolation cuts in ATLFAST.

<sup>1</sup>Such a measurement can be useful in determining the strength of the Higgs coupling to gauge bosons. We completed this SM analysis and obtained a significance of  $8.5\sigma$  for a Higgs mass of 120 GeV and a cut of 66 GeV in  $\cancel{E}_T$ . We presented our result in an ATLAS note [45].

### 5.3.2 Analysis

We now describe a set of cuts which can be used to isolate those  $pp \rightarrow \gamma\gamma$  events which also involve significant amounts of missing energy. We then use these cuts to quantify the smallest size for  $a$  which can be expected to be detectable.

We first establish our criteria for identifying two isolated photons. In the ATLAS detector, photons are detected if they are emitted with pseudorapidity in the range  $|\eta| < 2.5$ . We consider such photons to be isolated if their transverse momentum satisfies  $P_T^\gamma > 5.0$  GeV, and if there is less than 10 GeV of energy deposited by all other particles within a cone of radius  $\Delta R = \sqrt{(\Delta\phi)^2 + (\Delta\eta)^2} < 0.4$  around the photon of interest.

Part of the reducible background consists of jets which are misidentified as photons, and so we need also define our criteria for jet reconstruction. For this we use the cone algorithm, with a cone radius of  $\Delta R = 0.4$ , a pseudorapidity coverage of 5.0 and a minimal jet energy threshold of 10 GeV.

The first cuts to be imposed are those which optimize the significance of the  $h \rightarrow \gamma\gamma$  signal for the standard Higgs search at ATLAS, as in [52]. To this end we require:

**Cut 1:** The two photon candidates, ordered in  $p_T$ , must have transverse momenta which are in excess of 40 and 25 GeV. (That is, we choose  $P_T \geq 40$  GeV for photon 1 and  $P_T \geq 25$  GeV for photon 2.)

**Cut 2:** Both photon candidates must lie in the pseudorapidity interval  $|\eta| < 2.4$  and have a pseudorapidity separation of at least 0.15 ( $\Delta\eta > 0.15$ );

**Cut 3:** The reconstructed mass of the two photons, the two jets, or the jet +  $\gamma$  final state must have an invariant mass which is sufficiently close to the Higgs mass. Quantitatively, we demand:  $M_H - 1.4\sigma_H < M_{\gamma\gamma} < M_H + 1.4\sigma_H$ , where  $\sigma_H$  is the  $h \rightarrow \gamma\gamma$  resolution quoted in table 3.2.

Assuming an integrated luminosity of  $100 \text{ fb}^{-1}$ , after imposing these cuts and a 80% efficiency for detecting each photon, we are left with a total of 45,000 background events, 1,500 standard  $h \rightarrow \gamma\gamma$  events and 16  $hZ \rightarrow \gamma\gamma \nu\nu$ . We know that the exact initial number of signal events —  $pp \rightarrow \gamma\gamma + \cancel{E}_T$  — depends on the value of  $a$  (e.g. 8930 events before the cut for  $a = 0.5$ ). Since this coupling value is unknown, it is impossible to say how many events will survive the cuts. However, by studying the distributions, we evaluate that 38% of this initial number of signal events will be left after imposing the cuts (this corresponds to 3393 events for  $a = 0.5$ ).

In order to decide whether the missing-energy signal can be winnowed out of the background, we first recall that the previous ATLAS analyses [52] indicate that these same cuts would permit the standard Higgs boson signal to be identified with a significance of  $6.2 \sigma$  (using  $S/\sqrt{B}$  as the significance criterion). After cuts, an effective coupling of size  $a = 0.5$  produces roughly the same number of  $pp \rightarrow h\phi$  events as from the Standard Model  $pp \rightarrow h$  process, for  $m_h = 120 \text{ GeV}$ , even if the cross section is somewhat lower. This is due to the fact that the final-state Higgs bosons are more transverse in energy, leading to a larger acceptance of photons. Therefore, we roughly expect couplings of this size to be detectable at the  $6 \sigma$  level given  $100 \text{ fb}^{-1}$  of data. The significance for the Higgs signal itself is thus doubled. Since the  $h\phi$  production rate scales like  $a^2$ , a coupling  $a = 0.44$  would correspond roughly to a  $5 \sigma$  significance. For couplings this large, roughly half of the Higgs particles are produced in association with  $\phi$  emission into the extra dimensions.

This situation is illustrated in Fig. 5.7, which shows both the Standard Model and Higgs- $\phi$  production events as a function of the invariant mass of the two photons, assuming a Higgs mass of  $120 \text{ GeV}$ . The signal for Higgs- $\phi$  emission is clearly visible on top of the irreducible background plus the standard Higgs signal. These figures are also qualitatively the same as those obtained for the standard  $h \rightarrow \gamma\gamma$  process alone, which are published in the ATLAS Detector and Physics Performance Report [52].

As might be expected, and as we shall now see explicitly, those events where Higgses are produced in association with bulk scalars can be more efficiently identified

by imposing a cut on the total missing energy of the event. This is shown in Fig. 5.8, which plots the number of background, standard Higgs and  $h\phi$  events as a function of the total missing energy,  $\cancel{E}_T$ . As this figure shows, very few background or standard Higgs events have more than 50 GeV of missing energy, while about half of the  $h\phi$  events do. The high energy tail in the background  $\cancel{E}_T$  distribution is due principally to the processes  $Zh$  and  $Wh$ .

The larger the missing energy required in the event, the more the background and Standard Model Higgs boson events are excluded from the event sample, but also the fewer  $h\phi$  events there are. Fig. 5.9 shows how this trade-off scales with the effective coupling  $a$ , by showing the  $5\sigma$  coupling reach which is obtained as a function of the size of the missing energy cut. In this figure the standard Higgs production is counted as part of the background when computing the significance, since our goal is to identify the  $5\sigma$  discovery potential for the particular process of Higgses produced in association with  $\phi$ 's. If we define a discovery signal as a sample of at least 10 events which has significance greater than  $5\sigma$ , then the smallest coupling for which discovery is possible (with  $100 \text{ fb}^{-1}$  of data) is  $a = 0.09$ .

These considerations lead to the optimal missing-energy cut:

**Cut 4:** The missing transverse energy of the entire event must satisfy:

$$\cancel{E}_T > 78 \text{ GeV.}$$

Imposing such a cut, 14.3 signal events are left on a total background of 8.2 events consisting of  $\sim 0$  events of  $\gamma\gamma + \text{QCD}$ , 8.0 events of  $h, Zh, Wh, t\bar{t}h$  and 0.2 events of  $Z\gamma\gamma$  and  $W\gamma\gamma$ . Note that systematic errors on the measurement of the  $\cancel{E}_T$  may be large. A proper evaluation of this uncertainty is beyond the scope of this study but we do not expect that it will affect significantly the main conclusions. Fig. 5.10 shows the number of events vs invariant two-photon mass for the limiting case where  $a = 0.09$ . We see from this figure that even this marginal case yields a clear peak at the Higgs mass, leaving unambiguous evidence for Higgs production in association with missing energy.

More generally, for larger values of  $a$  than the above limit, the significance for

discovery of the Higgs boson itself can be much improved, since the Standard Model backgrounds are considerably reduced. This can be seen in Fig. 5.11, which plots the significance of the  $\gamma\gamma$  signal as a function of Higgs boson mass, for several choices of missing energy cut. As is clear from this figure, the curves with a nontrivial missing energy cut are more significant than the one with no cut, simply because of the dramatic reduction of background relative to signal which the cut allows. The range of Higgs masses which are accessible similarly increases, as can also be seen in Fig. 5.11, by cutting on  $\cancel{E}_T$ . For instance, while the mass range accessible with no cut is  $105 \text{ GeV} < m_h < 145 \text{ GeV}$ , this is extended to  $60 \text{ GeV} < m_h < 180 \text{ GeV}$  or more once cuts are applied. This figure assumes  $a = 0.5$ , but other values of the coupling are easily incorporated using the result that the missing-energy cross section scales as  $a^2$ .

We note in passing that the existence of a perturbative anomalous coupling, eq. 3.15 should not invalidate the earlier LEP searches for a Standard Model Higgs. On the other hand, this coupling should enhance the number of events found when searching with the Standard Model channel  $e^+e^- \rightarrow hZ \rightarrow b\bar{b}\nu\bar{\nu}$ , if a loose cut on the missing mass is applied.

### 5.3.3 Summary and Conclusions on scalar-Higgs coupling

The analysis presented here reconsiders some of the observational consequences of the existence of bulk scalars within a 6 dimensional scenario involving large extra dimensions. We have done so, motivated by the recent proposals of supersymmetric large extra dimensions, both as contributions towards understanding the small size of the cosmological constant [11] and as alternative realizations of low-energy supersymmetry [12].

Using the effective interaction presented in chapter 2, we computed there the rate for the process  $pp \rightarrow h\phi \rightarrow \gamma\gamma \cancel{E}_T$ , in order to see how large an effective coupling can be detected given reasonable assumptions as to the performance of a detector like ATLAS at the LHC. Our calculation assumed that the proton reaction is dominated by the contribution of gluon fusion at the parton level, and we computed the cross

section for the process  $gg \rightarrow h\phi$ . Given the sensitivity to  $a$  which we obtain, we believe there is sufficient motivation to go back and perform more detailed studies of bulk-scalar production at colliders. It must be noted that the coupling of a bulk scalar to a more massive Higgs boson can lead to clean signatures, such as in the case  $h \rightarrow ZZ^{(*)} \rightarrow 4\ell$ .

By comparing the number of signal events to the expected Standard Model backgrounds, we calculate the size of the effective couplings to which experiments at the LHC can expect to be sensitive. We find that couplings of order  $a = 0.5$  imply that as many Higgs particles are being produced in association with bulk scalars as are being produced without them. We find that the imposition of a missing energy cut  $\cancel{E}_T > 78$  GeV, greatly improves the signal relative to background, and allows a  $5\sigma$  detection of the effective interaction provided the effective coupling is  $a > 0.09$ . These limits would begin to probe the upper limit of the size of coupling which is obtained from a generic 1-loop estimate.

We also notice that the existence of Higgs production in association with missing energy is of considerable practical interest in the detection of the Higgs itself. It allows experiments to be sensitive to a much wider range of Higgs boson masses (at a given level of significance) than would otherwise be possible in the SM  $\gamma\gamma$  decay channel.

We regard these results to be encouraging and — together with the strong motivations for bulk supersymmetry — to further motivate the study of the phenomenology of extra dimensional fields (besides the higher-dimensional metric) within the framework of large extra dimensions.

This completes our analysis of the possibilities of testing SLED predictions at LHC. However, our work is not complete yet. We will now study the phenomenology at the LHC if we allow, consistent with SLED, the SM particles to propagate in smaller extra dimensions (TeV<sup>-1</sup> size). This is what is called Universal Extra Dimensions.

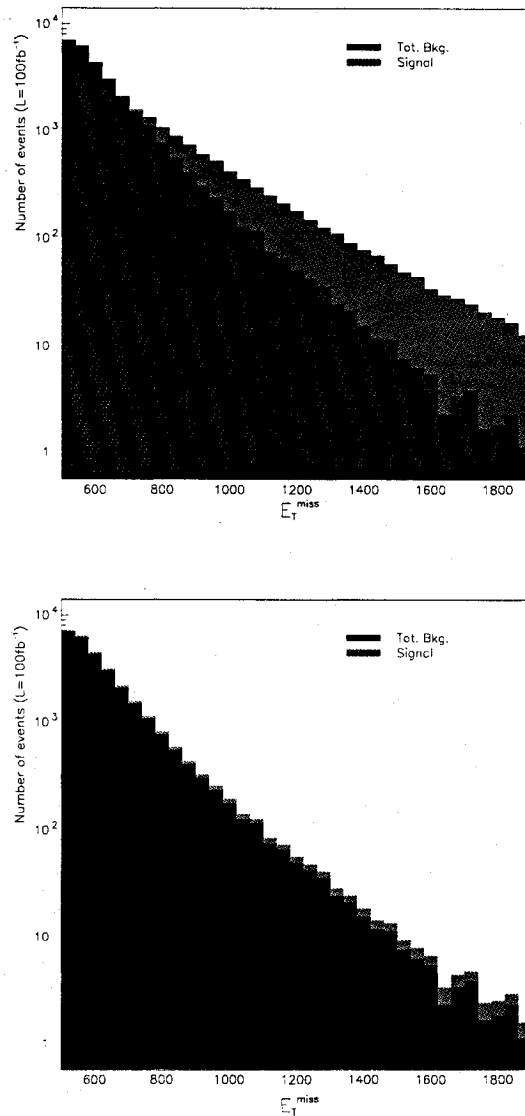


Figure 5.4: Distributions of missing  $E_T$  for background and signal when: (top) the cross section for bulk scalar production is the same as the graviton one; (bottom) this cross section is at its discovery limit.

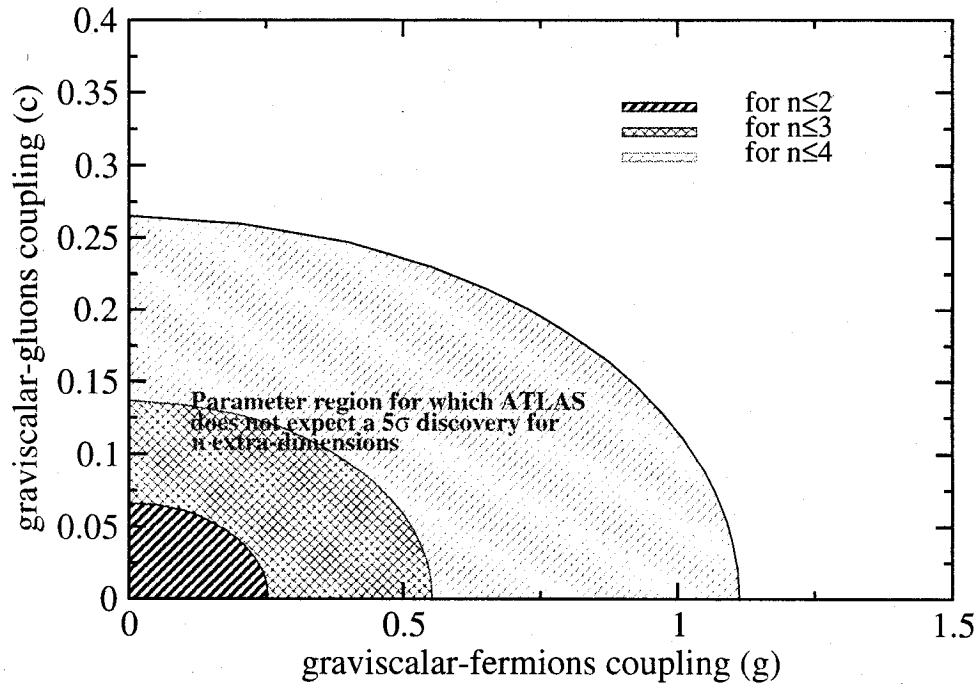


Figure 5.5: Parameters region for bulk scalar theory at second order in  $E/M_D$  that allows testable and valid physical predictions at ATLAS, for different number of extra dimensions. The bulk scalar-fermions and bulk scalar-gluons dimensionless couplings are effectively combinations  $(g^2 + g_5^2)^{1/2}$  and  $(c^2 + c_5^2)^{1/2}$

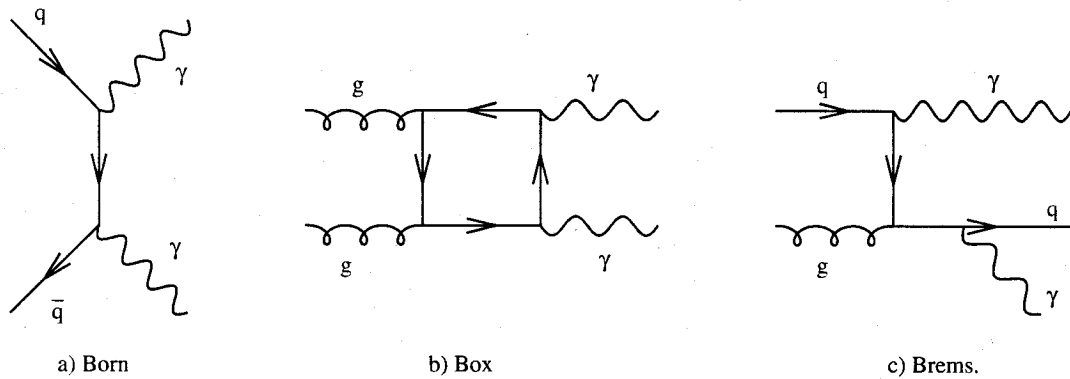


Figure 5.6: Feynman graphs of the irreducible backgrounds. In a) we have the Born process, in b) the box diagram process and in c) the quark bremsstrahlung process.

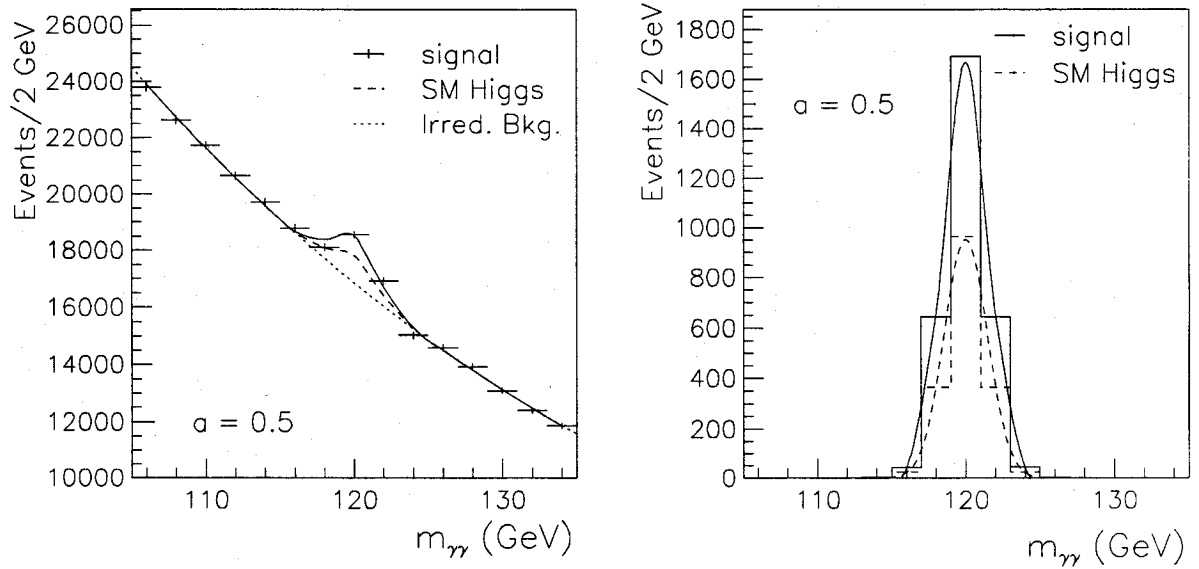


Figure 5.7: Expected  $h + \phi$  signal for  $M_H = 120$  GeV, for an integrated luminosity of  $100 \text{ fb}^{-1}$  and with  $hh\phi$  coupling value chosen as  $a = 0.5$ . The left panel shows the signal on top of the irreducible background, while the right one shows the reconstruction of the mass pic.

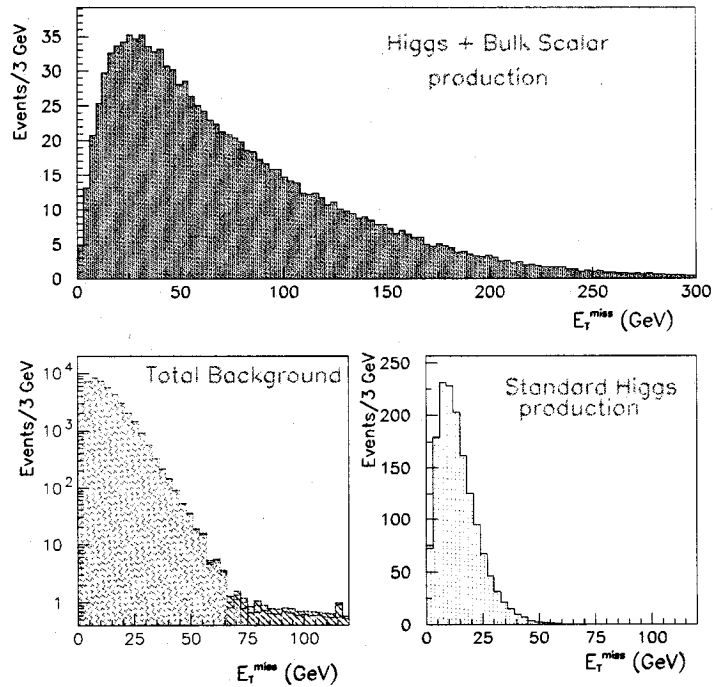


Figure 5.8: Distribution of  $E_T^{\text{miss}}$  for the Higgs + bulk scalar signal, assuming  $a = 0.5$  (top), the total background (bottom-left) including the  $Zh \rightarrow \gamma\gamma \nu\nu$  production (dashed blue) and the  $pp \rightarrow h$  process, with  $m_H = 120$  GeV (bottom-right). The plots are normalized for an integrated luminosity of  $100 \text{ fb}^{-1}$ .

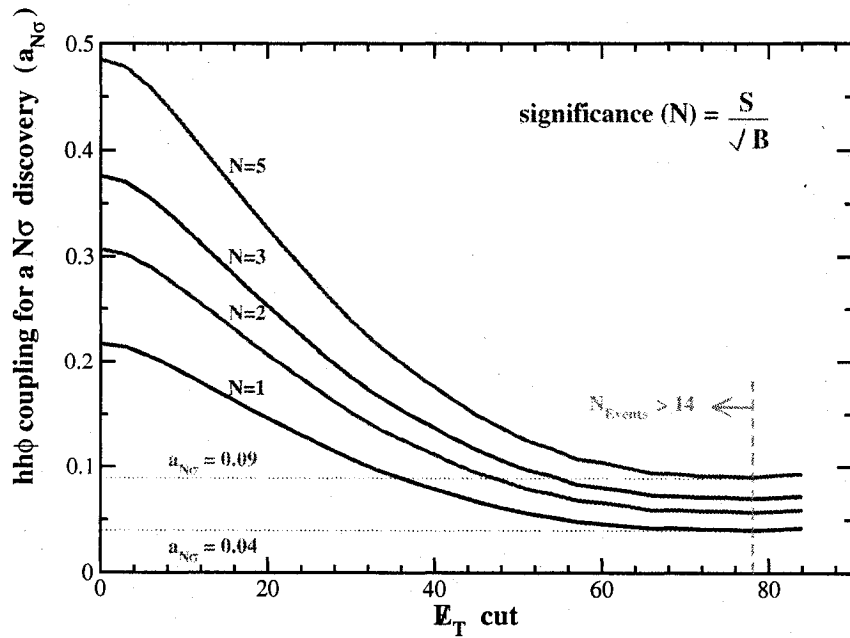


Figure 5.9: Value of the  $hh\phi$  coupling needed for different significances of the signal, as function of a cut on  $E_T$ .

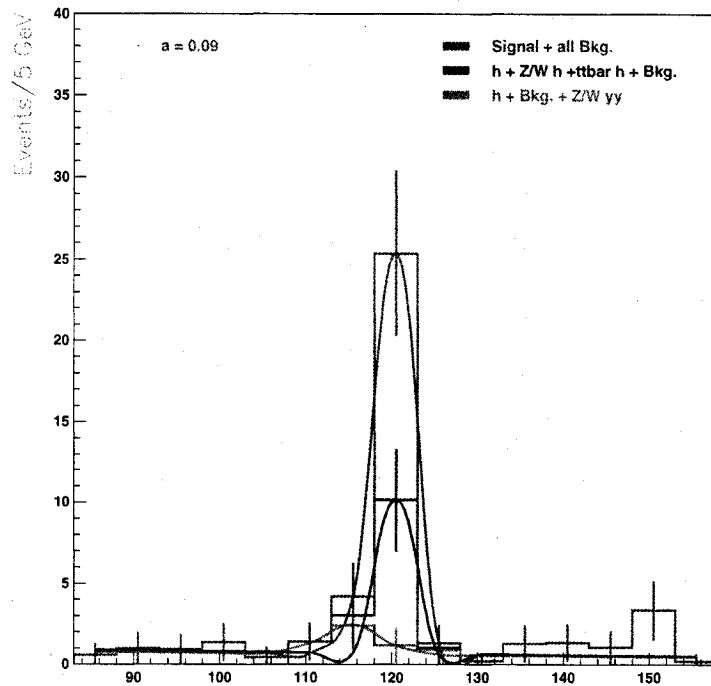


Figure 5.10: Number of events (including backgrounds) for  $h\phi$  and standard  $h$  production, as a function of the two-photon invariant mass. This plot assumes the smallest-detectable coupling  $a = 0.09$ , and uses the optimal missing-energy cut,  $E_T > 78$  GeV.

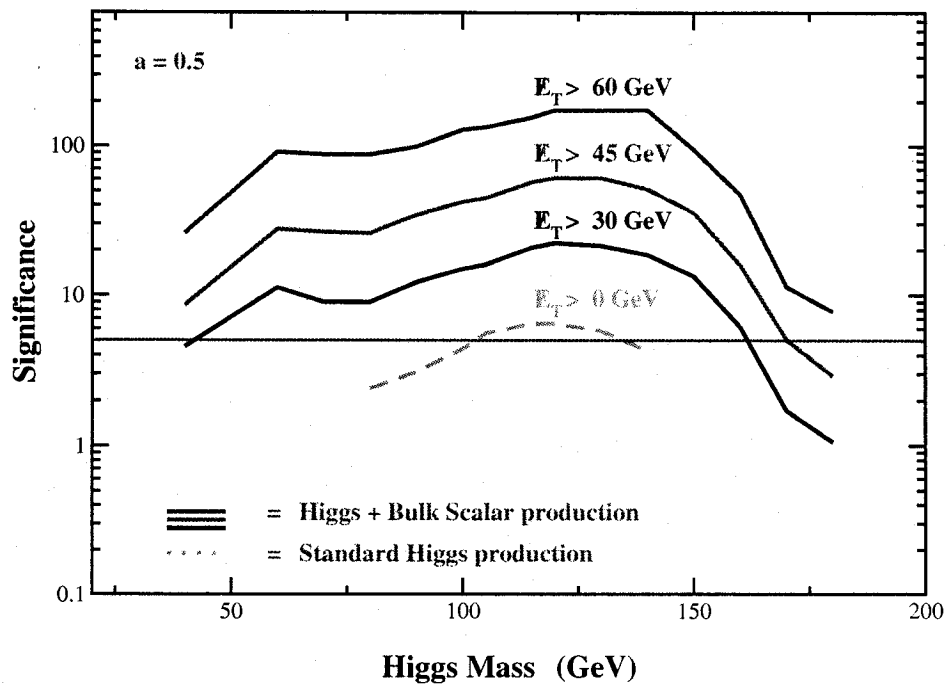


Figure 5.11: The significance of the  $\gamma\gamma$  signal alone as function of the Higgs mass for different values of the cut on  $\cancel{E}_T$ . The figure assumes the choices  $a = 0.5$  and an integrated luminosity of  $100 \text{ fb}^{-1}$ . The dotted line corresponds to what can be obtained from the standard  $h \rightarrow \gamma\gamma$  process making no cut on  $\cancel{E}_T$ . This shows that a considerable gain in Higgs reach is possible should Higgs production be possible in association with missing energy.

---

---

## UNIVERSAL EXTRA DIMENSION

---

---

### 6.1 *Why Universal Extra Dimensions?*

We have seen in section 2.3.3 that SLED realizes SUSY in a different way than does the MSSM (or its extensions). We then mentioned that this new approach to supersymmetry has many theoretical advantages compared to MSSM because, among other reasons, it offers a complete solution to the hierarchy problem and to the cosmological constant problem, principal motivations for this scenario. We met a drawback, however, in the implementation of SUSY in the SLED scenario, compared to the MSSM: a priori SLED does not predict any unification of the Standard Model gauge symmetries. In fact, in this scenario it may appear that the fundamental scale at which unknown new physics becomes important is much lower than the GUT (Grand Unified Theory) scale of the Standard Model describing the physics on our brane, therefore invalidating any unification predictions made from such an incomplete theory. (Although it is generally argued that the MSSM allows a precise convergence of the  $U(1)_Y$  (electromagnetic),  $SU(2)_L$  (weak) and  $SU(3)_c$  (strong) couplings, the Standard Model also predicts such a convergence but with a poorer precision, as can be seen in figure 6.1.) This implies that the fundamental reason why SLED, as stated in chapter 1, does not predict a unification is because, in whatever way SLED realizes SUSY at low energy, completely new and unknown physics (string modes, etc) will dominate at scales much lower than the GUT scale such that any prediction for a unification of couplings that does not involve this new physics will be invalid.

The idea of grand unification is profoundly attractive. The most obvious reason is

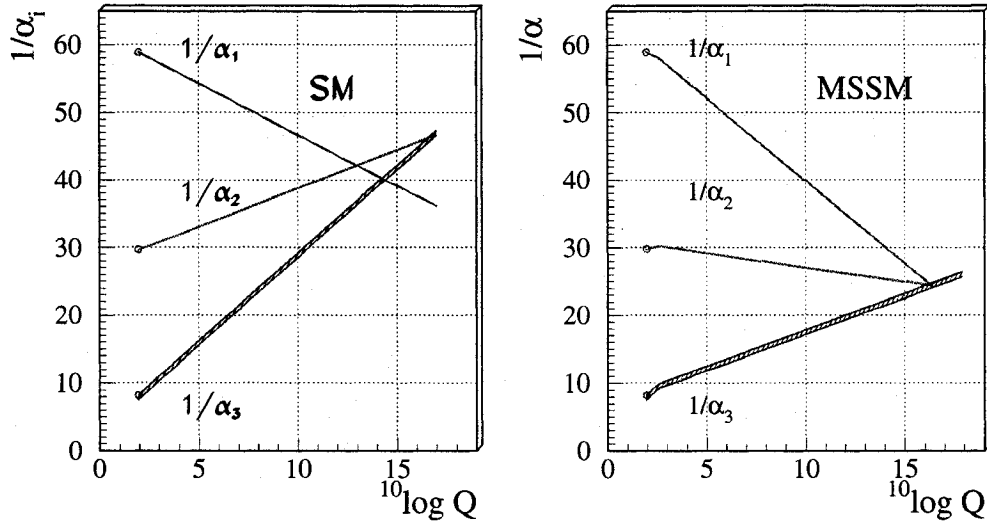


Figure 6.1: Unification of the electromagnetic, weak and strong coupling constants for the Standard Model (left) and the MSSM (right)

that such a theory unifies the diverse set of particle representations and parameters found in the low energy theory into a single, comprehensive and hopefully predictive framework. This implies that the number of arbitrary input parameters of the unified theory will be considerably reduced compared to that of its by-products. It will thus definitely constitute a fundamental step toward a self-sufficient, complete theory (not an effective theory) that can indeed be a fundamental and profound theory of Nature. For example, unification can provide an explanation for the various quantum numbers of fermions, for the origin of mass, for the quantification of electric charge and for the baryon/anti-baryon asymmetry [39, 63]. It is thus of fundamental importance for a high-energy theory to predict unification.

Is the SLED scenario sentenced to abandon this precious feature of fundamental high-energy physics theories? Not necessarily. In fact, what has been stated so far is not that it is impossible for SLED to yield such a unification but rather that, in order to achieve it, something must be added to the running of the Standard Model gauge couplings so that we arrive at unification by a different mechanism. The MSSM predicts a unification of its gauge groups thanks to extra-matter states added to the

SM spectrum, changing the running of the coupling constant related to each gauge group. Adding arbitrary extra-matter states to those included in SLED will not help, however, since all these fields will only couple gravitationally with our brane degrees of freedom and will therefore not change the Standard Model running of the fields that live on our brane. What we need is thus a new mechanism that will be consistent with SLED and which will lower the unification scale closer to the weak scale, the only true scale of Nature according to our model.

Why do the SM and the MSSM predict such a high value of the unification scale? The key to the answer lies in the fact that the running of the different coupling constants is due to quantum fluctuations of gauge fields, ie, formally, to quantum loop corrections to the propagator of gauge bosons [39, 30]. If we solve the renormalization group equations taking into account quantum corrections for the various coupling constants of the Standard Model, we will conclude that they run only logarithmically with the energy scale  $\mu$  [39]. Thus, given the different values of these couplings at low-energy, one must extrapolate over many orders of magnitude in energy before reaching a unification. Clearly, if there were a way to change the running of the gauge couplings so that they ran more quickly, we would have a chance to achieve a more rapid unification. Remarkably, there does exist a simple way in which a power-law rather than a logarithmic running can arise, as shown by Dienes *et al.* in [61]: the appearance of small ( $\mathcal{O}(\text{TeV}^{-1})$ ) extra space-time dimensions accessible to SM particles. In fact, if we consider that our brane has a small thickness of the  $\text{TeV}^{-1}$  size<sup>1</sup>, then at high energy (above the TeV scale) the de Broglie wavelength of the SM fields becomes smaller than the size of these extra dimensions, and the SM particles wavefunction thus travels in these extra dimensions subject to boundary conditions. This allows extra degrees of freedom to contribute to the quantum corrections of gauge

---

<sup>1</sup>Note that string theory predicts six extra dimensions and allows the possibility to devise models with asymmetrical compactification, i.e. with compactified dimensions of different radii. Since the SLED proposal considers that only two of them are large, string theory therefore leaves four other extra dimensions, in the thickness of the brane, free to play a different role in our understanding of particle physics

interactions. From this, we therefore expect a much faster running of the coupling constant of brane fields if the brane itself has a small thickness. Now if we embed this fat brane in large extra dimensions, this may not change the picture presented in chapter 1 for the solution to the cosmological constant problem. This scenario could thus constitute an extension of the SLED scenario in which a unification of the SM couplings is restored.

To achieve such a power-law running that allows for a low unification scale, we only need to consider that these  $\mathcal{O}(\text{TeV}^{-1})$  extra dimensions are accessible to Standard Model gauge bosons and to the Higgs boson. There are more theoretical motivations to allow these extra dimensions to be accessible to Standard Model particles, including chiral fermions. First, string theory, which provides the fundamental motivation for extra dimensions, generically treats every degree of freedom as higher dimensional string modes and not only gauge bosons. Moreover, it simplifies model building because it does not need a special mechanism to constrain some Standard Model fields to a thin 3-brane and others to a thick 3-brane: it treats every known particles on the same footing. Finally, and this is an important point, it has to satisfy weaker collider bounds than the scenario where only gauge bosons propagate in the small extra dimensions [62]. This is because it implies conservation of momentum in the extra dimensions, therefore forbidding brane observer vertices that involve only one non-zero KK-mode. Consequently there are no tree-level contributions to the electroweak observables and KK-modes may only be produced in pairs at colliders, thus reducing considerably the constraints from previous collider measurements [62, 63]. This scenario where every field will be described in a higher dimensional space is called the Universal Extra Dimension (UED) scenario.

Lower and higher experimental bounds on the compactification scale  $M_C \sim 1/R$  of UED models with only one  $\text{TeV}^{-1}$  size extra dimension can be estimated. The scale  $M_C$  is most strongly constrained at the lower end from precision electroweak measurements which would obtain contributions from KK states at the one-loop level, more precisely from the contribution of the KK modes associated with the top quark

and the Higgs bosons [62]. The current lower bound from LEP on the  $T$  parameter of Peskin and Takeuchi [64], which encodes the splitting in the  $W$  and  $Z$  masses due to physics beyond the Standard Model, leads to a lower bound on the compactification scale of approximately  $M_C \gtrsim 300$  GeV [62]. There is no relevant constraint from the new physics correction to the electroweak gauge boson propagators, encoded in the  $S$  parameter. This bound is however slightly raised by the current limit on direct production of KK excitations at colliders. Run II of the Tevatron sets this lower limit at about 350-400 GeV [62]. On the higher end, the electroweak scale sets a natural theoretical limit on the compactification scale. In fact, since the minimal Standard Model in  $4 + d$  dimensions has gauge, Yukawa and quartic-Higgs dimensionful couplings, it is an effective theory valid below a cutoff scale somehow related to the string scale  $M_s$ . To avoid fine-tuning the parameters in the Higgs sector, and in order for the  $D$ -dimensional theory to remain perturbative for a range of energies above  $M_C$ , the compactification scale should not be much higher than the weak scale  $M_W$ . This is consistent with the SLED scenario in which our UED braneworld is embedded since the cutoff of such a theory is the  $D$ -dimensional Planck scale  $M_D \sim M_W$ . Energies achievable at the LHC will therefore cover a significant part of the theoretical parameter space.

Here again, what interests us is the ATLAS phenomenology of such a scenario. In this chapter, we will first briefly review how a weak scale unification is possible by letting the SM fields evolve in  $n$  extra dimensions (we will choose  $n = 1$ ). To this end we only need to consider gauge fields. We will then describe the UED model and its Lagrangian and finally explain what the effects expected from embedding this thick brane in two large extra dimensions will be as predicted by the SLED scenario. We will complete this topic by discussing the physical predictions and performing a phenomenological analysis in the next chapter.

## 6.2 *Extra dimension and gauge coupling unification*

Here we want to explain, following Dienes *et al.* [61], how the running of gauge couplings is affected by extra dimensions in which gauge bosons propagate, and in which sense we can speak of a “unification” of the SM gauge couplings. Let us recall first that a particle propagating in  $4+n$  dimensions, where the  $n$  extra dimensions are compactified, will correctly be described in the 4D point of view as an infinite tower of Kaluza-Klein modes that only differ in their masses. The mass splitting between two modes depend on the size  $R$  of the extra dimensions:  $m_n - m_{n-1} \equiv R^{-1}$  (for massless particles). This means that in contrast with the case of large extra dimension, TeV $^{-1}$  size extra dimensions scenarios involve KK particles that largely differ in their mass. They will therefore not be considered as a continuously massive state.

The fundamental point of this gauge unification scenario is that it involves two different mass scales related to two approximations that legitimately allow to define a running of the gauge couplings. We explain here what these two mass scales are, why approximations are conceptually needed and how they provide a running of gauge couplings that can yield a unification at the weak scale.

The first mass scale is obvious: it is the energy scale corresponding to the radius of the extra dimensions  $\mu_0 \equiv R^{-1}$ . In fact, at energy scales much smaller than  $\mu_0$  the energy of the system is much less than the mass of the first Kaluza-Klein state  $M = \sqrt{m^2 + \mu_0^2}$  (with  $m$  being the mass of the 0-mode SM particle of this KK tower) and the existence of such KK states can be ignored. In this limit, our theory reduces to the usual four-dimensional Standard Model (on a thin brane) and the running of the couplings will be described by the usual beta functions of the Standard Model renormalization group equations. It is therefore beyond the scale  $\mu_0$  that an acceleration in the running can eventually yield a unification at a scale lower than the GUT scale. Indeed, at scales above  $\mu_0$ , the Kaluza-Klein excitations of the known particles will start to be produced. We will have to include them in every physical prediction, and in particular in the loop corrections to gauge couplings. These KK contributions will tend to accelerate the running of gauge couplings, ultimately

changing the scale-dependence of these gauge couplings from logarithmic to power-law as a function of the energy scale  $\mu > \mu_0$  at which this physical prediction is evaluated. This new energy dependence reflects, however, the fact that beyond the scale  $R^{-1}$ , a certain subset of the SM brane physics has essentially been considered as higher-dimensional and that the effective radius of these extra dimensions has been taken to be infinite relative to the energy scale  $\mu$  (We should remember that we are talking here of smaller size extra dimensions probed by brane physics, ie an extension of the SLED scenario). The Kaluza-Klein excitations indeed derive from a low-energy 4D description of a D-dimensional spacetime with  $D > 4$ , but these are the consequence of compactified extra-dimensions, which is not equivalent to a theory with  $4 + n$  flat and of infinite size dimensions because of boundary conditions. It is therefore fundamental for our purpose to make the approximation that at energies higher than  $\mu_0$  the small extra dimensions (brane thickness) probed by the brane fields are flat because it is such a D-dimensional flat theory that allows to change the energy dependence of gauge couplings to a power-law above the scale  $\mu_0$ . In fact, as is well-known [39], higher-dimensional field theories enhance the divergence structure of its physical predictions. An easy way to see this is that extra dimensions add extra momentum powers in the numerator of loop integrations, therefore increasing their superficial degrees of divergence. With this approximation we thus expect a power-law dependence on some mass scale after regularization of the divergences, rather than a logarithmic one, confirming its importance for our new unification scenario. According to references [61, 14], this is a good approximation for low-energy predictions.

This adds a subtle complication in our running picture: higher-dimensional field theories are non-renormalizable and, as such, it makes no sense to talk of a “running” of gauge couplings as a function of a floating energy scale  $\mu$  for  $\mu > \mu_0$ . For the high-energy sector, we have to find a new interpretation to such a “running”. It is here that the second scale announced earlier will play a role. To avoid infinities, one will have to regularize its predictions by introducing a cutoff scale  $\Lambda > \mu_0$ , on

the magnitude of which the gauge couplings will explicitly depend. In our case, this mathematical dependence on the cutoff is identical to the scale dependence that would have been naïvely calculated if the theory had been renormalizable [61]. We can thus still formally talk of a running of couplings with the scale  $\mu = \Lambda$ . The question is to find out if this running is just a question of wording or if indeed there is some physical meaning.

The problem with this question is that in general a cutoff  $\Lambda$  depends on the form and on the normalization of the specific regularization procedure used in an explicit calculation. It does not rely on any physical interpretation. However, in our UED scenario, we can naturally associate the cutoff parameter with a mass scale of physical significance [61]. Since our theory is non-renormalizable, it can only be considered as an effective theory valid up to a scale  $M$  where a more fundamental theory such as string theory becomes relevant. We already saw in the SLED scenario that the string theory description will be needed above the D-dimensional Planck scale  $M_D$ . We can therefore speculate that the cutoff scale of our UED scenario is conceptually related to the SLED scenario cutoff scale, ie  $M \sim \Lambda \sim M_D$ . Because of this, we can truncate the full D-dimensional theory, ie that we can make the sufficiently good approximation to consider that, at energies lower than  $M_D$ , all the KK-modes that can significantly contribute to our physical predictions have a mass below this scale  $M_D$ . This truncation avoids an infinite number of KK-modes contributing to our physical predictions and thus restores the renormalizability of our theory. Note that even if this renormalizable truncated D-dimensional field theory is only an approximation of the full D-dimensional theory, both the truncated and the full theories give essentially the same results for most of the calculations at energies smaller than the scale  $M_D$  above which neither of these theories anyway describe properly the physics. This truncated scenario allows thus to relate the cutoff scale  $\Lambda$  to the fundamental scale  $M_D$  [61] thus providing a physical significance to this parameter. Figure 6.2 sketches the different scales involved in the whole problem.

Now that we know that, for the price of a small but fundamental approximation,

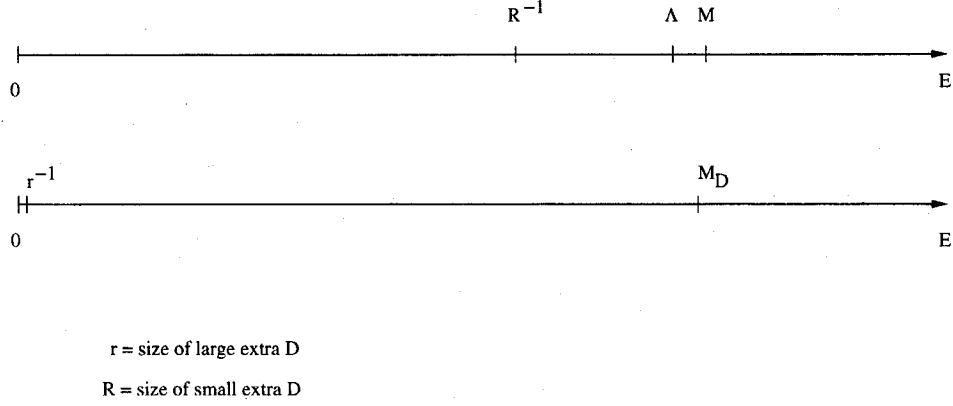


Figure 6.2: (top) Scales involved in the UED scenario, with  $R$  being the size of the small extra dimensions; (bottom) scales involved in the SLED scenario, with  $r$  being the size of the large extra dimensions.

the cutoff scale  $\Lambda$  can be interpreted as a physical quantity (the scale at which new physics become important), let us come back to the question of the running of the gauge couplings. We mentioned earlier that for energies smaller than  $\mu_0$ , the behavior of the various coupling constants is correctly described by the Standard Model. This imposes a matching condition: the value of the effective four-dimensional couplings must agree with the value of the D-dimensional coupling constants  $\alpha_i$  ( $i = 1, 2, 3$ ) at the scale  $\mu_0$ . This means that the running of any coupling constant will follow the Standard Model behavior at energy scales lower than  $\mu_0$ . From this condition we can compute the one-loop exact gauge couplings in the presence of an infinite tower of KK modes with  $\delta$  compactified extra dimensions of radius  $R$  [61]:

$$\alpha_i^{-1}(\Lambda) = \alpha_i^{-1}(\mu_0) - \frac{b_i - \bar{b}_i}{2\pi} \ln \frac{\Lambda}{\mu_0} - \frac{\bar{b}_i}{4\pi} \int_{r\Lambda^{-2}}^{r\mu_0^{-2}} \frac{dt}{t} \left[ \vartheta_3 \left( \frac{it}{\pi R^2} \right) \right]^\delta \quad (6.1)$$

where  $b_i$  are the SM one-loop beta-function coefficients,  $\bar{b}_i$  are the new beta-function coefficients,  $r$  is a parameter that numerically relates the cutoff scales  $\mu_0$  and  $\Lambda$  to physical scales ( $r \equiv \pi(V_\delta)^{-2/\delta}$  with  $V_\delta$  the volume of the unit sphere in  $\delta$  dimensions) and  $\vartheta_3$  is the Jacobi function defined as  $\vartheta_3(\tau) \equiv \sum_{-\infty}^{\infty} \exp(i\pi\tau n^2)$ .

The difficulties related to the non-renormalizability of the full theory will come with the integration of this Jacobi function [61]. However the second approximation justified above (truncation of the KK tower), which provides the  $\Lambda$  dependence with

a physical significance, formally consists in approximating this Jacobi function by  $\vartheta_3\left(\frac{it}{\pi R^2}\right) \approx R\sqrt{\frac{\pi}{t}}$  [61]. Now, if we numerically evaluate the value of the coupling constant before and after this approximation for an energy higher than  $\mu_0$  but lower than  $M_D$ , we obtain the same result, confirming the validity of the approximation. At the end of the day, the  $\Lambda$  dependence of the various gauge couplings at one-loop will thus be given by:

$$\alpha_i^{-1}(\Lambda) = \alpha_i^{-1}(\mu_0) - \frac{b_i - \bar{b}_i}{2\pi} \ln \frac{\Lambda}{\mu_0} - \frac{\bar{b}_i V_\delta}{2\pi\delta} \left[ \left( \frac{\Lambda}{\mu_0} \right)^\delta - 1 \right] \quad (6.2)$$

We note from this expression the power dependence on  $\Lambda$  expected for a faster running. This result stays true and valid for any value of the mass scales  $\mu_0$  and  $\Lambda$  [61]. In particular, after setting  $\mu_0$  to  $R^{-1}$  we can always find a value of  $\Lambda$ , that we can call  $\Lambda_{\text{GUT}}$  for which all the three gauge couplings unify [61]. This property is robust because it occurs independently of the number  $\delta$  of small extra dimensions, independently of the scale  $\mu_0 = R^{-1}$  at which they appear and independently of the number of chiral SM generations that feel these extra dimensions. Thus, since these gauge couplings are distinct at the scale  $\mu_0$  but take the same value at the scale  $\Lambda_{\text{GUT}}$  (which is also closely related to the fundamental scale  $M \sim M_D$  where our scenario breaks down), we can conclude that they run through all the intermediate cutoff scales between  $\mu_0$  and  $\Lambda_{\text{GUT}}$ . We can then consider that all these intermediate cutoff scales  $\mu_0 < \Lambda < \Lambda_{\text{GUT}}$  provide the energy dependence of  $\mu$  parameterizing the running of the coupling constants. We can therefore conclude that for every UED scenarios we will have a running of the brane gauge couplings that will unify at an energy scale that can be much lower than the usual GUT scale, as we expected since the beginning of this chapter.

In figure 6.3 (taken from [61]) we can see such running and unification for different values of  $\mu_0$  in the case of one small extra dimension. In this figure, the gauge couplings  $\alpha_i^{-1}(\mu)$  are given by equation 6.2 where we interpret the intermediate cutoff scale  $\Lambda$  as an energy parameter  $\mu$ . These figures are for parameter values quite different from what we are considering in our analysis, but the general shape is the same (we can see on the figure that it does not change over various energy scales).

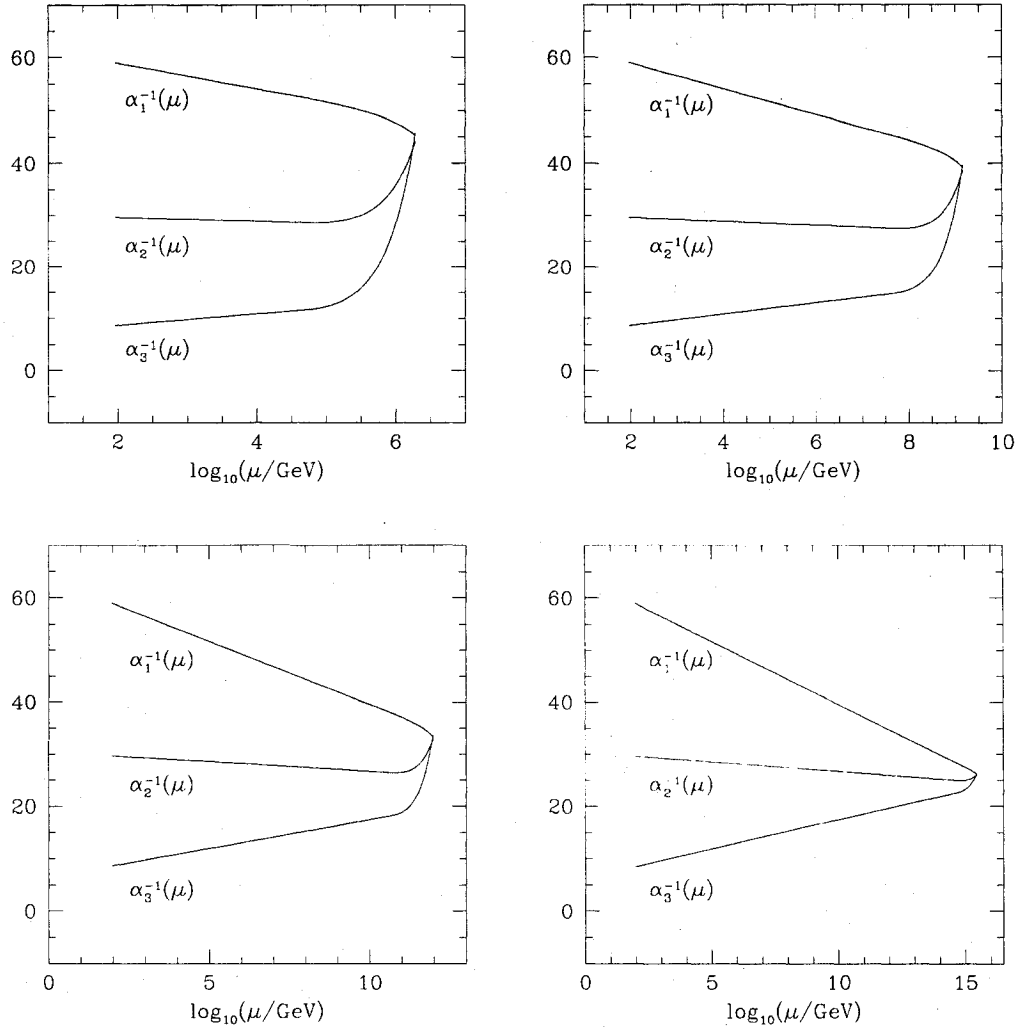


Figure 6.3: Unification of gauge couplings in the presence of extra space-time dimensions in the case where only gauge bosons and Higgs field propagate in the extra dimensions as computed by ref. [61]. Four cases have been considered:  $\mu_0 = 10^5$  GeV (top left),  $\mu_0 = 10^8$  GeV (top right),  $\mu_0 = 10^{11}$  GeV (bottom left) and  $\mu_0 = 10^{15}$  GeV (bottom right). In each case they considered only one small extra dimension ( $\delta = 1$ ).

We clearly notice the Standard Model running up to the scale  $\mu_0$  and the power-law running above this scale.

We have seen in previous chapters that SLED predicts a fundamental scale  $M_D$  of the order of 10 TeV. Since above the scale  $\mu_0$ , the gauge couplings unify at a scale  $\Lambda_{\text{GUT}}$  of roughly one order of magnitude higher than  $\mu_0$ , as can be seen in the figure, and since our interpretation of this running can only make sense if this unification scale is approximately the cutoff scale above which our theory is not anymore reliable and new physics become important (ie  $\Lambda_{\text{GUT}} \sim M_D$ ), we can then speculate, in a SLED scenario, that  $\mu_0 \sim \mathcal{O}(1 \text{ TeV})$ . This means that the size of these small extra dimensions are predicted to be of the order of  $1 \text{ TeV}^{-1}$  by SLED scenario. This is a good news since we will show in the next chapter that ATLAS is expected to be sensitive to such sizes of universal extra dimensions.

### 6.3 *The Universal Extra Dimension model*

In the previous section we discussed how unification can be achieved in the SLED scenario by letting the SM particles propagate in extra dimensions of  $\text{TeV}^{-1}$  size. This constitutes the basic motivation for the phenomenological analysis that is the object of the rest of this thesis. We will now develop briefly a model Lagrangian that will be used to compute physical predictions. We refer to original works by [62, 63].

Our starting point is the minimal Standard Model in  $D = 4 + \delta$  space-time dimensions. Because our phenomenological analysis will later be restricted to only one such extra dimension, we will take from now on  $\delta = 1$ . This has the advantage to be automatically anomaly-free [62]. Also our analysis will focus on the direct production of KK-modes at the LHC, i.e. of the hadronic sector. We will therefore consider only the coupling of KK-quarks with KK-gluons and the trilinear KK-gluon couplings. Finally, since the first KK excitation is expected at a mass of about 1 TeV (following previous discussions), ATLAS will mostly be sensitive to only the first mode of each KK-tower. From all these considerations and because the Lagrangian density will consist in the generalization of the SM one to its 5D analog, our UED theory will be

given by:

$$\mathcal{L}_5 = -\frac{1}{4}\mathcal{G}_{MN}^a(x,y)\mathcal{G}^{MNa}(x,y) - i\bar{Q}(x,y)\{\Gamma^M[\partial_M + ig_5 T^a A_M^a(x,y)]\}Q(x,y) \quad (6.3)$$

where  $\mathcal{G}_{MN}^a$  is the gluon field strength  $\mathcal{G}_{MN}^a = \partial_M G_N^a - \partial_N G_M^a + g_5 f^{abc} G_M^b G_N^c$ ,  $G_M^a$  the gluon field,  $g_5$  is the 5D strong coupling,  $M$  is the 5D analog of the Lorentz index  $\mu$ , ie  $M \in \{\mu, 4\}$ ,  $\Gamma^M$  are the gamma matrices in 4 + 1 dimensions and  $T^a$  are the Lie algebra generators of the  $SU_c(3)$  symmetry.

To derive the 4-dimensional point of view on this effective 5D theory, valid at energies lower than  $M_D$ , we must Fourier expand the 5D fields in terms of the coordinate  $y$  of the extra dimension and integrate over this  $y$  coordinate. Because this extra dimension is compactified on a given geometry, this integration will have finite limits. We will choose to compactify on a  $S^1/Z_2$  orbifold [62, 63] to provide matching of the zero mode with the observed SM spectrum. This geometrically corresponds to a circle cut in half, such that the limits of integration for  $y$  will be:  $0 \leq y \leq \pi R$ , with  $R$  being the radius of the extra dimension. By this procedure, we will obtain the SM Lagrangian with new physics terms that will involve the KK excitations of the quark and gluon fields. These new terms provide the masses of the KK modes as well as the Feynman rules for the new vertices and propagators. This is our goal in this section, but before that, let us see how the 5D fields are Fourier expanded.

The 5D analogue of the quark multiplets (under  $SU_L(2)$ ) consists of massless four-component vector-like quarks (non-chiral fermions, ie fermions for which the left-handed and the right-handed component have the same quantum number such that they don't violate parity in weak interaction), which we denote in the equations by  $Q(x,y)$ ,  $U(x,y)$  and  $D(x,y)$ . This vector-like structure comes from the fact that chiral fermions exist only when the number of extra dimensions  $\delta$  is even [62, 63] (because of the representation of the Lorentz group and more specifically of the gamma matrices). Since we consider only one extra dimension, the fermions are therefore non-chiral, ie vector-like. It implies that when these 5D fields are decomposed into 4D fields, corresponding to each 4D field are a left-handed and a right-handed term, depending on the parity of each Fourier mode component under the transformation  $y \rightarrow -y$ . To

decide whether it is the left-handed modes that are even under this transformation or the right-handed ones, we ask that the 0-modes that are not projected to zero by imposing this transformation (those for which the Fourier modes are even, ie the cosine modes) be the Standard Model fields. This expansion will thus be given by:

$$\begin{aligned}
Q(x, y) &= \frac{1}{\sqrt{\pi R}} \left\{ \begin{pmatrix} u(x) \\ d(x) \end{pmatrix}_L + \sqrt{2} \sum_{n=1}^{\infty} [Q_L^n(x) \cos\left(\frac{ny}{R}\right) + Q_R^n(x) \sin\left(\frac{ny}{R}\right)] \right\} \\
U(x, y) &= \frac{1}{\sqrt{\pi R}} \left\{ u_R(x) + \sqrt{2} \sum_{n=1}^{\infty} [U_R^n(x) \cos\left(\frac{ny}{R}\right) + U_L^n(x) \sin\left(\frac{ny}{R}\right)] \right\} \\
D(x, y) &= \frac{1}{\sqrt{\pi R}} \left\{ d_R(x) + \sqrt{2} \sum_{n=1}^{\infty} [D_R^n(x) \cos\left(\frac{ny}{R}\right) + D_L^n(x) \sin\left(\frac{ny}{R}\right)] \right\} \\
A_\mu^a(x, y) &= \frac{1}{\sqrt{\pi R}} \left[ A_{\mu 0}^a(x) + \sqrt{2} \sum_{n=1}^{\infty} A_{\mu, n}^a(x) \cos\left(\frac{ny}{R}\right) \right] \\
A_4^a(x, y) &= \frac{\sqrt{2}}{\sqrt{\pi R}} \sum_{n=1}^{\infty} A_{4, n}^a(x) \sin\left(\frac{ny}{R}\right)
\end{aligned}$$

Note that because we choose to work in the unitary gauge, we can apply the gauge choice  $A_{4, n}^a = 0$ , ie that these scalars get eaten by the other modes. By substituting these expressions in equation 6.3 and integrating over  $y$  between 0 and  $\pi R$ , we will obtain the effective 4D Lagrangian in term of  $Q_L$ ,  $Q_R$ , etc. Let us do it more explicitly for the quark kinetic term. From this we will predict the mass of the KK partons (see the previous section). Keeping all the KK modes, we have:

$$\begin{aligned}
i \int_0^{\pi R} \bar{Q}(x, y) \Gamma^M \partial_M Q(x, y) dy &= i \left[ (\bar{u}(x) \bar{d}(x))_L \gamma^\mu \partial_\mu \begin{pmatrix} U(x) \\ d(x) \end{pmatrix}_L \right. \\
&\quad + \sum_{n=1}^{\infty} [\bar{Q}_L^n(x) \gamma^\mu \partial_\mu Q_L^n(x) + \bar{Q}_R^n(x) \gamma^\mu \partial_\mu Q_R^n(x) \\
&\quad \left. + i \frac{n}{R} \bar{Q}_L^n(x) Q_R^n(x) + i \frac{n}{R} \bar{Q}_R^n(x) Q_L^n(x) \right]
\end{aligned}$$

We recognize the SM kinetic Lagrangian in the first term of the right-handed side of this equation. The next two terms are the kinetic terms of the quark KK excitations while the last two are mass terms due to the quantization of momenta in the extra dimension. Note that there are similar expressions for  $U(x, y)$ ,  $D(x, y)$  and  $G_\mu^a(x, y)$ .

Additional mass contributions arise from the Yukawa couplings of the 5D quark multiplets via Higgs vev's. In fact, given the 5D generalization of the SM Yukawa terms and integrating again over  $y$  yields:

$$i \int_0^{\pi R} [\lambda_u^5 \bar{Q}(x, y) i\sigma_2 H^*(x, y) U(x, y) + \lambda_d^5 \bar{Q}(x, y) H(x, y) D(x, y) + h.c.] dy =$$

$$i \left\{ M_u \left[ \bar{u}(x) u(x) + \sum_{n=1}^{\infty} [\bar{Q}_L^n(x) U_R^n(x) + \bar{Q}_R^n(x) U_L^n(x)] \right] + M_d terms \right.$$

$$\left. + \lambda_u \left[ \bar{u}(x) u(x) h(x) + \sum_{n=1}^{\infty} [\bar{Q}_L^n(x) U_R^n(x) + \bar{Q}_R^n(x) U_L^n(x)] h(x) \right] + \lambda_d terms \right\}$$

where  $\lambda \equiv \lambda_u^5 / \sqrt{\pi R}$  and  $M_u \equiv \lambda \langle H \rangle$ . The  $(Q^n(x), U^n(x))$  mass matrix, including these Yukawa contributions as well as the kinetic terms is therefore:

$$\begin{pmatrix} \bar{Q}^n(x) & \bar{U}^n(x) \end{pmatrix} \begin{pmatrix} \frac{n}{R} & M_u \\ M_u & -\frac{n}{R} \end{pmatrix} \begin{pmatrix} Q^n(x) \\ U^n(x) \end{pmatrix}$$

Since the Yukawa couplings  $\lambda$  and the Higgs vev are SM parameters,  $M_u$  corresponds to the SM prediction on the mass of the up quark. We can therefore diagonalize this mass matrix and get the net mass  $M_n$  of the KK modes in terms of the mass of the corresponding quark field  $M_q$  and the mass from the compactification scale  $n/R$ :

$$M_n = \sqrt{\frac{n^2}{R^2} + M_q^2} \quad (6.4)$$

Since  $1/R \sim \mathcal{O}(\text{TeV}^{-1})$ , in our subsequent calculations we will neglect the SM quark masses except for the top quark,  $M_t$ . Note also that we get a similar result for the excited KK gluons with  $M_g = 0$ .

Before deriving the final effective 4D Lagrangian density, we can combine the indistinguishable interactions involving the  $Q$ ,  $U$  and  $D$  fields using the following expressions:

$$Q_{L,R}^n(x) \equiv P_{L,R} \begin{pmatrix} u_n^\bullet(x) \\ d_n^\bullet(x) \end{pmatrix}$$

$$U_{R,L}^n(x) \equiv P_{R,L} u_n^\circ(x)$$

$$D_{R,L}^n(x) \equiv P_{R,L} d_n^\circ(x)$$

where  $P_{R,L} = \frac{1}{2}(1 \pm \gamma_5)$ . These two distinct quark towers  $q^\bullet$  and  $q^\circ$  will have the same masses given by equation 6.4 and will interact identically except for the vertices that will be differentiated by the helicity projectors  $P_R$  or  $P_L$ . After computing the algebra from the 5D Lagrangian density of equation 6.3, we have the 4D trilinear effective Lagrangian needed to study the production of KK pairs of quarks and gluons in the case where the SM partons can propagate in 1 extra dimension of the  $\mathcal{O}(\text{TeV}^{-1})$  size is [63]:

$$\begin{aligned}
\mathcal{L}_{int} = & -g \left\{ \bar{q}(x) \gamma^\mu T^a q(x) A_{\mu,0}^a(x) - \frac{1}{2} f^{abc} A_{\mu,0}^b(x) A_{\nu,0}^c(x) [\partial^\mu A_0^{\nu a}(x) - \partial^\nu A_0^{\mu a}(x)] \right. \\
& + 3 f^{abc} A_{\mu,0}^b \sum_{n=1}^{\infty} A_{\nu,n}^c(x) [\partial^\mu A_n^{\nu a}(x) - \partial^\nu A_n^{\mu a}(x)] \\
& + \sum_{n=1}^{\infty} [\bar{q}_n^\bullet(x) \gamma^\mu T^a q_n^\bullet(x) + \bar{q}_n^\circ(x) \gamma^\mu T^a q_n^\circ(x)] A_{\mu,0}^a(x) \\
& + \sum_{n=1}^{\infty} [\bar{q}(x) P_L \gamma^\mu T^a q_n^\bullet(x) + \bar{q}_n^\bullet(x) \gamma^\mu T^a P_L q(x)] A_{\mu,n}^a(x) \\
& + \sum_{n=1}^{\infty} [\bar{q}(x) P_R \gamma^\mu T^a q_n^\circ(x) + \bar{q}_n^\circ(x) \gamma^\mu T^a P_R q(x)] A_{\mu,n}^a(x) \\
& + \frac{1}{\sqrt{2}} \sum_{n,m,l=1}^{\infty} [-\bar{q}_n^\bullet(x) \gamma^\mu \gamma_5 T^a q_m^\bullet(x) + \bar{q}_n^\circ(x) \gamma^\mu \gamma_5 T^a q_m^\circ(x)] A_{\mu,l}^a \delta_{l,m+n} \\
& \left. + \frac{1}{\sqrt{2}} \sum_{n,m,l=1}^{\infty} [\bar{q}_n^\bullet(x) \gamma^\mu T^a q_m^\bullet(x) + \bar{q}_n^\circ(x) \gamma^\mu T^a q_m^\circ(x)] A_{\mu,l}^a \delta_{l,|m-n|} \right\}
\end{aligned}$$

We recognize on the first line the SM interaction terms of quarks and gluons, while all the other terms involve the coupling of one SM field with two KK excitations of SM partons.

The Feynman rules can be directly read from this Lagrangian density. They are summarized in figure 6.4 (taken from [63]). Note that, as we mentioned already, for phenomenological reasons we will only be interested in the first KK excitation of the various particles. We can therefore drop the summation and take  $n = 1$  in the above equation. The last four terms also are irrelevant for physical predictions at the LHC. We wrote them here nevertheless for completeness and because of what



they imply. We clearly see from the Feynman rules, computed from the Lagrangian density, that we can draw 1-loop diagrams with different KK numbers on each side of the loop (for example, taking the bottom left and the bottom right Feynman rules of figure 6.4 and connecting together the quark propagators of each vertex yield a 1-loop diagram for which on one side of the loop we have  $g_{m+n}^*$  and on the other side we have  $g_{|m-n|}^*$ ). The conservation of KK numbers holding at tree-level (because of the conservation of momentum in this small extra dimension) and which dictates that  $N$  KK modes  $n_1, n_2, \dots, n_N$  can only couple to each other if they satisfy the relation  $|n_1 \pm n_2 \pm \dots \pm n_{N-1}| = n_N$ , will therefore not hold at the loop-level. The higher modes can thus decay to the lower one. However, the lowest-lying KK modes of the light quarks and massless gluons will be completely stable unless there exists another form of new physics to serve as a decay mechanism (because if  $m+n=1$  then  $|m-n|=1$  as well). SLED will provide such a decay mechanism (more of that in the next section). Because of the different physics theories responsible for the production and for the decay of KK states, this kind of event can be studied in two cases: first a pair of stable (in the thick brane)  $N=1$  KK excitation of SM partons is produced, conserving momentum then partons which decay because of the new mechanism to be introduced. This is how our simulation program is written.

Note finally that the decay type that we just talked about is between states of different KK numbers. There is another decay procedure that conserves the KK number: it is the analogue of the SM decays. For example, the first KK excitation of a top quark can decay in an excited W boson and a SM bottom quark, exactly like the SM channels. These decays have calculable branching ratio in the UED scenario itself. However, because of the huge mass of the first KK excitation compared to the mass of the SM partons, to a pretty good approximation equation 6.4 reduces to  $M_1 \sim \frac{1}{R}$ . This is why all the partons except the top quark are taken to be degenerate (they have the same mass  $\frac{1}{R}$ ). This degeneracy forbids all the different SM-like decay channels (because they are kinetically highly suppressed), and the  $n=1$  modes of the parton will be considered stable in this scenario. This is again just a tree-level

approximation. In fact, it has been shown in [65] that radiative corrections lift this degeneracy, thus allowing the first excitation level to decay into the lightest KK particle, the  $\gamma^*$ , along the following two decay chains:

$$\begin{aligned} q_1^\bullet &\rightarrow q Z_1^* \rightarrow q l l_1^\bullet \rightarrow q l l \gamma_1^*, & \text{Br. } \sim 33\% \\ q_1^\bullet &\rightarrow q W_1^* \rightarrow q l' l_1^\bullet \rightarrow q l' l \gamma_1^*, & \text{Br. } \sim 65\% \end{aligned}$$

For simplicity we will not consider these kinds of decay but we will continue to take every  $n = 1$  parton to be stable on the thick brane. We will also consider a decay mechanism of the lowest-lying KK modes that may dominate the above chains under certain circumstances. We will now look more precisely at what this mechanism can consist in.

#### 6.4 *Decay mechanism of the lowest-lying KK mode*

There are various decay schemes that have been considered so far in the literature [62, 66, 67]. However, reference [63] argues that provided that the KK excitations decay within the detector, all the specific decay mechanisms will yield approximately the same phenomenological final state distributions. The analysis of the signature will thus only tell whether or not these KK excitations have decayed. We have nevertheless to choose one such mechanism to perform our simulations.

Since our first motivation for studying UED was to provide the SLED scenario with a possible unification mechanism, we shall perform our UED analysis in this context. It turns out that when it is assumed that the small universal extra dimension gives a thickness to a  $D_4$  brane in which the SM particles propagate and that this brane is embedded in a  $5 + 2$  dimensional space in which gravity can propagate (these new extra dimensions have a radius  $r$  much larger than the thickness  $R$  of the brane) then the interactions between gravity and the KK excitations of the SM fields can violate the conservation of momentum (as has been seen in the first chapters) allowing these KK excitations to decay [63, 66]. In fact, the graviton wave function will overlap with those of KK 0-modes and those of the SM parton KK excitations, therefore inducing

transitions of the form  $\text{KK}(n = 1) \rightarrow \text{KK}(n = 0) + G$ , where the graviton immediately escapes into the large extra dimension [66]. This kind of events where a pair of  $n = 1$  partons decay will appear as 2-jets plus missing  $\cancel{E}_T$  in the detector. We thus see that our motivation provides us with a decay mechanism of the lowest-lying KK modes.

The Feynman rules for the couplings of the graviton fields to the UED fields are related to the corresponding couplings of the graviton fields to the SM fields by a form factor:

$$|\mathcal{F}_1(\frac{M_G}{M_{KK}})|^2 = \frac{4M_G^2}{\pi^2(M_{KK}^2 - M_G^2)}(1 + \cos(\pi \frac{M_G}{M_{KK}})) \quad (6.5)$$

where  $M_G$  is the continuous mass of the graviton and  $M_{KK}$  is obviously the mass of the decaying KK excitation. SLED predicts that there will also be couplings of the UED KK excitations with other bulk states such as the bulk scalar that has been considered throughout this thesis. However, for simplicity, we will not consider them here, ie we will take all the other form factors to be 0. The KK excitations of SM partons will thus decay exclusively to graviton in our further analysis. The branching ratio of this channel will therefore be 1 and the total cross section for producing these KK excitations will not be modified by their decay to jet plus graviton. The lifetime of these KK states into gravitons will thus be very short, sufficiently so to justify our simplification to forget about the decay chain presented in the last section. We can nevertheless compute a decay rate for this KK state  $\rightarrow$  jet + graviton process because this will determine the graviton masses that will be “sampled” in this forced graviton decay. The total decay width is given by [66]:

$$\Gamma = \frac{2\pi\bar{M}_{pl}}{M_D^4} \int_{r^{-1}}^{M_{KK}} dM_G M_G \frac{|\vec{p}_i|}{M_{KK}^2} |\mathcal{F}_1(\frac{M_G}{M_{KK}})|^2 \quad (6.6)$$

where  $\bar{M}_{pl}$  is the reduced 4D Planck mass,  $M_D$  is the fundamental Planck scale and  $p_i$  is the momentum of the decaying KK modes. Performing the integration numerically yields the results of figure 6.5 taken from ref [66]. This figure shows that this mechanism provides for a very rapid decay over almost all of the parameter space as we argued before.

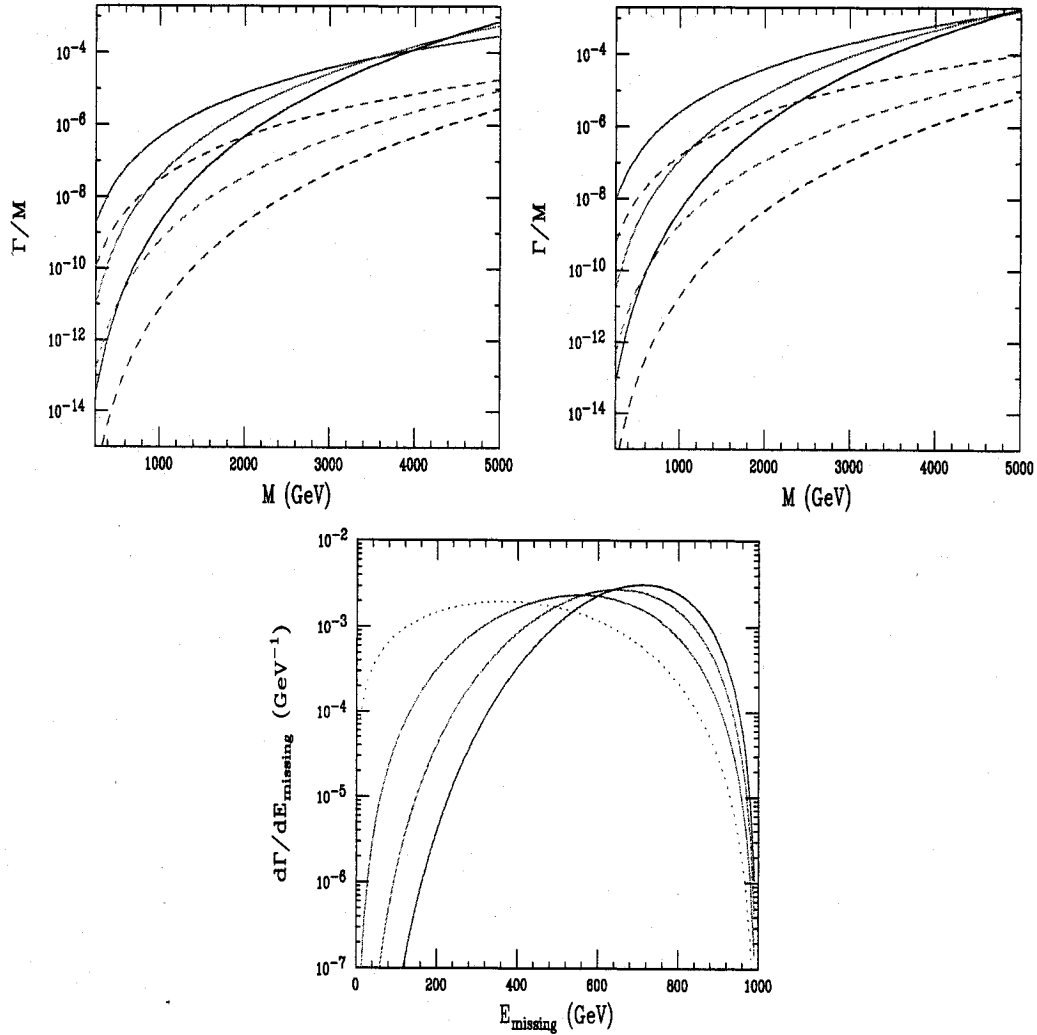


Figure 6.5: Width for the decay of the first excited KK state (even-top left panel, odd-top right panel) into the corresponding zero mode and a graviton tower as a function of the mass of the KK state. The solid (dashed) lines are for  $M_D = 5(10)$  TeV and from top to bottom in each case the curves correspond to  $\delta = 2, 4, 6$  large extra dimensions respectively. The lower panel shows the missing energy distribution for these decays for the same cases assuming a KK mass of 1 TeV. These graphs have been taken from [66]

Note that the graviton masses will be sampled proportionally to the distribution  $\frac{d\Gamma}{dM_G}$  as a function of  $M_G$ , ie, since the graviton is responsible for most of the missing energy of the event, following the distribution of  $\frac{d\Gamma}{dE_T}$  of the previous picture. We can note, from this distribution, that in the SLED scenario (two large extra dimensions) the graviton masses will be approximately uniformly sampled on all the interval of energy allowed by the kinematics of the event. These decays will not be performed by PYTHIA (again used to simulate our processes). Instead, we do it in a separate step. We perform the decay in the rest frame of the decaying KK parton, and Lorentz boost it to the lab frame before filling the simulated event. The implementation of this decay process is thus only a matter of kinematics. The number of events and most of their distributions will be mainly affected by the direct production. We can now turn our discussion to the study of the direct production of parton KK excitations and to their phenomenological analysis, considering that immediately after being produced they each emit a graviton.

---



---

## PHENOMENOLOGICAL ANALYSIS OF THE UED SCENARIO

---



---

In this chapter, we will perform a detailed analysis of dijet signals in the ATLAS detector arising from KK states of quarks and gluons in the embedded UED model. We will provide a realistic upper limit on the value of the compactification scale  $M_C$  which can be detected at the LHC. More precisely we will first show that a value of  $M_C$  close to the present lower bound would provide a clear signal of the existence of Universal Extra Dimension embedded in a bulk of large extra dimension, and we will then give the maximum value that  $M_C$  can take and still allow a  $5\sigma$  discovery with the ATLAS detector. But first, we summarize, the physical predictions that follow from the UED model presented in the previous chapter.

### 7.1 Physical predictions

Having in mind the production of pairs of the first KK excitations of gluons,  $g_1^*$ , and quarks,  $q_1^\bullet$  and  $q_1^\circ$ , in proton-proton collisions at the LHC, we can use the Lagrangian density and Feynman rules for the vertices rederived in the previous chapter to compute analytically the differential cross section for the various processes at parton tree-level. Due to KK number conservation, the final states will consist of two  $n = 1$  KK partons. The KK propagators that can be involved in the relevant diagrams are given, respectively for gluons and quarks, by [63, 68]:

$$-i\Delta_{\mu\nu}^{ab}(p^2) = -i\delta^{ab} \frac{g_{\mu\nu} - \frac{p_\mu p_\nu}{M_{KK}^2}}{p^2 - M_{KK}^2} \quad (7.1)$$

$$-i\Delta^{a'b'}(p^2) = i\delta^{a'b'} \frac{\not{p} + M_{KK}}{p^2 - M_{KK}^2} \quad (7.2)$$

For simplicity, we will not consider the top quark excitations in this analysis since they are less likely to be stable (we already mentioned that at tree-level all the other partons are degenerate).

The differential cross section for the different processes that yield two  $n = 1$  KK partons in the final state have been calculated in reference [63]. However, we found and reported to the authors a number of mistakes in their published results, some of which were typographical errors. Since many subprocesses were off, in some cases by more than one order of magnitude, we recalculated the differential cross section for every subprocess (using the same techniques as the one presented in chapter 2) in order to obtain a proper evaluation of the total production rate for pairs of KK partons at the LHC. The calculations have been tested by evaluating them in the massless limit where these KK partons become SM particles. In terms of the redefined Mandelstam variables  $s \equiv \hat{s}$ ,  $t \equiv \hat{t} - M_{KK}^2$  and  $u \equiv \hat{u} - M_{KK}^2$ , where  $s+t+u = 0 \Leftrightarrow \hat{s} + \hat{t} + \hat{u} = 2M_{KK}^2$ , the results are:

$$\text{process } gg \rightarrow g_1^* g_1^* \quad (7.3)$$

$$\begin{aligned} \bar{\sum} |\mathcal{M}|^2 &= \frac{9}{8} \alpha_s^2 \frac{1}{(stu)^2} [M^4(6t^4 + 18t^3u + 24t^2u^2 + 18tu^3 + 6u^4) \\ &\quad + M^2(6t^4u + 12t^3u^2 + 12t^2u^3 + 6tu^4) \\ &\quad + 2t^6 + 6t^5u + 13t^4u^2 + 15t^3u^3 + 13t^2u^4 + 6tu^5 + 2u^6] \end{aligned}$$

$$\text{process } qg \rightarrow q_1^* g_1^* \quad (7.4)$$

$$\bar{\sum} |\mathcal{M}|^2 = \frac{-1}{36} \alpha_s^2 \frac{1}{(stu)^2} [12su^5 + 5s^2u^4 + 22s^3u^3 + 5s^4u^2 + 12s^5u]$$

$$\text{process } qq \rightarrow q_1^* q_1^* \quad (7.5)$$

$$\begin{aligned} \bar{\sum} |\mathcal{M}|^2 &= \frac{1}{72} \alpha_s^2 \frac{1}{(tu)^2} [M^2(8t^3 + \frac{4}{3}t^2u + \frac{4}{3}tu^2 + 8u^3) \\ &\quad + 8t^4 + \frac{56}{3}t^3u + 20t^2u^2 + \frac{56}{3}tu^3 + 8u^4] \end{aligned}$$

process  $gg \rightarrow q_1^\bullet \bar{q}_1^\bullet$  (7.6)

$$\begin{aligned} \bar{\sum} |\mathcal{M}|^2 &= \frac{5}{6} \alpha_s^2 \frac{1}{(stu)^2} [-M^4(4t^4 + 8t^3u + 8t^2u^2 + 8tu^3 + 4u^4) \\ &\quad - M^2(4t^4u + \frac{15}{2}t^3u^2 + 4t^2u^3 + \frac{1}{2}tu^4) \\ &\quad + t^5u - \frac{1}{4}t^4u^2 + 2t^3u^3 - \frac{1}{4}t^2u^4 + tu^5] \end{aligned}$$

process  $q\bar{q} \rightarrow q_1^\bullet \bar{q}_1^\bullet$  (7.7)

$$\begin{aligned} \bar{\sum} |\mathcal{M}|^2 &= \frac{2}{9} \alpha_s^2 \frac{1}{(st)^2} [M^2s(4t^2 - st - s^2) \\ &\quad + 4t^4 + 3st^3 + \frac{11}{12}t^2s^2 - \frac{2}{3}s^3t + s^4] \end{aligned}$$

process  $q\bar{q} \rightarrow q_1^\bullet \bar{q}'_1^\bullet$  (7.8)

$$\bar{\sum} |\mathcal{M}|^2 = \frac{16}{9} \alpha_s^2 \frac{1}{s^2} [2M^2s + s^2 + 2st + 2t^2]$$

processes  $qq' \rightarrow q_1^\bullet q'_1^\bullet$ ,  $q\bar{q}' \rightarrow q_1^\bullet \bar{q}'_1^\bullet$  and  $q\bar{q}' \rightarrow q_1^\bullet \bar{q}_1^\bullet$  (7.9)

$$\bar{\sum} |\mathcal{M}|^2 = \frac{2}{9} \alpha_s^2 \frac{1}{t^2} [-M^2s + s^2 + \frac{1}{4}t^2]$$

processes  $q\bar{q}' \rightarrow q_1^\bullet \bar{q}'_1^\bullet$  and  $qq' \rightarrow q_1^\bullet q'_1^\bullet$  (7.10)

$$\bar{\sum} |\mathcal{M}|^2 = \frac{1}{18} \alpha_s^2 \frac{1}{t^2} [4M^2s + 4s^2 + 8st + 5t^2]$$

process  $qq \rightarrow q_1^\bullet q_1^\bullet$  (7.11)

$$\bar{\sum} |\mathcal{M}|^2 = \frac{1}{36} \alpha_s^2 \frac{1}{(tu)^2} [-8M^2(t^3 + t^2u + tu^2 + u^3) + 8t^4 + 4t^2u^2 + 8u^4]$$

where  $M$  is the mass of the first KK excitation of light partons ( $M \equiv M_1^{KK}$ ).  $q'$  is a different quark flavor than the ones that collide and the summation is taken over the polarization and color states (sum on the final states and average on the initial ones). For the process  $gg \rightarrow q_1^\bullet \bar{q}_1^\bullet$  we multiplied the cross section by 5 to account for all the possible quark flavors that can be produced in the final state (remember that we restrained our analysis to the light quarks). For a similar reason the process  $q\bar{q} \rightarrow q_1' \bar{q}_1'$  has been multiplied by 4 (this process requires that the final state quark flavors be different than the initial one, therefore leaving four final state flavor possibilities). Note finally that for every process except the mixed ones (ie those involving a  $q^\bullet$  and a  $q^\circ$  in the final state) we will have two exact copies of each process, one for each of the two possible quark towers<sup>1</sup>.

The total cross section can be obtained, as we saw in previous chapters, by convoluting the differential cross section with the Parton Distribution Function (PDF), integrating over the phase space and finally summing on the quarks flavors. The general expression is:

$$\sigma^{tot}(pp \rightarrow 2\text{-KK}) = \sum_j \int_{\frac{4M_1^2}{s}}^1 dx_A \int_{\frac{4M_1^2}{sx_B}}^1 dx_B f(x_A, Q) f(x_B, Q) \quad (7.12)$$

$$\times \int_{-1}^1 dz \frac{\pi \sum |\mathcal{M}_j|^2}{2\hat{s}} \sqrt{1 - \frac{4M_1^2}{\hat{s}}}$$

where the functions  $f$  are the CTEQ5L PDF [58],  $j$  identify the processes enumerated above and  $z = \cos \theta$  with the cosine given by the relation  $\hat{t} = -\frac{\hat{s}}{2}(1 - \sqrt{1 - \frac{4M_1^2}{\hat{s}} \cos \theta}) + M_1^2$  in the center of mass system. The numerical integration is performed as before

<sup>1</sup>One process that should contribute to the total cross section for the direct production of excited KK partons has not been presented so far:  $q\bar{q} \rightarrow g_1^* g_1^*$ . After discussion with the authors, we came to the agreement that the published result is one order of magnitude bigger than what the right answer must be. For simplicity we therefore implemented the published result and divided it by a factor 10. This is just an approximation, but it will have no impact on our phenomenological results since the ratio of the cross section of this process to the combined cross section of all the processes is about 0.004.

with PYTHIA [49] which also selects the events and performs the hadronization, the initial state and the final state radiation. In table 7.1, we can see the processes of interest with their computed cross section for a KK mass of 1.3 TeV. Adding all these numbers yields a total cross section of 2.4 pb, which is large enough to be detectable easily at the LHC. Of course, this cross section drops with increasing value of the compactification scale  $M_{KK}$ , as can be seen in figure 7.1.

We now analyze the results of our simulation, taking the backgrounds into account, to see what the expected significance of such a signal is and at what mass range ATLAS is sensitive.

Processes	$\sigma$ fb	Processes	$\sigma$ fb	Processes	$\sigma$ fb
$gg \rightarrow g^*g^*$	212	$q\bar{q} \rightarrow g^*g^*$	14	$qg \rightarrow q^*g^*$	605
$qq \rightarrow q^*q^*$	175	$q\bar{q} \rightarrow q^*\bar{q}^*$	25	$gg \rightarrow q^*\bar{q}^*$	11
$q\bar{q} \rightarrow q'^*\bar{q}'^*$	22	$qq' \rightarrow q^*q'^*$	121	$q\bar{q}' \rightarrow q^*\bar{q}'^*$	26
$qq \rightarrow q^*q^\circ$	222	$q\bar{q} \rightarrow q^*\bar{q}^\circ$	16	$qq' \rightarrow q^*q'^\circ$	84
$q\bar{q}' \rightarrow q^*\bar{q}'^\circ$	38				

Table 7.1: Cross sections for the different processes that yield a KK pair production at LHC assuming  $M_{KK} = 1.3$  TeV and an integrated luminosity of  $100 \text{ fb}^{-1}$ .

## 7.2 Detailed Simulations

As was done previously, to perform a detailed analysis of the expected signals, accounting for Standard Model backgrounds, and incorporating detector effects, we first assign incoming parton flavors for each event according to the CTEQ 5L parton distribution functions [58] evaluated at the renormalization scale  $Q^2 = M_n^2 + p_T^2$  and we apply color flow between these partons. ATLAS detector effects are again incorporated using the fast Monte Carlo program ATLFAST [59].

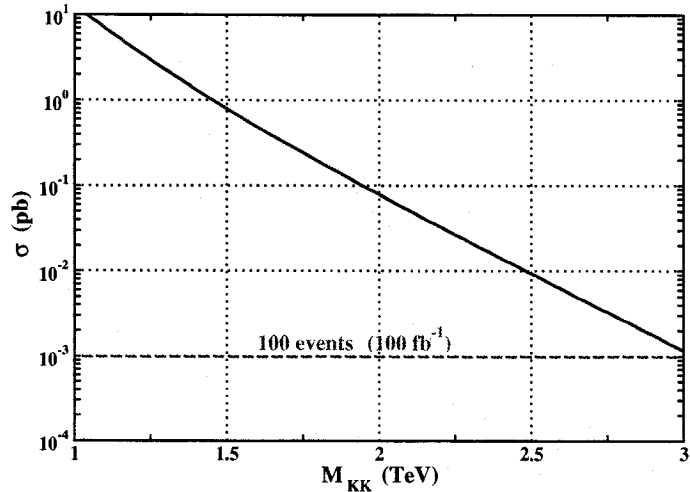


Figure 7.1: The total cross section for the production of two KK final states at the LHC is shown in function of the KK mass of these states. A annual luminosity of  $100 \text{ fb}^{-1}$  has been considered here. The dashed line mark 100 events at this luminosity.

### 7.2.1 Standard Model Backgrounds

The phenomenology of interest is the production of a pair of KK partons each of which immediately decays into its associated parton plus a graviton. Since the graviton will quickly escape into the large extra dimensions, the signal that we are looking for is two energetic jets accompanied by a large amount of missing  $E_T$ . The Standard Model backgrounds for this process involve two jets and neutrinos in the final state. The principal backgrounds having these features are  $pp \rightarrow 2 \text{ jets} + Z(\rightarrow \nu\nu)$  and  $pp \rightarrow 2 \text{ jets} + W(\rightarrow \ell\nu)$  where we miss the lepton. Although PYTHIA does not generate these  $Z/W + 2 - jets$  events from matrix element calculations, it does generate  $Z + jet$  and  $W + jet$  events with additional energetic jets produced from initial or final state QCD radiation and from parton showering. In order to estimate the systematic error due to this approximate simulation of the second jet, we will need to use a next-to-leading order generator such as Sherpa [69] which simulates  $Z/W + 2-jets$  with matrix element code. Here, we will be content, in a first analysis, with the estimate of PYTHIA.

The simulated backgrounds and their cross sections in the phase space region  $E_{T,jet}^{\min} > 100 \text{ GeV}$  and  $E_{T,jet}^{\min} > 250 \text{ GeV}$  are given in table 7.2 while the cross

sections for different mass scenarios of the signal with  $E_{T,jet}^{\min} > 250$  GeV can be read from figure 7.1 ( $\sigma = 1.96$  pb in the case  $M_{KK} = 1.3$  TeV).

Processes	cross-section (pb)	
	100 GeV	250 GeV
$pp \rightarrow \text{jet} + Z (\rightarrow \nu\nu)$	129.1	5.11
$pp \rightarrow \text{jet} + W (\rightarrow e\nu_e)$	176.7	6.75
$pp \rightarrow \text{jet} + W (\rightarrow \mu\nu_\mu)$	176.7	6.75
$pp \rightarrow \text{jet} + W (\rightarrow \tau\nu_\tau)$	176.6	6.74

Table 7.2: S.M. backgrounds to the production at ATLAS of a pair of KK partons which each decay in a jet plus an undetectable graviton and their cross sections for 2 different phase space regions.

### 7.2.2 Analysis

Here, we first apply experimental selection criteria to the sample of simulated data in order to isolate our signal. We then use these cuts to quantify the largest size of the compactification scale ( $M_C = \frac{1}{R} \approx M_1$ ) which can be expected to be detectable at a  $5\sigma$  significance with the ATLAS detector. Throughout this analysis, jets are reconstructed using the cone algorithm with a cone radius  $\Delta R = \sqrt{(\Delta\eta)^2 + (\Delta\phi)^2} = 0.4$ . In the ATLAS detector, leptons are detected if they are emitted in the range of pseudorapidity  $-2.5 < \eta < 2.5$ . They are also defined as isolated if the energy deposited by other particles in a cone of radius  $\Delta R$  is less than 10 GeV.

As a first cut we require:

**Cut 1:** No isolated lepton (electron or muon) with  $p_T > 6$  GeV allowed in the event.

This eliminates most of the  $W \rightarrow e\nu_e$  and  $W \rightarrow \mu\nu_\mu$  events, leaving only those for which the leptons are not properly reconstructed in the detector. It does not eliminate events such as  $W + jet \rightarrow \tau\nu_\tau + jet$  in which the  $\tau$  decays hadronically.

We will first want to eliminate the dominant background, ie the  $pp \rightarrow jet + Z \rightarrow jet + \nu\nu$ . Since we expect to have two high energetic jets in our signal coming from

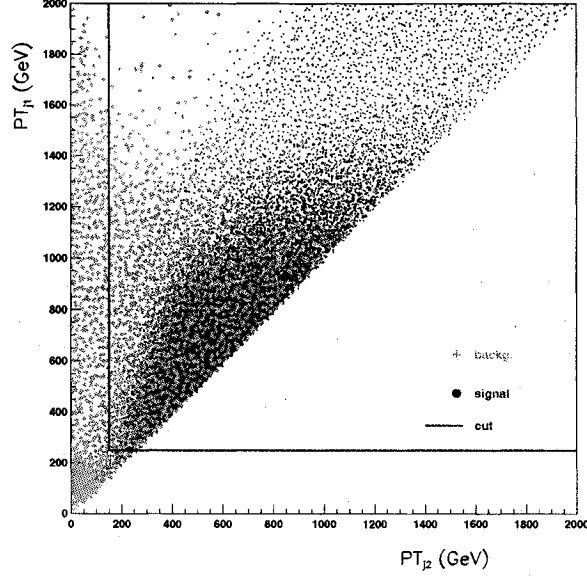


Figure 7.2: Comparison of the  $p_T$  distributions of the two most energetic jets for the signal and the background.

the decay of the two final state KK partons, it is useful to compare the transverse momentum distributions of the two most energetic jets of the signal events with the corresponding distributions for the background sample. This comparison is shown in Fig. 7.2. It is clear, from this figure, that with the following cuts:

**Cut 2:** Only events with a jet having a transverse momentum greater than 250 GeV are kept: ( $p_T^{jet-1} > 250$  GeV).

**Cut 3:** We keep only events for which  $p_T^{jet-2} > 150$  GeV, where jet-2 is the jet with second-highest  $p_T$ .

combined to the **Cut 1**, we can reject most of the background events ( $\sim 92\%$  for W+jets and  $\sim 96\%$  of the Z+jets events) while keeping most of the signal. (About 35% of the signal events are lost by these two cuts).

For the  $W + jet \rightarrow \tau\nu_\tau + jet$  background, we expect, in this case, to have also an energetic low-multiplicity jet opposite, in the azimuthal plane, to the principal jet. Following [43, 50], a cut on the difference in azimuthal angles between the two most

energetic jets is found to help in eliminating this  $\tau$  background. Indeed, even after making cut 3 above on the second most energetic jets of the events, a cut on the difference in the azimuthal angle of the two most energetic jets will not be redundant, as we can see on the top panel of Fig. 7.3. This figure shows that indeed the main contribution to the background after cuts 1 to 3 have been applied is  $W \rightarrow \tau\nu_\tau$ . The bottom panel of Fig. 7.3, shows that we optimize the significance ( $\text{Signal}/\sqrt{\text{Background}}$ ) of the signal when we impose the following cut:

**Cut 4:** Only events for which  $|\varphi_{j_1} - \varphi_{j_2}| < 2.6$  radians are kept.

Finally, because the emission of massive gravitons from our signal is expected to leave in general much more missing energy than the emission of neutrinos from vector boson decays, we consider the possibility of a cut on  $\cancel{E}_T$ . We see in Fig. 7.4 (left picture) that the distribution of this variable is clearly different for the signal and the background. On the right picture of the same figure we show the significance of the signal as a function of an applied cut on the missing transverse energy and determine the optimum value of that cut. On the basis of this figure, we further require:

**Cut 5:** We keep only events for which  $\cancel{E}_T > 775$  GeV.

### 7.2.3 Results

The above cuts leave us with only 0.07% (or 1789 events for an integrated luminosity  $\mathcal{L} = 100 \text{ fb}^{-1}$ ) of the initial number of background events, for the phase space region  $E_{T,jet}^{\min} > 250$ ) and 14.4% (or 28210 events) of the total number of signal events for a significance of 670 and  $M_{KK} = 1.3$  TeV. It will therefore be easy to detect a pair of 1.3 TeV KK particles with the ATLAS detector. A  $5\sigma$  significance can be reached with a luminosity of only  $6 \text{ pb}^{-1}$ . Imposing the same cuts on the signal samples of different masses yields the curve of figure 7.5. With an integrated luminosity of  $100 \text{ fb}^{-1}$ , ATLAS will allow a  $5\sigma$  discovery if the mass of the first excited KK partons is

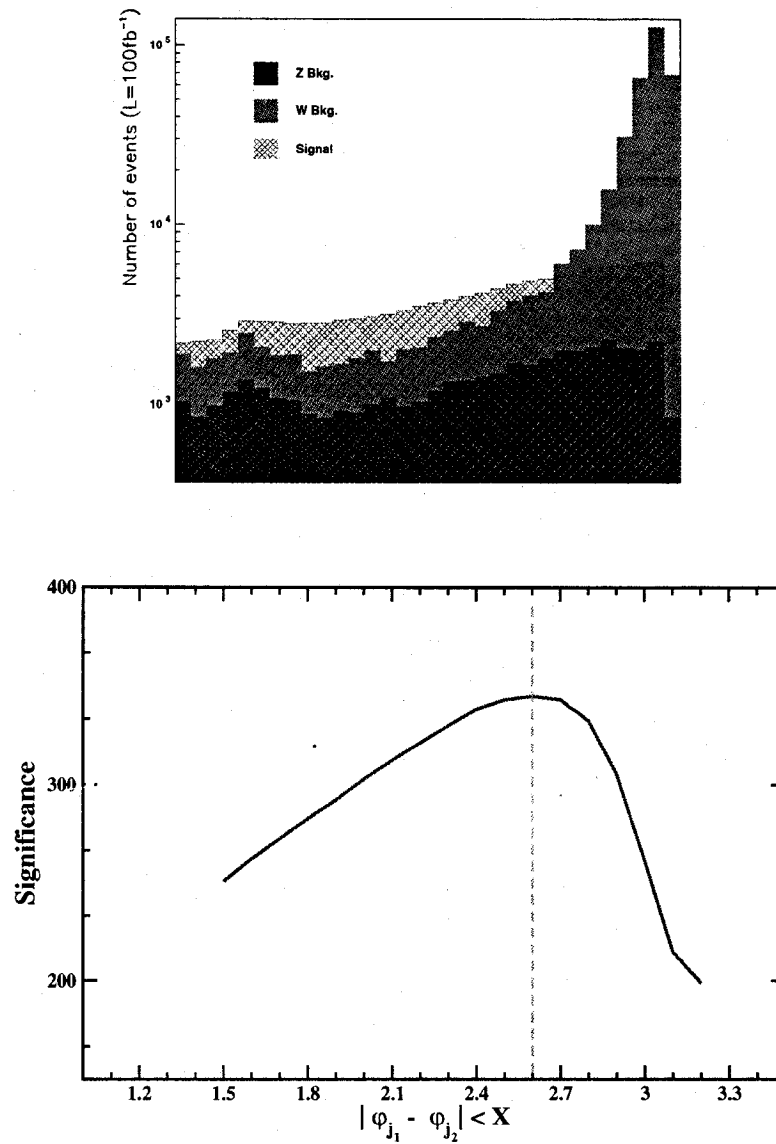


Figure 7.3: top: Distribution of the difference in the azimuthal angle between the two most energetic jets of an event for the signal and the each background on top of it. A KK mass of 1.3 TeV is used as reference. Cuts 1-3 have been applied. bottom: Significance of the signal for different values of a cut on the difference in the azimuthal angle between the most energetic jets of an event.

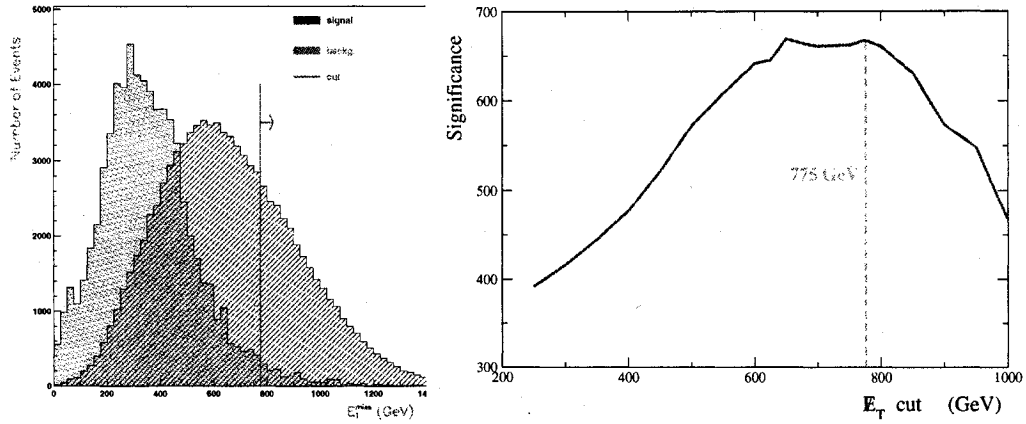


Figure 7.4: Left: Comparison of  $E_T$  distribution for signal and background events. Right: Variation of the significance of the signal as a function of the cut on  $E_T$

$< 2685$  GeV (ie it is sensitive to a compactification radius of the extra dimension of  $\sim 2.7$  TeV $^{-1}$ ).

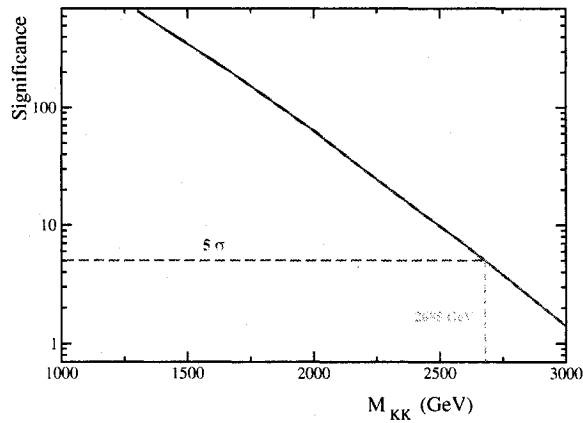


Figure 7.5: Variation of the significance of the signal in function of the mass of the first KK excitation state.

We note also that such a high cut on missing transverse energy will help to discriminate the principal large extra dimension signals (one jet and missing energy) where only one of the gravitational modes (graviton or its superpartners) are produced.

With such an analysis we therefore prove that if the mass of the compactification scale is higher than the actual experimental lower bound ( $M_c \gtrsim 400$  GeV), we will be able to see this signal at more than  $5\sigma$  significance. For example, if  $M_C = 1.3$  TeV we can probe these UED with an only  $6$  pb $^{-1}$  luminosity, which is indeed a clear

signal. We can finally conclude from our analysis that if there is one small extra dimension that can be universally probed by Standard Model particles and if the thin brane that it forms is embedded in a bulk of large extra dimensions as is predicted by Supersymmetric Large Extra Dimensions scenario [12, 44], then ATLAS will allow us to make a  $5\sigma$  discovery for such a signal for a compactification scale up to 2700 GeV.

---

---

## SUMMARY AND CONCLUSION

---

---

The Supersymmetric Large Extra Dimension (SLED) scenario offers the possibility of building low-energy effective fields theories, or even microphysics models valid beyond the  $(4 + n)$ -dimensional Planck scale ( $M_D$ ), which don't suffer from the cosmological constant problem. We have seen in chapter 2 that this theory requires that a 3-brane, where the Standard Model fields live, be embedded in a  $(4 + 2)$ -dimensional space, with the two extra dimensions compactified on a geometry of about a micron size. We have also seen that this scenario requires a gravitational supersymmetric bulk space (with SUSY only weakly broken by the presence of the brane), but non-supersymmetric brane degrees of freedom for energy scales lower than the weak scale ( $M_W \sim M_D \sim 10$  TeV). These features thus predict a low-energy realization of supersymmetry that differs completely with what is expected from the popular Minimal Supersymmetric Standard Model (MSSM). Moreover, with the number and the size of the extra dimensions fixed in this scenario by the requirement of a solution to the cosmological constant problem, SLED also provides a solution to the hierarchy problem without involving fine tuning. By solving all these problems, the SLED scenario therefore offers the inestimable possibility of greatly improving our understanding of high-energy physics and cosmology.

Inspired by the strong scientific value and the novelty of such a theoretical framework, this thesis has aimed to provide this scenario with the concrete phenomenological analysis needed for fixing and orienting future experimental tests of SLED theories. In particular we wanted to study the possibility of testing the direct production of bulk scalars (superpartners of the graviton) at the LHC and to evaluate the

capabilities of the ATLAS detector to discover their presence. To this end, we considered the lowest mass-dimensional effective Lagrangian describing the interactions of Kaluza-Klein states of a generic bulk scalar with SM quarks, gluons and Higgs boson at low energy and we used it to compute the differential cross section of the processes  $q\bar{q} \rightarrow g\phi$ ,  $qg \rightarrow q\phi$ ,  $gg \rightarrow g\phi$  and  $gg \rightarrow h\phi$ . This was presented in chapter 3. After a brief description in chapter 4 of the LHC and of the expected performances of the ATLAS detector, we have explained how Monte Carlo generators were produced and we have presented our complete phenomenological analysis of these processes in the fifth chapter using Monte Carlo simulations. The results are the following.

We first found out that a  $5\sigma$  discovery of such a generic bulk scalar is possible with the ATLAS detector for a wide range of values of the bulk scalar-gluon coupling and the bulk scalar-fermion couplings, even if ATLAS is more sensitive to the first one. We then showed that this sensitivity is higher when the number of extra dimensions is small, being maximal for the  $n = 2$  SLED scenario. Finally, we compared these results with those of graviton production and found that they are comparable in size and shape. The number of events expected for each of these two processes can only be evaluated in the SLED scenario because it is the only extra dimensional framework which fixes the number and size of the large extra dimensions on which depend the cross sections of these processes. This confirms the stronger predictability and scientific value of the SLED scenario compared to any other Large Extra Dimension (LED) proposal.

In a second analysis, we studied the dimensionless trilinear interaction of SM Higgs bosons with a bulk scalar. We mentioned that the interest in such a coupling is that it is independent of any mass scales. A large coupling is therefore a specific prediction of the SLED scenario, and it must dominate at the LHC energy scale. Studying the channel where the Higgs boson decays in two photons (and the bulk scalar again leaves missing energy in the detector), we showed that a  $5\sigma$  discovery will be possible for an integrated luminosity of  $\mathcal{L} \text{ fb}^{-1}$ , if the dimensionless Higgs-bulk scalar coupling  $a$  is higher than 0.09, when a cut of 78 GeV on the missing transverse energy of the

events is applied. If ATLAS indeed sees such signal, it will be strong evidence for the SLED scenario. Moreover, we showed that such a channel would help the discovery and the measurement of the Higgs boson even in the context of the Standard Model.

Finally, in the last part of this work, we studied the possibility of observing a Universal Extra Dimension signal, when the final KK states decay into a parton plus a graviton because of the large extra dimensions predicted by SLED. Here again we showed that such a signal will be detectable and lead to a discovery at the LHC, provided that the compactification scale of the small extra dimension (corresponding to a brane thickness) is lower than  $(2675 \text{ GeV})^{-1}$ .

This work constitutes a guide for an experimental analysis when data become available. It provides information on what can be seen in a detector like ATLAS, on how the signals of the physical processes that we considered can be isolated and on how we can interpret them. We find our results encouraging since they confirm that with the ATLAS detector it will be possible to verify or falsify the powerful SLED scenario. More work can still be done to complete this analysis with the study of other possible channels and processes, but we are already excited. We are awaiting impatiently the first collisions at the LHC, in 2008, as we know that we could, hopefully, confirm the proposed solution of the cosmological constant problem.

---

---

## BIBLIOGRAPHY

---

---

- [1] L. Alvarez-Gaume and M.A. Vazquez-Mozo, *Topics in String Theory and Quantum Gravity*, lecture notes for the Les Houches Summer School on Quantum Gravity held in July 1992;  
J.H. Schwarz, *Introduction to Superstring Theory*, Lectures presented at the St. Croix NATO Advanced Study Institute on Techniques and Concepts of High Energy Physics, Report-no: CALT-68-2293, CITUSC/00-045 [hep-ex/0008017];  
A. Belhaj, *Introduction à la Théorie des Cordes*, Cours de DESA-Physique des Hautes Énergies, Faculé des Sciences de Rabat, hivers 2003.
- [2] C.L. Bennett, *First Year Wilkinson Microwave Anisotropy Probe (WMAP) Observations: Preliminary Maps and Basic Results*, *Astrophys.J.Suppl.* **148** (2003) 1, [astro-ph/0302207]
- [3] A.E. Lange *et al.*, *First Estimations of Cosmological Parameters from BOOMERanG*, *Phys. Rev.* **D63** (2001) 042001 [astro-ph/0005004]; P. de Bernardis *et al.*, *A Flat Universe from High-Resolution Maps of the Cosmic Microwave Background Radiation*, *Nature* **404** (2000) 955-959 [astro-ph/0004404]; J.R. Primack, *Cosmological Parameters*, [astro-ph/0007187] (2000).
- [4] N.A. Bahcall, J.P. Ostriker, S. Perlmutter and P.J. Steinhardt, *The Cosmic Triangle: Assessing for the State of the Universe*, *Science* **284** (1999) 1481-1488 [astro-ph/9906463].
- [5] E. Witten, *Nucl. Phys.* **B471** (1996) 135 (hep-th/9602070); J. Lykken, *Phys. Rev.* **D54** (1996) 3693 (hep-th/9603133); P. Horava and E. Witten, *Nucl. Phys.* **B475** (1996) 94 (hep-th/9603142); I. Antoniadis, N. Arkani-Hamed, S. Dimopou-

- los and G. Dvali, Phys. Lett. **B436** (1998) 257 (hep-ph/9804398); Nucl. Phys. **B460** (1996) 506 (hep-th/9510209); I. Antoniadis, Phys. Lett. **B246** (1990) 377.
- [6] G.F. Giudice, R. Rattazzi and J.D. Wells, Nucl. Phys. **B544** (1999) 3–38, [hep-ph/9811291].
- [7] E.A. Mirabelli, M. Perelstein and M.E. Peskin, Phys. Rev. Lett. **82** (1999) 2236–2239, [hep-ph/9811337]; J.L. Hewett, Phys. Rev. Lett. **82** (1999) 4765–4768, [hep-ph/9811356]; T Han, J.D. Lykken and R.-J. Zhang, Phys. Rev. **D59** (1999) 105006, [hep-ph/9811350]; I. Antoniadis, K. Benakli and M. Quiros, Phys. Lett. **B460** (1999) 176–183, [hep-ph/9905311]; S. Cullen, M. Perelstein and M.E. Peskin, Phys. Rev. **D62** (2000) 055012, [hep-ph/0001166].
- [8] M. Battaglia, D. Dominici, J.F. Gunion and J.D. Wells, Proceedings of the Les Houches Workshop 2003: “*Physics at TeV Colliders*”, ed. F. Boudjema (hep-ph/0402062);  
A. Datta, K. Huitu, J. Laamanen and B. Mukhopadhyaya, hep-ph/0404056
- [9] S. Dimopoulos and G. Landsberg, Phys. Rev. Lett. **87** (2001) 161602, [hep-ph/0106295]; S.B. Giddings and S. Thomas, Phys. Rev. **D65** (2002) 056010, [hep-ph/0106219]; D.M. Eardley and S.B. Giddings, Phys. Rev. **D66** (2002) 044011, [gr-qc/0201034]; R. Emparan, Phys. Lett. **B526** (2002) 393–398, [hep-ph/0108060]; G.F. Giudice, R. Rattazzi and J.D. Wells, Nucl. Phys. **B630** (2002) 293–325, [hep-ph/0112161]; J.L. Feng and A.D. Shapere, Phys. Rev. Lett. **88** (2002) 021303, [hep-ph/0109106]; R. Emparan, M. Masip, R. Rattazzi, Phys. Rev. **D65** (2002) 064023, [hep-ph/0109287]; S. Hossenfelder, S. Hofmann, M. Bleicher and H. Stoecker, Phys. Rev. **D66** (2002) 101502, [hep-ph/0109085]; Phys. Lett. **B548** (2002) 73–76, [hep-ph/0112186]; K. Cheung, Phys. Rev. Lett. **88** (2002) 221602, [hep-ph/0110163]; R. Casadio and B. Harms, Int. J. Mod. Phys. **A17** (2002) 4635–4646, [hep-th/0110255]; L.A. Anchordoqui, J.L. Feng, H. Goldberg and A.D. Shapere, Phys. Rev. **D65** (2002) 124027, [hep-ph/0112247]; A. Ringwald and H. Tu, Phys. Lett. **B525** (2002) 135–142, [hep-ph/0111042];

- M.B. Voloshin, Phys. Lett. **B518** (2001) 137-142, [hep-ph/0107119]; S.N. Solodukhin, Phys. Lett. **B533** (2002) 153-161, [hep-ph/0201248]; T.G. Rizzo, JHEP 0202 (2002) 011, [hep-ph/0201228]; E. Kohlprath and G. Veneziano, JHEP 0206 (2002) 057, [gr-qc/0203093]; S.D.H. Hsu, Phys. Lett. **B555** (2003) 92-98, [hep-ph/0203154].
- [10] For recent reviews with more references, see: P. Kanti, *Black holes in theories with large extra dimensions: A review*, [hep-ph/0402168]; J. Hewett and M. Spiropulu, *Particle Physics Probes Of Extra Spacetime Dimensions*, Ann.Rev.Nucl.Part.Sci. 52 (2002) 397, [hep-ph/0205106]; G. Azuelos et al., *The Beyond the Standard Model Working Group: Summary Report*, proceedings of the Workshop 'Physics at TeV Colliders', Les Houches, 2001 [hep-ph/0204031]; B. C. Allanach et al., *LES HOUCHES PHYSICS AT TEV COLLIDERS 2003, BEYOND THE STANDARD MODEL WORKING GROUP: SUMMARY REPORT* proceedings of the Workshop 'Physics at TeV Colliders', Les Houches, 2003 [hep-ph/0402295].
- [11] Y. Aghababaie, C.P. Burgess, S. Parameswaran and F. Quevedo, Nuclear Physics **B680** (2004) 389-414, [hep-th/0304256];  
C.P. Burgess, *Supersymmetric Large Extra Dimensions and the Cosmological Constant: An Update*, Annals of Physics (to appear) [hep-th/0402200]
- [12] C.P. Burgess, J. Matias and F. Quevedo, *MSLED: A Minimal Supersymmetric Large Extra Dimensions Scenario*, [hep-ph/0404135];  
C.P. Burgess, *Towards a Natural Theory of Dark Energy: Supersymmetric Large Extra Dimensions*, [hep-th/0411140]
- [13] Y. Aghababie, C.P. Burgess, J.M. Cline, H. Firouzjahi, F. Quevedo, G. Tasinato and I. Zavala, Journal of High Energy Physics **0309** (2003) 037, 48 pages [hep-th/0308064];  
Y. Aghababaie, C.P. Burgess, S. L. Parameswaran and F. Quevedo, JHEP **0303** (2003) 032, [hep-th/0212091].

- [14] N. Arkani-Hamed, S. Dimopoulos and G. Dvali, Phys. Lett. **B429** (1998) 263 (hep-ph/9803315); Phys. Rev. **D59** (1999) 086004 (hep-ph/9807344); I. Antoniadis, N. Arkani-Hamed, S. Dimopoulos and G. R. Dvali, Phys. Lett. B **436** (1998) 257 [hep-ph/9804398].
- [15] L. Randall, R. Sundrum, Phys. Rev. Lett. **83** (1999) 3370 [hep-ph/9905221], Phys. Rev. Lett. **83** (1999) 4690 [hep-th/9906064].
- [16] Real graviton emission is discussed in E. A. Mirabelli, M. Perelstein and M. E. Peskin, Phys. Rev. Lett. **82**, 2236 (1999) [hep-ph/9811337]; T. Han, J. D. Lykken and R. Zhang, Phys. Rev. **D59**, 105006 (1999) [hep-ph/9811350]; K. Cheung and W.-Y. Keung, Phys. Rev. **D60**, 112003 (1999) [hep-ph/9903294]; S. Cullen and M. Perelstein, Phys. Rev. Lett. **83** (1999) 268 [hep-ph/9903422]; C. Balázs et al., Phys. Rev. Lett. **83** (1999) 2112 [hep-ph/9904220]; L3 Collaboration (M. Acciarri et al.), Phys. Lett. **B464**, 135 (1999), [hep-ex/9909019], Phys. Lett. **B470**, 281 (1999) [hep-ex/9910056].
- [17] There is an extensive literature examining the effects of virtual graviton exchange. For a review, along with a comprehensive list of references, see K. Cheung, talk given at the 7th International Symposium on Particles, Strings and Cosmology (PASCOS 99), Tahoe City, California, Dec 1999, hep-ph/0003306.
- [18] E. Accomando, I. Antoniadis and K. Benakli, Nucl. Phys. **B579**, 3 (2000) [hep-ph/9912287]; S. Cullen, M. Perelstein and M. E. Peskin, [hep-ph/0001166].
- [19] H. Ohanian and R. Ruffini, *Gravitation and Spacetime*, W.W.Norton & Company, 1994;  
H. Lam, Notes from the course *Introduction to Modern Physics*, McGill University.
- [20] S. Eidelman et al., *Particle Data Book*, Phys. Lett. B 592, 1 (2004)
- [21] S. Weinberg, *The Cosmological Constant Problem*, Reviews of Modern Physics **Vol. 61** No. 1 (1989) 1-23.

- [22] M. Kaku, *Quantum field Theory: A Modern Introduction*, Addison Wesley (1995).
- [23] C.D. Hoyle, D.J. Kapner, B.R. Heckel, E.G. Adelberger, J.H. Gundlach, U. Schmidt and H.E. Swanson, *Sub-millimeter Tests of the Gravitational Inverse-square Law*, Phys.Rev. **D70** (2004) 042004, [hep-ph/0405262]
- [24] S. Cullen and M. Perelstein, *Phys.Rev. Lett.* **83** (1999) 268 [hep-ph/9903422]; V. Barger, T. Han, C. Kao, R.-J. Zhang, *Phys. Lett.* **B461** (1999) 34-42, [hep-ph/9905474]; C. Hanhart, D.R. Phillips, S. Reddy, M.J. Savage, *Nucl. Phys.* **B595** (2001) 335 [nucl-th/0007016]; J.A. Pons, D.R. Phillips and S. Reddy, *Phys. Lett.* **B509** (2001) 1-9, [astro-ph/0102063].
- [25] S. Hannestad and G. Raffelt, *Phys. Rev. Lett.* **87** (2001) 051301, [hep-ph/0103201]; *Phys. Rev. Lett.* **88** (2002) 071301, [hep-ph/0110067]; *Phys. Rev.* **D67** (2003) 125008, Erratum-ibid. **D69** (2004) 029901, [hep-ph/0304029]; S. Hannestad, *Phys. Rev.* **D64** (2001) 023515, [hep-ph/0102290].
- [26] C.P. Burgess, *String Theory and Inflation*, Seminar presented at McGill University and at 2003 CAP meeting at Charlottetown.
- [27] For recent summary of experimental bounds on deviations from General Relativity, see C.M. Will, Lecture notes from the 1998 SLAC Summer Institute on Particle Physics [gr-qc/9811036]; C.M. Will [gr-qc/0103036].
- [28] A. Albrecht, C.P. Burgess, F. Ravndal and C. Skordis, *Natural Quintessence and Large Extra Dimensions*, *Phys.Rev.* **D65** (2002) 123507 [astro-ph/0107573]
- [29] I. Antoniadis, K. Benakli, A. Laugier and T. Maillard, *Brane to bulk supersymmetry breaking and radion force at micron distances*, *Nucl. Phys. B* **662** (2003) 40 [hep-ph/0211409]; M. Klein, *Loop-effects in pseudo-supersymmetry*, *Phys. Rev. D* **67** (2003) 045021 [hep-th/0209206]; C. Angelantonj and I. Antoniadis, *Nucl.Phys. B* **676** (2004), 129-148 [hep-th/0307254].

- [30] S. Weinberg, *The Quantum Theory of Field vol.1, 2 and 3*, Cambridge University Press, 1996.
- [31] J.-W. Chen, M.A. Luty and E. Pontón, JHEP **0009** (2000) 012 [hep-th/0003067].
- [32] G. Giudice, R. Rattazzi and J.D. Wells, Nucl. Phys. **B595** (2001) 250, [hep-ph/0002178].
- [33] D. Atwood, C.P. Burgess, E. Filotas, F. Leblond, D. London and I. Maksymyk, Physical Review D **63** (2001) 025007 (14 pages) [hep-ph/0007178];
- [34] D. Gross, Phys. Lett. **B197** (1987) 129, Nucl. Phys. **B303** (1988) 407; D. Amati, Phys. Lett. **B197** (1987) 81; Int. J. Mod. Phys. **A3** (1988) 1615; H. Verlinde and E. Verlinde, Nucl. Phys. **B371** (1992) 246-268, [hep-th/9110017].
- [35] For a recent review with later references, see: P. Kanti, *Black holes in theories with large extra dimensions: A review*, [hep-ph/0402168].
- [36] A. Salam and E. Sezgin, Physics Letters B **Vol. 147** (1984) 47-51; H. Nishino and E. Sezgin, Physics Letters B **Vol. 144** (1984) 187-192; N. Marcus and J.H. Schwarz, Physics Letters B **Vol. 115** (1982) 111-114.
- [37] M. F. Sohnius, Physics Report, **Vol. 128** (November 1985) 40-204
- [38] C. Houghton, Note from the course *Group theory and topology in physics*, given at Trinity College in Dublin (2004).
- [39] M. E. Peskin and D. V. Schroeder, *An Introduction to Quantum Field Theory*, Addison Wesley (1995)
- [40] R. N. Mohapatra, *Unification and Supersymmetry* (third edition), Springer (2002)
- [41] C.P. Burgess, *An Ode to Effective Lagrangians*, invited talk presented to RADCOR 98, Barcelona, September 1998; C.P. Burgess, *Goldstone and*

- Pseudo-Goldstone Bosons in Nuclear, Particle and Condensed-Matter Physics*, Phys.Rept. **330** (2000) 193-261, [hep-th/9808176]
- [42] E.I. Guendelman, *Scale Invariance, Inflation and the Present Vacuum Energy of the Universe*, Contribution to the conference "Energy Densities in the Universe", Les Arcs, France, January 2000, [gr-qc/0004011]; K. Ghoroku, M. Tachibana and N. Uekusa, *Dilaton coupled brane-world and field trapping*, Phys.Rev. **D68** (2003) 125002, [hep-th/0304051]
- [43] G. Azuelos, P.-H. Beauchemin and C.P. Burgess, *Phenomenological Constraints on Extra-Dimensional Scalars*, J. Phys. G: Nucl. Part. **31** (2005) 1-19 [hep-ph/0401125].
- [44] P.-H. Beauchemin, G. Azuelos, C.P. Burgess, *Dimensionless Coupling of Bulk Scalars at the LHC*, J. Phys. G: Nucl. Part. **30** (2004) N17-N31 [hep-ph/0407196].
- [45] P.-H. Beauchemin and G. Azuelos, *Search for the Standard Model Higgs in the  $\gamma\gamma + E_T^{miss}$  channel*, (submitted)
- [46] P. Breitenlohner and A. Kabelschacht, Nucl. Phys. **B148** (1979) 96; N. Marcus and J.H. Schwarz, *Phys. Lett.* **115B** (1982) 111; P.S. Howe, G. Sierra and P. Townsend, Nucl. Phys. **B221** (1983) 331; L.J. Romans, Nucl. Phys. **B269** (1986) 691-711.
- [47] J. Cline, Note from the course *Special topic in quantum field theory: renormalization* given at McGill University during winter 2002.
- [48] R. Cutler and D. Sivers, *Quantum-chromodynamic gluon contributions to large- $p_T$  reaction*, Phys. Rev. D **Vol 17**, No 1 (1978) 196-211; H.-U. Bengtsson, *The Lund Monte Carlo for high- $p_T$  physics*, Computer Physics Communication **31** (1984) 323-355;
- [49] T. Sjöstrand *et.al.*, Comp. Phys. Comm. **135** (2001) 238.

- [50] L. Vacavant and I. Hinchliffe, *J. Phys., G* : 27 (2001) 1839 and ATL-PHYS-2000-016
- [51] The OPAL Collaboration, G. Abbiendi *et al.*, *Search for the Standard Model Higgs Boson in  $e+e-$  Collisions at  $\sqrt{s}=192-209$  GeV*, CERN-EP-2000-156, *Phys. Lett.* **B499** (2001) 38-52; A. Quadt, *Higgs Searches at LEP*, proceedings of the 37th Recontres de Moriond on Electroweak Interactions and Unified Theories, March 2002, [hep-ex/0207050]; P. Ferrari, *Higgs Boson Searches at LEP*, [hep-ex/0305039];
- [52] ATLAS Collaboration, *Detector and Physics Performance Technical Design Report*, vol. II, CERN-LHCC-99-15
- [53] J. Ellis, M.K. Gaillard and D.V. Nanopoulos, *Nucl. Phys.* **B106** (1976) 292; A.I. Vainshtein, M.B. Voloshin, V.I. Sakharov and M. Shifman, *Sov. J. Nucl. Phys.* **30** (1979) 711; E. Eichten, I. Hinchliffe, K. Lane and C. Quigg, *Rev. Mod. Phys.* **56** (1984) 579 M. Spira, A. Djouadi, D. Graudenz and P.M. Zerwas, *Nucl. Phys.* **453** (1995) 17.
- [54] C.P. Burgess, Q. Matias and M. Pospelov, *I.J.M.P.* **A17** (2002) 1841–1918, (hep-ph/9912459).
- [55] The PHD thesis that have been made within the ATLAS collaboration are accessible from the ATLAS web site at: <http://atlas.web.cern.ch/Atlas/documentation/thesis/thesis.html>. Here are the guiding references that has mostly been used in this chapter:
- P. Savard, *Potentiel de découverte d'un boson de Higgs lourd avec le détecteur ATLAS*, Thèse de doctorat présenté à l'Université de Montréal (1997);
- D.C. O'Neil, *Performance of the ATLAS Hadronic Endcap Calorimeter and The Physics of Electroweak Top Quark Production at ATLAS*, PHD thesis presented at the University of Victoria (1999);
- A.J. Barr, *Studies of Supersymmetry models for the ATLAS experiment at the*

*Large Hadron Collider*, PHD thesis presented at the University of Cambridge (2002).

- [56] D.H. Perkins, *Introduction to High Energy Physics*, Addison Wesley (1986).
- [57] O. Oye, *A full simulation analysis of the graviscalar discovery potential*, ATL-COM-PHYS-2005-009
- [58] H. L. Lai et al., *Eur.Phys.J. C*12 (2000) 375-392 [hep-ph/9903282]
- [59] E. Richter-Was, D. Froidevaux, L. Poggioli, *ATLFAST 2.0, a fast simulation package for ATLAS*, ATLAS-PHYS-98-131
- [60] J. Hewett and J. March-Russell, in *Review of Particle Physics*, K. Hagiwara et al. (Particle Data Group), *Phys. Rev. D* 66, 010001 (2002) [<http://pdg.lbl.gov>]; S. Hannestad and G. Raffelt, *Phys.Rev.Lett.* 88 (2002) 071301 [hep-ph/0110067]
- [61] K.R. Dienes, E. Dudas and T. Gherghetta, *Grand Unification at Intermediate Mass Scales through Extra Dimensions*, *Nucl.Phys.* **B537** (1999) 47-108, [hep-ph/9806292].
- [62] T. Appelquist, H.-C. Cheng and B.A. Dobrescu, *Bounds on Universal Extra Dimensions*, *Phys. Rev. D* **Vol. 64** 035002 (2001).
- [63] C. Macesanu, C.D. McMullen and S. Nandi, *Collider Implications of Universal Extra Dimensions*, *Phys.Rev. D* **66** (2002) 015009, [hep-ph/0201300]
- [64] M. Peskin and T. Takeushi, *Phys. Rev. Lett.* **65** (1990) 964; *Phys. Rev.* **D46** (1992) 381
- [65] C. Macesanu, C.D. McMullen and S. Nandi, *New Signal for Universal Extra Dimensions*, *Phys.Lett.* **B546** (2002) 253-260, [hep-ph/0207269].
- [66] T.G. Rizzo, *Phys. Rev. D* **64**, 095010 (2001) [hep-ph/0106336]
- [67] A. DeRujula, A. Donini, M.B. Gavela and S. Rigolin, *Phys. Lett.* **B482**, 195 (2000), [hep-ph/0001335]

- [68] D.A. Dicus, C. Macesanu and S. Nandi, *Collider Implications of Kaluza-Klein Excitation of the Gluons*, Phys.Rev. D **65** (2002) 076007, [hep-ph/0012259]
- [69] T. Gleisberg, S. Höche, F. Krauss, A. Schälicke, S. Schumann and J.C. Winter; JHEP **0402** (2004) 056